INTEGRATION OF REMOTE SENSING DATA ON PRECIPITATION, EVAPOTRANSPIRATION & LEAF AREA INDEX INTO THE DISTRIBUTED GLOBAL HYDROLOGICAL MODEL PCR-GLOBWB

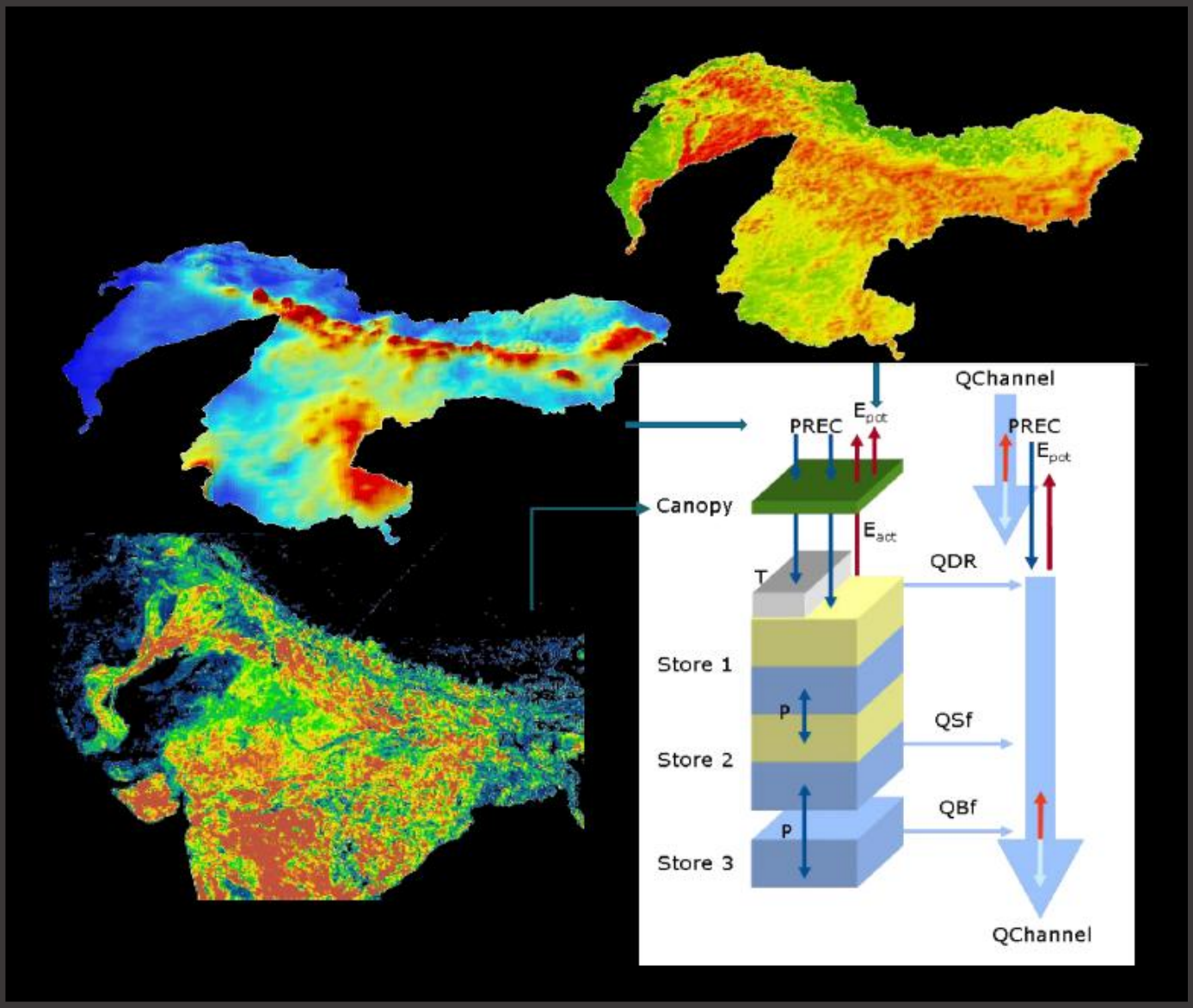

Chinmay Deval

Universiteit Utrecht

3920321

INTEGRATION OF REMOTE SENSING DATA ON PRECIPITATION, EVAPOTRANSPIRATION & LEAF AREA INDEX INTO THE DISTRIBUTED GLOBAL HYDROLOGICAL MODEL PCR-GLOBWB

Master Thesis

Student Number: 3920321

Supervisors:

Dr. Wim Bastiaanssen

Dr. Walter Immerzeel

Dr. Marc Bierkens

by

Chinmay Deval

August 2016

ABSTRACT

Using the Indus, Ganges, Brahmaputra, Mahi, Narmada, Tapi and Godavari River basins as an example, the present study examines the extent to which the remote sensing hydrological information can help improve the hydrological modelling. The leaf area index (LAI) derived from satellite remote sensing was incorporated into the PCR-GLOBWB model to add an inter-annually dynamic vegetation cycle. Four different precipitation products (CRU TS 3.21, APHRODITE, corrected-APHRODITE, and CHIRPS) were used in the different simulations to assess which product helps in better simulation of the historical river discharge in the aforesaid basins. An ensemble evapotranspiration product based on six different remote sensing ET models, was combined with the model to correct for the bias. It was concluded that the remote sensing LAI and Upper Indus Ganges Brahmaputra (UIGB)-corrected-APHRODITE precipitation products have a significant impact on the model. The P-RSLAI-ET-cor-APHRO model run performed significantly better in simulating the temporal variability of the river discharge at daily and monthly scales across the most gauging stations, while the P-RSLAI-cor-APHRO run captures the inter-annual variability and magnitude of discharge fairly well. The model improvements indicate that the incorporation of remote sensing hydrological information into the hydrological model did not only provide greater model accuracy and better representation of historic river flow but can also, to an extent, assisted in representing the the model related uncertainties in the simulations.

Keywords: *Remote sensing, Hydrological Modelling, PCR-GLOBWB*

ACKNOWLEDGEMENTS

First of all, I would like to express my deepest gratitude and warm regards to Dr. Wim Bastiaanssen for providing me with the opportunity to carry out my thesis in his research group at UNESCO-IHE and Dr. Walter Immerzeel for co-supervising the thesis. I take immense pleasure in thanking, both, Wim and Walter for their invaluable guidance and useful suggestions throughout the research period. They provided me with much time for discussions about the research and addressed every query with great patience, steering me in the right directions.

I would like to thank Dr. Rens van Beek and Dr. Edwin Sutanudjaja for getting me started with the PCR-GLOBWB model and guiding me with all queries regarding the model. I am in particular greatly indebted to Dr. Edwin Sutanudjaja who, literally, always found time in his busy schedule to help me with the python scripting, resolving model errors that I faced and in modifying the model to cater to my research objectives.

In addition, I would like to thank Marc Bierkens for providing his valuable time and guidance in the initial stages of the research. I would also like to thank Dr. Lal Muthuwatta (IWMI) for kindly providing the river discharge data, Dr. Arthur Lutz (FutureWater) for providing the UIGB correction grid, Tim Hessels (UNESCO-IHE) for guiding me through the methodology for ET ensemble preparation and also for providing the ET ensemble product itself. I would also like to express my gratitude to Dr. Elga Salvadore (UNESCO-IHE) for her able guidance and suggestions throughout the study.

I would like to extend my appreciation to Utrecht university and Utrecht university foundation for funding my Master Studies through the Utrecht Excellence Scholarship, without which the study would have been impossible.

Lastly, I would like to thank my family. Without their constant moral support and encouragement this would have been incomplete.

Chinmay Deval

August, 2016

TABLE OF CONTENTS

LIST OF TABLES

LIST OF FIGURES

CHAPTER 1

INTRODUCTION

1.1 Background and Motivation

Water is the most fundamental resource and is pivotal for the continued existence of life on earth. Yet, the water resources are continually threatened by the anthropogenic activities. Throughout the course of the 20th century, the world has witnessed about a sevenfold increase in the withdrawals of freshwater resources (Gleick, 2000). During the last few decades, the global water crisis has become increasingly evident owing to the growing gap between the availability and demand of the water resources. In the most recent edition of the global annual risk assessment report published by the World Economic Forum, the water crisis has been listed among the top ten long-term global risks in terms of societal impact (World Economic Forum, 2016), further emphasizing on the global water concern. The unprecedented proliferation of the population coupled with increased areas under food production and improved living standards, among some others, have been commonly recognized as the principal factors behind this growing water scarcity (Vorosmarty, 2000; Mekonnen and Hoekstra, 2016). The majority of the these freshwater withdrawals (approximately 70%) have been documented to be consumed by the agricultural sector, while the consumption of the remaining amount of the withdrawals has been attributed to domestic and industrial sectors (Wada et al., 2013; Wisser et al., 2009; Gleick, 2003; Shiklomanov, 2000). Besides these anthropogenic pressures on water resources, the variability of climate has further implications on the spatial and temporal availability of freshwater water. For instance the drought in several parts of the world such as Asia, Africa and USA are closely linked with the global climate phenomenon El Nino Southern Oscillation (ENSO) (Fauchereau et al., 2003; Hoerling and Kumar, 2003; Richard et al., 2000; Mo and Schemm, 2008) and the severity of such phenomena has a direct consequence on water availability both in time and space. Subsequently, water availability has direct repercussions on the development of such water stressed areas, especially in terms of the progression of the economy of the region. Previous estimates had indicated about the six-fold rise in the number of people, amounting to about 5 out of 8 billion people, living

in the circumstances of water stress by the year 2025 (Postel, 1999; Arnell, 1999b). The recent research reports that already 4 billion people throughout the globe live in the water scarce conditions at least for a month every year (Mekonnen and Hoekstra, 2016). Notably, a significant number of this population lives in the developing parts of the world. For instance, the population in India, Pakistan and Bangladesh combined, accounts to approximately 1.2 out of the 4 billion people facing the water scarce conditions. These countries are not only very densely populated which leads to extensive water withdrawals for domestic and industrial use, but are also home to one of the worlds largest and most intense irrigated area networks. In addition, these countries experience a large variation in seasonal as well as inter-annual water availability which leads to the situations where the amount of water withdrawn in certain months exceeds the availability. Such situations when exist over an extended period of time manifest into reduced amount of river discharge, inflow to the lakes and groundwater depletion. Extensive documentation corroborating the propagation of such situations into the eventual decline of water levels in the ground and surface water bodies exists. For instance Wada et al. (2010); Reddy (2007); Prigent et al. (2012).

In the light of these increased pressures on the water resources, developing an accurate knowledge base about the water balance is imperative for fundamental understanding the hydrological system of the area, forecasting the water availability, developing appropriate water management plans and decision making. However, detailed knowledge about the spatial and temporal variability of the water balance is often lacking. This inadequacy of knowledge can be attributed to numerous factors which include, amongst others, the intricacy of the area and lack of observed data and measurements. Also, the partitioning of the hydrological variable such as precipitation into different processes of the hydrological cycle (e.g. infiltration, runoff, and evaporation) is largely determined by the spatiotemporal variability of the precipitation itself, the surface characteristics (e.g. land cover, soil characteristics and slope) and the antecedent moisture conditions in the area. In addition, these different processes of the hydrological cycle take place at wide spatial and temporal scales (see figure 1.1). The interaction and feedback between these different processes at varying space and time eventually leads to an overall complex response of the catchment. Furthermore, the anthropogenic influences are enormous, for

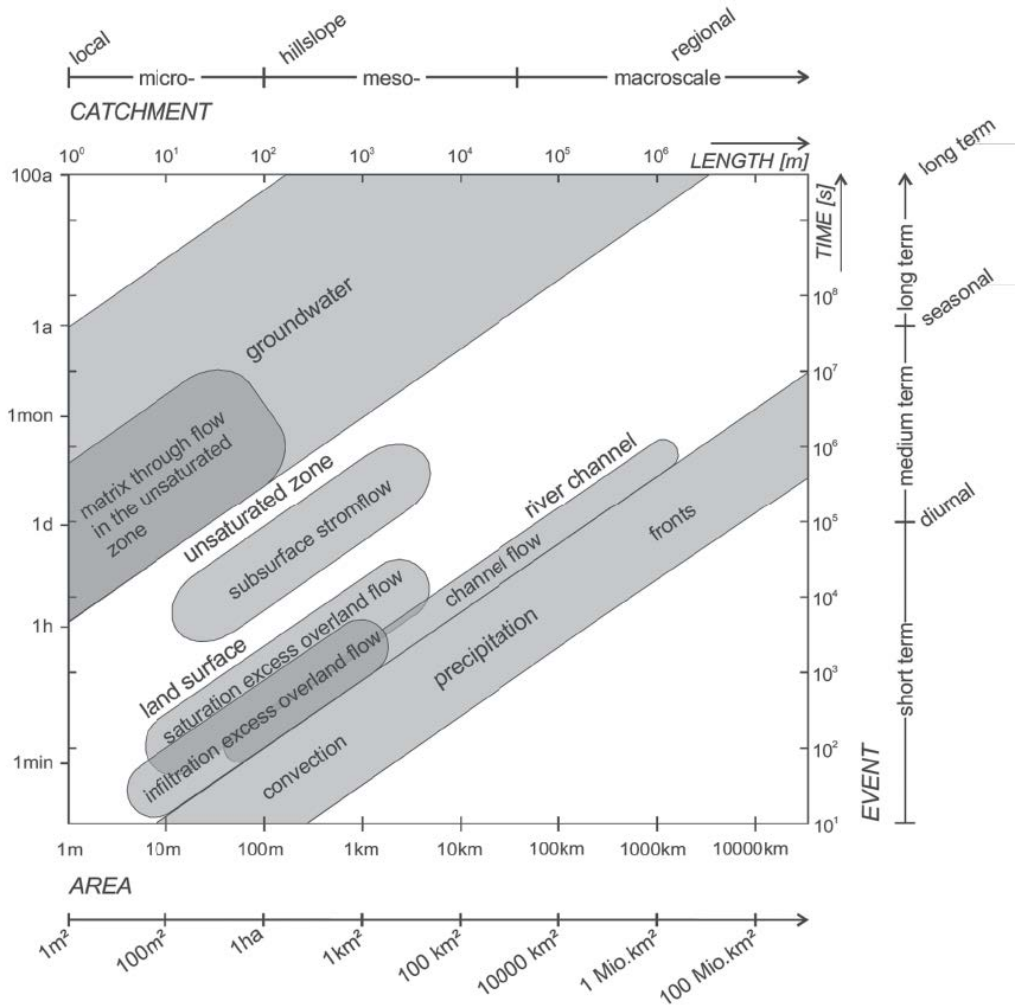

Figure 1.1: The Schematic relationship between spatial and temporal processes for various hydrological processes. Adpoted from (Bronstert et al., 2005)

instance, irrigation water withdrawals, which add to the complexity of water accounting and completely alter the understanding of the dynamics of water balance in a particular area. All these factors together complicate the modelling the water balance of the area.

Over the years, the understanding of the hydrological processes and water budget of the area has been improved extensively by developing global climate and hydrological models. These models, when forced with climatic and hydrological data-sets, are capable of simulating the hydrological system at global scales and at varying levels of details or complexity. The level of these

details or complexity is a function of how the model has been parametrized and how the model has been structured; i.e. how the interaction of different elements such as the topography, ground vegetation cover and its interaction with soil and atmosphere, composition of underlying soils, etc. are incorporated in the model (Widén-Nilsson et al., 2007). One such global hydrological model is PCRaster Global Water Balance (PCR-GLOBWB), developed by van Beek and Bierkens (2009). The present study was carried out using this model for seven river basins in south Asia, namely Indus, Ganges, Brahmaputra, Mahi, Narmada, Tapi, and the Godavari. This study area is of particular interest because the area not only experiences extreme dry and wet events but also suffers from large volumes of water withdrawals, much of which are consumed by the widespread irrigated agricultural. All of it combined, makes this area, a ground of highly intricate and large scale water-related issues and challenges. Numerous studies highlighting the intricacy of natural, social and economic water pressures in Indus, Ganges, and Brahmaputra river basins have been carried out. For e.g. (Biemans et al., 2013; Gain and Wada, 2014; Sharma et al., 2010). Yet, the efficient management of the water resources and dealing with the array of pressures that the region faces continues to be a persistent challenge. It, therefore, makes the present study essential to better understand the nature of water budget in these basins which is relevent for effective adaptation to the rising water-related pressures.

This study attempts to evaluate the coupled suitability of open-access satellite derived hydrological information and one of the leading global hydrological models, PCR-GLOBWB for assessing water resources in the river basins that lack comprehensive understanding of their water budget. The study specifically investigates the efficacy of integrating the satellite derived leaf area index, different precipitation products and an ensemble product of several evapotranspiration data-sets with the distributed hydrological model PCR-GLOBWB.

1.2 Problem description

The field of global hydrology and global hydrological modelling has progressed a lot over last few decades. However, there are large number of issues that are

yet to be dealt with and several challenges that require attention in order to expand the capabilities and application areas of the global hydrological models. Some of these challenges include improved integration of the global models with the remote sensing data sets and reducing the inherent model uncertainties that mainly arise from poor quality input data sets especially the precipitation products (Sood and Smakhtin, 2014). In addition, improvements in incorporating the anthropogenic water demand and use in the global hydrological model remains a challenge along with the issue of improving the structural processes like the model evapotranspiration and runoff generation processes (Bierkens, 2015). Resolving these issues and addressing the challenges can lead to further improvements in the representation of global hydrology.

Furthermore, contemporary large-scale hydrological models are typically being forced with gridded data sets and calibrated using a set of gauge data sets such as the observed discharge data. However, such calibrations using only the observed discharge does not ensure that other model state variables have been simulated appropriately (Sutanudjaja et al., 2014) and that the different model processes are accurately simulated across the entire model domain. Consequently, major components of the hydrological system, especially the unsaturated zone, remains uncalibrated (Wanders et al., 2014b). Several new calibration techniques aimed at improving the accuracies of the models have been developed. One of the established model calibration strategies is data assimilation. It is a mathematical technique, which is predominantly used for estimating state variables by merging observed data with model predictions. This produces an updated model state variable which is a more precise estimation of the real system state (Smith et al., 2013). The technique further helps reduce the contributions of model errors on the estimates of model parameters(Clark and Vrugt, 2006). As such, the data assimilation can be accomplished with both field measurements and remote sensing measurements. Calibration of hydrological models using data assimilation techniques has been carried out on large scale, especially in the context of soil moisture (Crow and Ryu, 2008; Wanders et al., 2014b; Jhorar et al., 2004) and snow cover (Pulliainen, 2006; Lark et al., 2006; De Lannoy et al., 2010). Much of the hydrological modelling while assimilating hydrological variable, especially in PCRaster environment has been carried out using both the field measurements and remotely sensed information (Thirel et al., 2013; Lopez Lopez et al., 2015; Wanders et al., 2014a,b).

The distributed hydrological models are highly intricate and consist of large number of parameters that represent the characteristics of the catchment. Determining the exact values of these parameters is difficult because the hydrological process occur at varying spatial and temporal scales (Bárdossy and Singh, 2008). The calibrations of such models is often done by estimating the optimum value for model parameters such that the simulations make a good fit with the observed data. The underlying assumption of these optimization procedures is that the parameters have an optimal value range for a particular model application(Beven, 1989). On the contrary, Beven and Freer (2001) argue that equally good model fit with the observed data can be achieved by using different parameter values in the same model. This issue of variety of parameter values, commonly referred to as 'equifinality' in the hydrological models introduces uncertainty in the model simulations (Beven, 2006). However, the strong advantage of utilizing remote sensing data is that it provides information of hydrologic variables in a distributed way. This data, as demonstrated by Silvestro et al. (2015), can be used to parametrise the hydrological models and set up constraints to the parameters during the calibration phase. The remote sensing information at the pixel resolution ensures pixel by pixel calibration of the hydrological model. This facilitates calibration across the entire model domain, rather than just on a particular location, usually basin outlets, which is typically the case when calibrating the model with the data assimilated from field measurements (point data). Hydrological information from remote sensing is available for several hydrological variables such as rainfall, evapotranspiration, soil moisture, snow cover and Leaf Area Index.

In addition, issues such as the need for calibration of global hydrological models at the catchment level arise especially because of poor quality forcing data-sets. For instance, a recent study comparing seven different global gridded precipitation estimates revealed that on an average there is 10% deviation in global annual means of these global gridded precipitation estimates at a river basin scale (Biemans et al., 2009). Such uncertainty can further propagate into the discharge estimates when the model is forced with these data-sets. Yet, most present-day global hydrological models are often forced using these gridded precipitation estimates. Some examples of such data-sets include Global Precipitation Climatology Centre (GPCC), Climate Research Unit (CRU) precipitation database, Global Precipitation Climatology Project (GPCP),

ERAreanalysis data, and Asian Precipitation Highly Resolved Observational Data Integration towards the Evaluation of Water Resources (APHRODITE). These estimates are a combined outcome from several sources such as the meteorological radars, rain gauge stations, and numerical prediction models and, therefore, contain some inherent uncertainty. Also, these data-sets are prepared by geostatistical interpolation of precipitation point data-sets (rain gauge stations). Such interpolation techniques have been reported to fail in representing the actual spatial variability of precipitation over the area in which gauge network is sparse (Cheema and Bastiaanssen, 2012). Besides, the aforementioned data-sets have a very coarse spatial resolution and varying temporal resolution making them more appropriate for global scale modelling but unsuitable for regional scale water management studies (Fekete et al., 2004).

The necessity of spatially accurate model inputs can be catered by the sensors aboard on various satellites. As briefly mentioned earlier, several satellite products for the different hydrological variable at various spatial and temporal resolutions and covering a wide range of spatial extent have emerged over time. Some examples of these products providing precipitation estimates include, Precipitation Estimation from Remotely Sensed Information using Artificial Neural Networks (PERSIANN) (Ashouri et al., 2015), Climate Prediction Centre morphing method (CMORPH) (Joyce et al., 2004), and Tropical Rainfall Measuring Mission (TRMM) (Yong et al., 2015). These data-sets are being widely used for the hydrological modelling at catchment to global scale. However, it has been extensively documented that the gridded precipitation products perform poorly in the intricate areas that have high relief and tend to underestimate the precipitation in those areas (Ménégoz et al., 2013; Krakauer et al., 2013; Andermann et al., 2011; Shrestha et al., 2008). A recent study attempted to address this issue by inversely estimating the precipitation from the glacier mass balance in the complex high altitude upper Indus basin. The study established that the precipitation in this area was underestimated by up to a factor of ten and that such underestimations have further implications on the planning and management of the water resources of the region (Immerzeel et al., 2015). Besides, a new addition to the remotely sensed precipitation archive has been made in the form of the Climate Hazards Group Infra-Red Precipitation with Stations (CHIRPS) data archive Funk et al. (2014). This data archive is a quasi-global product that extends from 50°S to 50°N and 180°E to 180°W and has a very fine

spatial resolution of 0.05°X0.05°i.e. approximately 5km^2 at equator. The added value of these newly emerged data-sets in understanding the water budget, when used as forcing to the global hydrological models, especially PCR-GLOBWB is yet to be explored.

Some other example of satellite derived information include moderate resolution imaging spectroradiometer (MODIS) products like MOD16 (Mu et al., 2007, 2011) that provides evapotranspiration estimates, MOD15A2 that provides vegetation phenology related information in the form of leaf area index and MOD10A1 and MYD10A1 products that give the snow cover estimates. Leaf area index (LAI), the one sided green leaf area above the give area of the ground, is a significant element determining the mass and energy exchange over the vegetated land surfaces (Running et al., 1986). The land cover specific and spatio-temporal information about the LAI is key for quantifying the physical processes such as mass and energy transfer to the ground and to the atmosphere (Gholz et al., 1976). Such LAI information can be translated into different land cover properties such as interception storage, vegetation ground cover and crop factors using the well established relationships. However, the existing vegetation parametrization of the PCR-GLOBWB model does not directly incorporate the LAI information from the remote sensing data. The LAI information used in the existing parametrization is generated using a growth function that is a function of temperature and moisture availability. This presents an excellent opportunity to investigate the model performance by replacing the default vegetation parametrization by the remote sensing information.

The goal of the present study was therefore to implement vegetation parametrization based on the satellite-based leaf area index data-set into the PCR-GLOBWB model. Further the study aims to calibrate the model using the ensemble product of remotely sensed evapotranspiration. This is of particular interest because in this way the influence of site-specific inter-annual vegetation dynamics can be directly incorporated into the model. Also, the calibration can be carried out at the pixel level thus facilitating the calibration across the entire model domain as against the contemporary way of calibrating the model at several discharge points. The study also attempts to examine the newly emerged precipitation products, namely CHIRSP and APHRODITE with corrected precipitation in the upper Indus, Ganges and Brahmaputra basins for

their effectiveness in simulating the water balance at the basin scale when used as the forcing to the model.

CHAPTER 2

LITERATURE REVIEW

2.1 Developments in Hydrological Modeling

Computer models that simulate entire or a part of the hydrological cycle are significant tools for understanding the hydrological system. These models can be categorized as physically-based or empirical, depending upon the degree of complexity of the model and how well the physical process are incorporated into the model (Beven, 1989; Refsgaard and Henriksen, 2004). The models are further classified, based on the degree of space discretization as lumped or distributed and time discretization as steady-state or dynamic (Dingman, 2015). Last five decades have witnessed an enormous development in both, the number and the intricacy of such hydrological models. In the second half of the 19th century, numerous hydrological models to simulate terrestrial processes of the hydrological cycle at catchment scale have been developed. However, around 1980's hydrologists argued that the alterations due to anthropogenic activities are already causing changes in the hydrological response at the continental scale and that the hydrological cycle being a global process needs a global scale hydrological outlook (Eagleson, 1986). Furthermore, achieving better accuracy in the global hydrological model simulations will improve the understanding of the way a certain hydrological system might respond to shifting scenarios such as changes in the water demand and management in the area, climate variability and dynamic land use and land cover.

Nowadays, several land surface models (LSMs) that simulate the land processes of the hydrological cycle exist. Some examples of these models include, bucket model (Manabe, 1969), National centers for environmental prediction/Oregon state university/Air Force/Hydrologic research Lab (Noah) model (Koren et al., 1999; Chen et al., 1996), and Variable Infiltration Capacity (VIC) model(Liang et al., 1994, 1996). Further advancements have led to the development of global climate models (GCMs) that incorporate LSMs and are devoted towards simulating land-atmosphere interactions at regional to global scale. During last few decades, several global hydrological models (GHMs) that are capable of simulating land surface processes at longer temporal

resolution and finer spatial resolution have been developed. Some examples of these models include WaterGAP (Alcamo et al., 1997), WBM (Vörösmarty et al., 1998), Mac-PDM (Arnell, 1999a) and WASMOD-M (Widén-Nilsson et al., 2007). These models were, however, largely focused on representing physical processes based on the climate variability and lacked the incorporation of the influence anthropogenic activities. Since the anthropogenic withdrawals largely influence the global water availability, the global hydrological models were further adapted to incorporate the anthropogenic influence on the global water cycle. Some examples of these include models like MATSIRO (Takata et al., 2003), H08 (Hanasaki et al., 2008), PCR-GLOBWB (Wada et al., 2014; van Beek et al., 2011; van Beek and Bierkens, 2009).

2.2 Role of Vegetation cover in Hydrological processes

Vegetation cover is a critical element of the land surface hydrology as it plays a determinant role in the soil-land-atmosphere interactions. Presence of vegetation cover can employ significant effects on runoff generation and evapotranspiration through factors such as interception (Eckhardt et al., 2003), rooting depths (Bayabil et al., 2016) and stomatal response to mention a few. Its spatiotemporal distribution and dynamics is, therefore, key to both, the evapotranspiration and runoff generation processes. Vegetation cover also influences the surface albedo (i.e. amount of insolation that is reflected back), thus driving the surface energy balance. Hence it is important to consider the influence of spatiotemporal vegetation cover dynamics on water budget. This can be achieved by including the vegetation properties such as LAI, rooting depths, etc. in the model.

Researchers, have increasingly utilised LAI information to improve the representation of spatial and temporal variation of land surfaces in the GCMs. For e.g. Sellers et al. (1996); Koster and Suarez (1992); Garratt (1993); Dickinson et al. (1993). In these models, the temporal allocation of this LAI information to the broad land cover classes was either kept constant throughout or varied seasonally. While, the information on ecosystem distribution (Olson et al., 1983) and global land cover archive (Wilson and Henderson-Sellers, 1985) formed the basis of the spatial dynamics of the land cover classes. Further algorithms were

developed for retrieving the information pertaining the vegetation dynamaics using the operational remote sensing data (Sellers et al., 1996; Los et al., 2000).

2.2.1 Leaf Area Index and Hydrological Modelling

GHMs that simulate the major hydrological components accounting for the closed water balance, in general, do take into account the effects of vegetation dynamics. But these may vary from model to model based on the properties of the vegetation which are simulated. Usually three physical characteristics of the vegetation cover namely, LAI, rooting depth and stomatal conductance form the basis of evapotranspiration parametrization in the distributed process based hydrological models. Since the late 1990's a number of researchers have investigated the relationship between the LAI and hydrological cycle. Fraedrich et al. (1999) examined the implications of vegetation extremes (i.e. globe land surfaces covered with dense vegetation v.s. globe land surfaces fully deserted) on the hydrological cycle and atmospheric simulations of a Hamburg climate model ECHAM4. In the scenario with densely vegetated globe, the experiment revealed a significant increase in the land surface evapotranspiration coupled with reduction in the surface temperatures and enhanced precipitation. Andersen et al. (2002) utilized the LAI information derived from the Advanced Very High Resolution Radiometer (AVHRR) for hydrological modelling of Senegal river basin using the modified version of the distributed model MIKE SHE. Comparison of the simulation using remote sensing LAI with the simulation using conventional vegetation properties revealed improvements in the discharge simulations using remote sensing LAI. The simulated actual evapotraspiration which comprised of the evaporation from soil and canopy and transpiration from the canopy also showed a noticeable change relative to the simulations with the default LAI values. Another experiment also using the distributed hydrological model MIKE SHE and remote sensing LAI information for simulations in semi-arid Jameson catchment in California, USA showed that the LAI information can help reduce the uncertainty in the simulated discharge (McMichael et al., 2006) . Zhang and Wegehenkel (2006) forced a simple spatially distributed model using remote sensing LAI over the Ucker catchment located in Germany and found that the seasonal variations in evapotranspiration and

runoff were closely related to those in LAI. Tesemma et al. (2015) determined the impact of inter-annual variability of LAI on the performance of Variable Infiltration Capacity (VIC) model in the GoulburnBroken catchment located in Australia. The assessment of the model efficiency showed improvements when the inter-annual variability of the LAI was incorporated in the model compared to the simulations when long term mean LAI was used instead. Also this inclusion of the inter annual variability proved useful in reducing the runoff overestimation and underestimations during dry and wet spans respectively. Parr et al. (2015), in a similar study, assessed the impacts of incorporating remote sensing LAI into VIC model for the Connecticut River basin. The study showed slight improvements in the soil moisture simulations and resulted in better representation of the inter- annual variability of river discharge, especially in the spring and winter seasons. Some other examples illustrating the role of LAI in the partitioning of the insolation and hydrological variables like leaf interception etc. include Lei et al. (2014); Gigante et al. (2009); Maltese et al. (2008); Bounoua et al. (2000)

2.2.2 Remote Sensing derived ET and Hydrological Modelling

It is evident from the previous sections that ET is a key element of surface hydrological cycle. However, obtaining ET estimates based on remotely sensed information is a relatively new field. Number of operational tools and models that resolve the surface energy balance and estimate evapotranspiration based on remote sensing information have been developed. Examples of these tools and models include Surface Energy Balance(SEBAL) (Bastiaanssen W.G.M. et al., 1998), MOD16 (Mu et al., 2009, 2011), Atmosphere Land Exchange Inverse (ALEXI) (Anderson et al., 2007; Kustas and Norman, 1997), CSIRO MODIS Reflectance Based Scaling ET (CMRSET) (Guerschman et al., 2009), Simplified Surface Energy Balance Model (SSEBop) (Senay et al., 2013), Global Land Evaporation: the Amseterdam Methodology (GLEAM) (Miralles et al., 2011), and ETMonitor (Hu and Jia, 2015) to mention a few. Yet, ET proves to one of the difficult component of the hydrological cycle to accurately measure or simulate. For instance, Kite and Droogers (2000) evaluated evapotranspiration estimates obtained from different hydrological models, in-situ observations and

satellite observations and found that the ET estimates were in varying range and that these different estimates did not exhibit any pattern. The study could not conclude whether one ET estimate evidently performing better than the other. In another study Weiß and Menzel (2008) undertook a comparative assessment of the impact of different equations for potential ET on the simulated discharge. The study found a significant impact of the equations used in simulating ET on the estimates of the discharge.

Less work has been down in terms of using the remote sensing derived ET for calibrating the distributed hydrological models. Schuurmans et al. (2003) assessed whether assimilating the latent heat flux derived from satellite observations into a physically based distributed hydrological model 'simulation of groundwater flow and surface water levels'(SIMGRO) can result into improved water balance computations. They used the NOAA-AVHRR data for the Drentse As catchment located in the Netherlands and translated it into latent heat flux using the SEBAL algorithm which was then assimilated into the model using the a constant gain kalman filter. The results showed improved simulation of latent heat flux in the high altitude areas of the basin where the flux was systematically underestimated prior to the data assimilation. Immerzeel (2008) successfully calibrated the Soil and Water Assessment Tool (SWAT) by incorporating the ET derived using SEBAL model over the Upper Bhima catchment in India. In contrast to the traditional way of calibrating the model against the discharge gauges, Immerzeel (2008) used spatially distributed ET values to constrain the fluxes thereby reducing the issue of equifinality. In a similar study Winsemius et al. (2008) used the SEBAL ET to constrain the land surface parameters of conceptual semi distributed hydrological model, that determine the rainfall-runoff behavior, for the ungauged Luangwa river basin in Zambia. This facilitated in imposing the constraints over the largest outgoing flux in the basin and resulted in a more realistic simulation of soil moisture in both space and time. Wipfler et al. (2011) evaluated the ability of land surface model HTESSEL to simulate spatial distribution of evaporation in response to patterns in the precipitation and land surface properties. The study was focused on Transdanubian region in Hungary and analysed the model simulated evaporation against the SEBAL ET estimates for the region. The study found out that the model simulated evaporation was slightly underestimated compared to the SEBAL estimates and at the pixel resolution the difference between model

simulated evaporative fraction and SEBAL evaporative fraction was as high as 30%. Also, the model displayed a low ability to simulated Evaporation in the dry areas and irrigated areas with low precipitation. Cheema et al. (2014) used the remote sensing ET derived by ETLook algorithm to calibrated the SWAT model for the Indus basin. The ETLook algorithm uses remote sensing soil moisture data and range of MODIS products to compute evaporation (E) and transpiration (T) by applying the two layered Penman-Monteith equation Bastiaanssen et al. (2012). Parameters such as depth of evaporation, holding capacity, relative root water uptake, and capillary rise front which have a substantial effect on ET were calibrated. The study reported significant improvements in the model after calibration determined by higher values of NSE (0.52 to 0.93) and Pearson correlation coefficient (0.78 to 0.93) along with reduction in the model bias from -17.3% to -0.4%. Parr et al. (2015) studied the impacts of incorporating remote sensing ET on model performance and future predictions in VIC hydrological model for Connecticut river basin. The ET product used in the study was from Fisher et al. (2008) which was estimated based on the surface radiation budget algorithm. The study, on incorporating ET, showed significant improvements in the discharge simulations at varying timescales. In a similar study by Kunnath-Poovakka et al. (2016), the CMRSET ET product was used in calibration of Australian Water Resource Assessment Landscape model (AWRA-L) model. The usefulness of this method was assessed based on the accuracy in simulating the discharge. Overall, the study concluded that calibrating hydrological model with spatially distributed information on Evapotranspiration proves to be a robust method for better discharge estimations.

CHAPTER 3

SCIENTIFIC AIM AND RESEARCH QUESTIONS

3.1 Thesis Focus

The thesis focuses on the large scale physically based spatially distributed model PCR-GLOBWB. Existing scripts and model that is at this time functional was used in this study. The scope of this study was to investigate (i) whether the spatially distributed hydrological information from the operational remote sensing data can help improve the water balance simulations in the aforementioned model and (ii) whether the fine resolution CHIRPS precipitation data and the APHRODITE data corrected for the upper Indus Ganges and Brahmaputra region provide additional value to the simulations of the water budget. The period chosen for this study includes the years from 2001 to 2007. The choice of this study period was based solely on the complete availability of all the data sets used in the present study.

3.1.1 Aim

As identified in the problem description section, it is evident that there is still a vast scope for improvements in the hydrological modelling especially in terms of vegetation parametrization using the remotely sensed LAI, exploration of the added value of new precipitation data sets and model calibration using remotely sensed ET. The present study, therefore, builds upon the previous hydrological modelling efforts but then contributes to improving previous water resource assessments, by answering several unsolved questions. The objective of the present study is to deliver improved understanding of the water budget of the complex hydrological system of the Indus, Ganges, Brahmaputra, Mahi, Narmada, Tapi and Godavari (IGBMNTG) river basins. While the upstream areas of some of these basin, namely Indus, Ganges and Brahmaputra is relatively free from anthropogenic activities and is home to large glaciers that function as a chief water source for large part of Asia, the downstream parts of these basins along with the Mahi Narmada Tapi and Godavari basins experience semi-arid climate coupled with the enormous anthropogenic water withdrawals.

Because of these anthropogenic influence on water budget, there is a spelled out need for an accurate estimation of water withdrawal information. The accurate withdrawal information can be drawn via indirect measurements such as soil moisture and evapotranspiration. This makes the present study of incorporating information on actual evapotranspiration into the model imperative for accurately understanding the water budget of the complex system. The knowledge from this study is anticipated to contribute to improved understanding of the complex hydrological system and further facilitate the decision making pertaining the water resources management of the region.

3.1.2 Research Questions

Ensuing the research objective, this study provides an improved quantitative analysis of the complex IGBMNTG basin using the global hydrological model PCR-GLOBWB. The main research questions that will be addressed in the study are enlisted below.

1. Can remote sensing based leaf area index and evapotranspiration estimates help in reliable quantification of hydrological fluxes?
2. Can incorporation of the high-altitude precipitation data corrected by (Immerzeel et al., 2015) using glacier mass balance and runoff in this hydrological modelling effort result in an improved simulation of the water budget of IGB basin?
3. Does the new fine resolution (0.05°X 0.05°) CHIRPS precipitation data archive provides added value in estimating the water budget using the global hydrological model PCR-GLOBWB?

3.2 Study Area

The present study was carried out in the Indus - Ganges - Brahmaputra - Mahi - Tapi - Narmada - Godavari (IGBMNTG) river basin. It occupies the large areas spanning between latitude 37.0°5′ 0″N to 16°32′ 60″N and longitude 66°9′

30″E and 97°46′ 30″E and spreads over seven countries namely India, Pakistan, Nepal, Afghanistan, Bangladesh, Bhutan and China. The elevation in the basin ranges between 0 to 8848m above mean sea level (a.s.m.l) (see figure 3.1. The

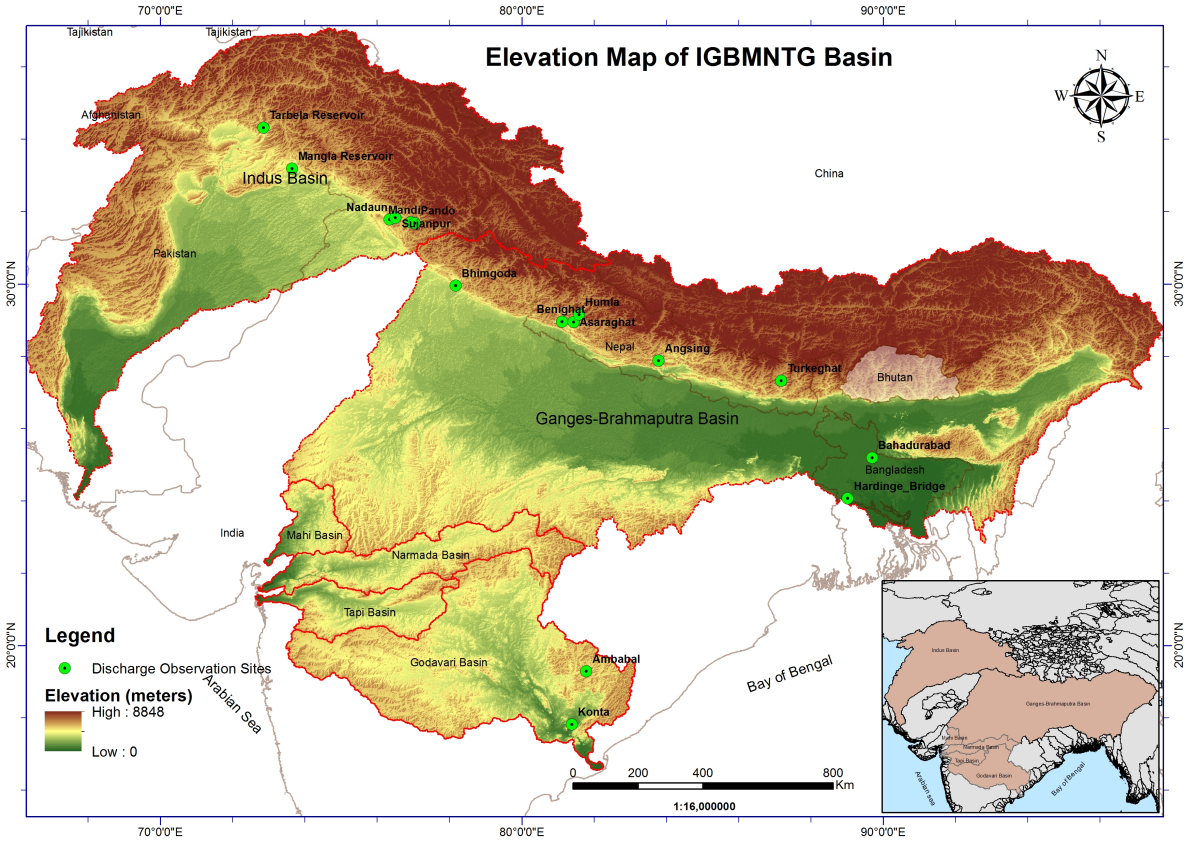

Figure 3.1: The map showing elevation in the IGBMNTG basin and the location of river discharge gauging stations used in this study (DEM Source: Cartosat-1 Satellite data).

head waters of Indus Ganges and Brahmaputra originate in the Himalayan mountain range in the north from where Indus flows south west draining into Arabian Sea while Ganges and Brahmaputra flow south east draining into the Bay of Bengal. The rivers Tapi, Mahi and Narmada originate in the Satpura and Vindhya mountain ranges and Amarkantak Plateau, all flowing westwards and draining into the Arabian sea. The river Godavari has its origin in the Brahmagiri mountain range located in the state of Maharashtra and flows south east to drain into Bay of Bengal. The total area covered by these river basins accounts to about 3.27 million km^2 of which major areas are occupied by Indus Ganges and

Brahmaputra accounting to about 20%, 31% and 33% of the total respectively, while Mahi, Narmada, Tapi and Godavari occupy about 1%, 3%, 10% and 2% of the total respectively. The basin exhibits intricate hydrological processes because of the variability in the climate as well as complex topography and land use. Figure 3.2 shows the land use and land cover map of the IGBMNTG basin. As

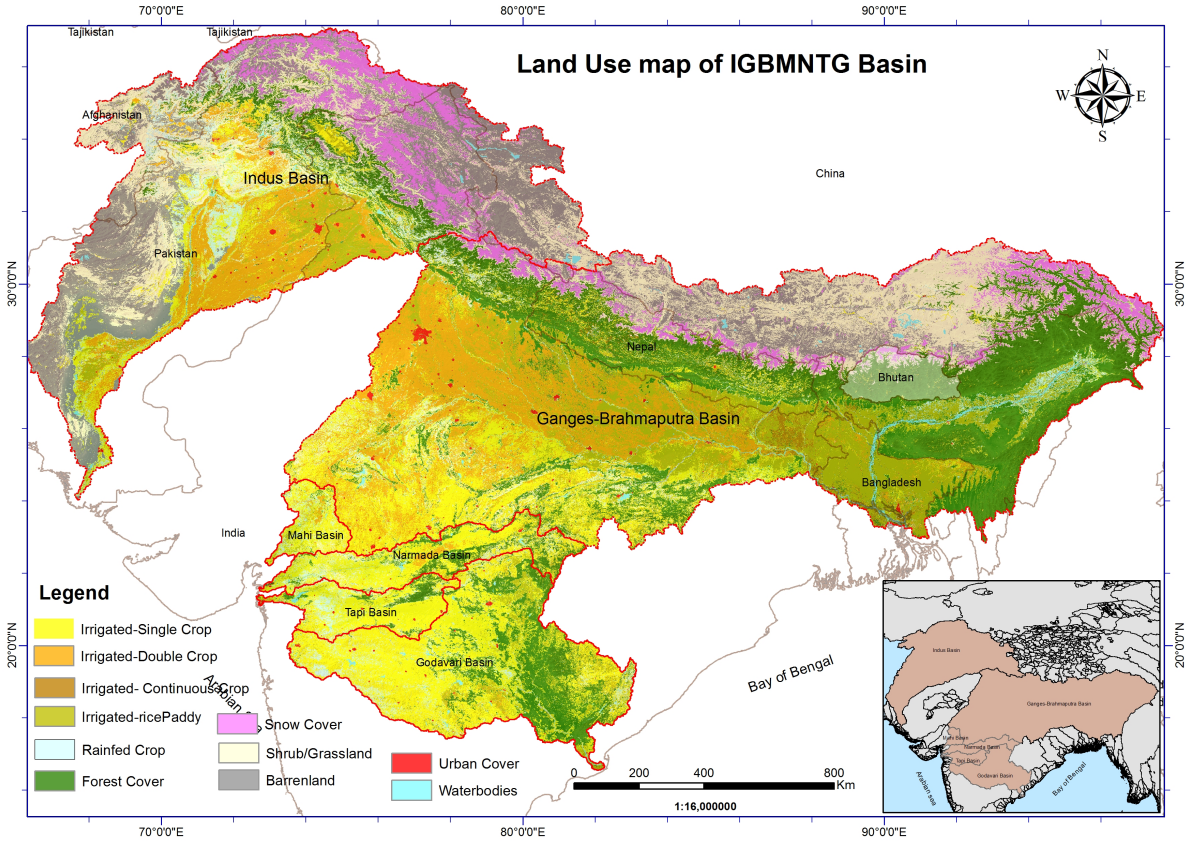

Figure 3.2: The map showing land use and land cover in the IGBMNTG basin (Data Source: IWMI,IRRI.)

can be seen in figure 3.2, agriculture is the most dominant land use in the area. Especially the region of Indo-Gangetic plains including the floodplains of the tributaries of these rivers is a large fertile area consisting of alluvial deposits.The net cropped area in this region has been estimated to be about 1.14 million Km^2 and almost 92% of the water withdrawals in this region are consumed by the agricultural sector (Sharma et al., 2008). Also, the Indus basin is home to worlds largest contiguous irrigation system (Laghari et al., 2012), commanding an irrigated area of about 0.1487 million Km^2. Overall, there are two distinct

agricultural seasons in the IGBMNTG basin, namely kharif (wet season) which approximately extends May to October and Rabi which extends from November to April (dry season). Major crops in the basin include rice, cotton, wheat,maize and sugarcane. Usually, a double cropping scheme is employed in the region during which rice is grown in kharif season while Wheat is grown in rabi.

These river basins experience a diverse climatic conditions. The temperatures in the basin can range from about -7°C in the northern mountain range to about 35°C in plains during summer and about -15°C in the northern mountain range to about 20°C in plains during Winter (see figure 3.3). The Figure on the right in 3.4 shows the spatial distribution of the seasonal mean precipitation for the years 2001 to 2007 over the study area. Clearly, the majority of the total precipitation in this region is because of the southwest monsoon winds, which again is unevenly distributed in space. The region also experiences some amounts of precipitation during the winter season which is caused by the Northeast monsoon winds and mainly occurs over the north and northeastern parts of the basin.

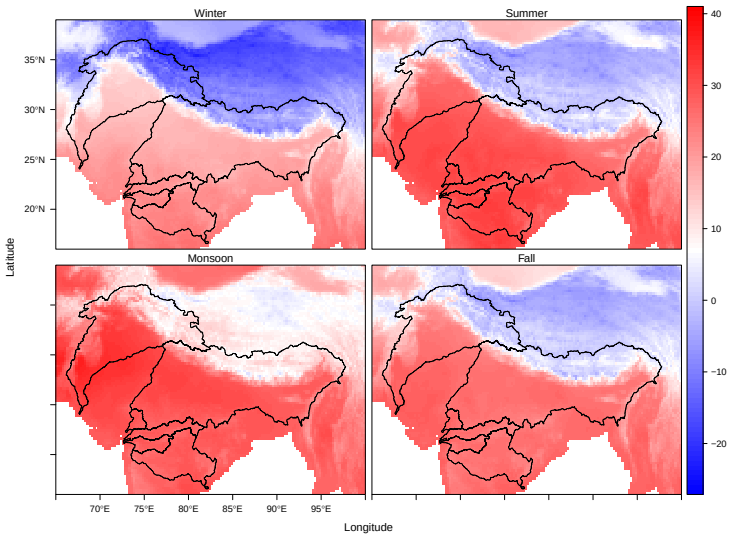

Figure 3.3: Plot showing spatial distribution of seasonal mean temperature(°C) over the IGBMNTG basin (Data Source: APHRODITE).

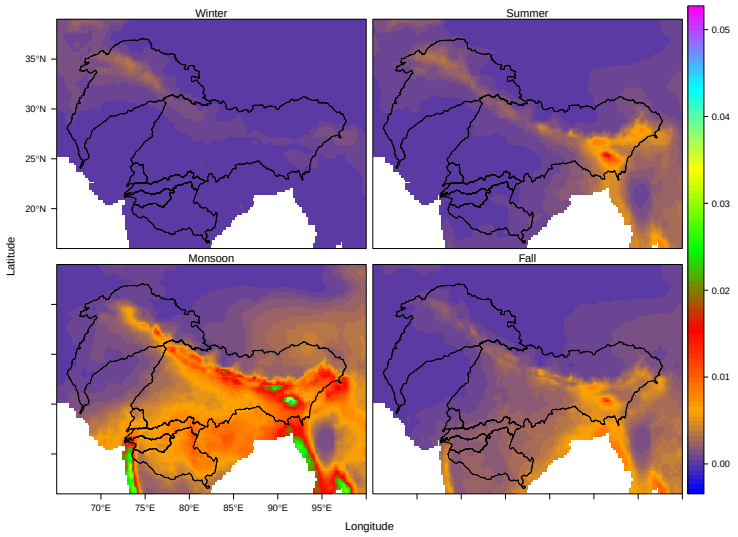

Figure 3.4: Plot showing spatial distribution of seasonal mean precipitation(m/day) (right) over the IGBMNTG basin (Data Source: APHRODITE).

CHAPTER 4

METHODOLOGY

4.1 Data Used in the Study

Data	Spatial-temporal Resolution	Description
Land Cover	0.002083°	Prepared by combining the irrigated area map of Asia prepared by IWMI (see, `http://waterdata.iwmi.org/applications/irri_area/` and Rice paddy map for south Asia prepared by citetgumma2011
Climate Research Unit (CRU) time series 3.21	0.50°,Monthly	Monthly CRU TS 3.21 for precipitation, temperature and reference evapotranspiration disaggregated into daily values using ERA-interim reanalysis dataset
APHRODITE precipitation	0.25°, Daily	Gridded daily precipitation product available at 0.25°spatial resolution
UIGB-Corrected -APHRODITE	0.25°, Daily	The APHRODITE precipitation product with corrections applied in the upper Indus-Ganges-Brahmaputra basin based upon the inverse glacier mass balance technique by Immerzeel et al. (2015).
CHIRPS 2.0	0.05°,Daily	A quasi-global precipitation product prepared by Climate Hazard group at University of California, Santa Barbara (Funk et al., 2014)
MOD15A2 LAI	0.0083333°, 8-day composites	MODIS leaf area index at approximately 1km spatial resolution available at the frequency of 8 days
ETensemble	0.0025°,Monthly	Global evapotranspiration ensemble prepared by the Water Accounting Group at UNESCO-IHE from seven different ET products at approximately 1km spatial resolution and downscaled to approximately 250m resolution based on the 250m MODIS NDVI (MOD13Q1) product

Table 4.1: List of data sets used in this study and their specifications

Table 4.1 gives provides an overview of all the datasets that were used in the

study along with their spatial and temporal resolution and other specifications. The land use and land cover map for the area was prepared by combining the two existing land cover maps namely the irrigated area map for asia prepared by International Water Management Institute (IWMI) and the rice paddy map for south Asia prepared by (Gumma, 2011). The two maps were overlayed and the irrigated agriculture areas in the irrigated area map that coincided with the rice paddy areas in the the rice paddy map were reclassified as the paddy irrigated areas. While those that did not coincide with the rice paddy class were classified as non-paddy irrigated areas. All the land cover classes apart from paddy-irrigated areas, non-paddy irrigated areas and forest were classified as grasslands.

The MOD15A2 LAI product which is available every 8 days and at a spatial resolution of approximately 0.008333°X 0.008333°was used in this study to determine the vegetation parametrization which includes ground vegetation cover, crop factor (K_c), and interception storage.

Meteorological forcing consisted of the CRU 3.21 time series of monthly precipitation, temperature and reference evapotranspiration data which is available at 0.5°X 0.5°spatial resolution. This data covers entire globe and is based upon the monthly point observations from the meteorological stations. Based on ERA-Interim reanalysis data, available at 1.5°X 1.5°resolution ,the monthly CRU time series has been disaggregated into daily values.

The meteorological forcing data sets other than the CRU time series included three different precipitation products namely APHRODITE, UIGB-Corrected-APHRODITE and CHIRPS and the ETensemble. The APHRODITE database provides gridded precipitation data over Asia and at the spatial resolution of about 0.25°X 0.25°. It has been primarily created by interpolating the daily observed point data obtained from numerous rain gauge stations across Asia. The UIGB-Corrected-APHRODITE data has the same spatial and temporal resolution as that of the APHRODITE. However the underestimations in the upper Indus Ganges and Brahmaputra basins in the APHRODITE have been corrected by Immerzeel et al. (2015) by using the inverse modelling approach. The correction grid obtained from Immerzeel et al. (2015) was used to prepare the UIGB-Corrected-APHRODITE data. CHIRPS 2.0 precipitation database provides daily quasi-global precipitation estimates

at the fine spatial resolution of approximately 0.05°X 0.05°. The data set is a combination of satellite estimates, infrared cold cloud estimates (CCD) and in-situ point measurements obtained from rain gauge stations across the globe.

The ETensemble is a product prepared by the water accounting group at UNESCO-IHE and is a combination of six different remote sensing derived ET products namely, ALEXI, CMRSET, SSEBop, MOD16, GLEAM and ETMonitor. It is a global product and is available at monthly temporal resolution and and at a finer spatial resolution of about 0.008333°X 0.008333°which has then been further downscaled to a spatial resolution of about 0.0025°X 0.0025°spatial resolution based on the MODIS NDVI (MOD13Q1) product.

4.2 Hydrological Model

Model Choice

To answer the research questions stated earlier, regionally downscaled version of global hydrological model PCR-GLOBWB was used. It is a physically based spatially distributed model scripted in PCRaster environment. The choice of this model was motivated by its ready availability as well as the accessibility. Furthermore the model is increasingly being used to simulate hydrological fluxes at the global scale. Yet, the model has been reported to exhibit limited performance in river basins in which the flow is dominated by snow melt. The simulated discharge in such basins tends to be underestimated as is mainly attributed to the under-catch of snow in the CRU forcing data set.(van Beek and Bierkens, 2009; van Beek et al., 2011). This provides an opportunity to evaluate the performance of the model in the snow melt driven catchments when forced with increasingly available global remotely sensed hydrological information.

Model Description

PCR-GLOBWB is a gridded model with a cell size of approximately 0.083333°X 0.083333°and functions at a daily temporal resolution. Each cell, as shown in figure 4.1, is bifurcated into three vertical layers called as stores. The first two

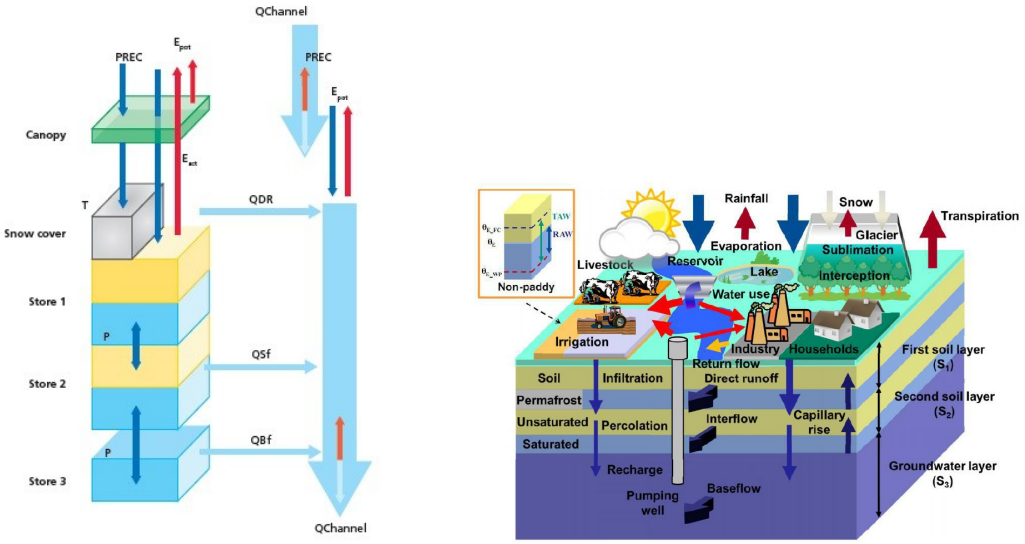

Figure 4.1: Graphical representation of hydrological processes in the PCR-GLOBWB model (on left,adopted from van Beek and Bierkens (2009)) and depiction of how anthropogenic processes have been incorporated into the model (on right, adopted from Wada et al. (2013))

stores represent soil with maximum depth of 0.3m and 1.2m respectively while the third store represents the groundwater. For each grid cell at a particular time step, the model simulates the water exchange between the three stores, and between the top store and the atmosphere. The top store is subjected to precipitation either in the form of snow, which then is stored on the surface until it turns into snow melt, or as rain which depending upon the soil saturation state end infiltrates or flows out as runoff. Also the water in the top store can evaporate. The model also takes into account the canopy interception and snow storage along with the sub-grid variability which is accounted by incorporation of different land cover (separated into tall and short vegetation and open water bodies) and soil types in the model (van Beek and Bierkens, 2009). Upward movement of water can also take place between the stores with the capillary rise. These upward and downward movements of water are a function of atmospheric conditions, the relative difference in soil saturation of stores and type of soil. The amount of precipitation on the cell that is not lost to evaporation or runoff can then either end up as in soil stores and groundwater store of the cell. This excess water can flow to the neighbouring cell, from groundwater store as baseflow

(QBf) and from second store as interflow (QSf). These sub-surface flows are governed by the local drainage directions that are defined by the topography of the area. The surface water flows too follows the local drainage directions and eventually exits the catchment, unless subjected to loss due to evaporation, re-infiltration or storage during the transport, as discharge. More detailed and thorough information about the model and its parametrization can be found in van Beek and Bierkens (2009). Parametrization only relevant to the present study are further described in detail in the following section.

4.2.1 Vegetation Parameterization

Green water requirement or the soil moisture required by the vegetation including the cropped land is replenished by infiltration and capillary rise processes. Calculation of irrigation water demand is also dependent on the amount of soil moisture present and it is calculated as the difference between the potential transpiration and the actual transpiration under the non-irrigated circumstances. This crop specific transpiration in the model is calculated as suggested in the food and agriculture organization of united nations (FAO) guidelines (Allen, 1998). Similarly the estimation of evapotranspiration in the model is based upon the standard method described in the FAO guidelines (Allen, 1998). The method makes use of crop factor [K_c] defined for individual vegetation cover types to translate the reference evapotranspiration [ET_o, ($m.day^{-1}$)] occurring due to the meteorological conditions over a well watered reference grass surface having a specified height of 0.12 m, an albedo of 0.23 and a surface resistance of 70 sm^{-1}, into the crop specific potential evapotranspiration [ET_c, ($m.day^{-1}$)] (see equation 4.1). The reference evapotranspiration imposed in the simulations is calculated using the variables in the CRU TS 2.1 data set. The crop factors represent the average effect of the individual crop conditions on the potential crop transpiration and bare soil evaporation. This crop factor method was originally developed for the real crop, however it can be expanded to the natural vegetation cover (Allen, 1998).

$$ET_c = K_c * ET_o \tag{4.1}$$

The seasonal dynamics of the vegetation phenology in the model is incorporated by developing a LAI climatology for different vegetation types. The vegetated surfaces in the model are defined by diving the land cover map obtained from the Global Land Cover Characteristics (GLCC) Data Base Version 2.0 (available at: `https://lta.cr.usgs.gov/glcc/globdoc2_0`), the global ecosystem classification system by Olson (1994a,b) into three categories namely, rain-fed crops, irrigated crops and natural vegetation. In order to calculate the LAI climatology, a growth factor (f_m), which is a function of monthly temperature (T_m) was used (see 4.2).

$$f_{\mathrm{m}} = 1 - [T_{\mathrm{max}} - T_{\mathrm{m}}/T_{\mathrm{max}} - T_{\mathrm{min}}]^2 \tag{4.2}$$

where T_{max} and T_{min} are the assumed maximum and minimum temperatures respectively for the growing and dormancy season. This temperature driven growth function is then used to model the LAI values using relationship shown in 4.3.

$$LAI = LAI_{\mathrm{min}} + f_{\mathrm{m}} * (LAI_{\mathrm{max}} - LAI_{\mathrm{min}}) \tag{4.3}$$

The LAI_{min} and LAI_{max} values in the equation 4.3, for all land cover types at the dormancy and peak growing stage, was based on the improved land surface parameter table by Hagemann (2002) that provides precise distinction between different vegetation types in varied climatic zones. This relationship determined the length of the growing season based on the temperature and the soil moisture availability criteria (van Beek and Bierkens, 2009). The LAI climatology values so obtained are then translated into the crop factors based on the equation 4.4 given by Allen (1998)

$$K_{\mathrm{c}} = K_{\mathrm{cmin}} + (K_{\mathrm{cfull}} - K_{\mathrm{cmin}}) * (1 - exp(-0.7 * LAI)) \tag{4.4}$$

Where K_{cmin} is the minimum value of crop factor for the bare soil and is set to 0.20. K_{cfull} is the crop factor under the vegetation full cover conditions. It is calculated by using the equation 4.5 under sub-humid and calm wind conditions (viz. minimum daily relative humidity of 45% and wind speed of 2 $m.s^{-1}$ at 2 m elevation).

$$K_{\text{cfull}} = 1.0 + 0.1h \tag{4.5}$$

where h represents the height of the vegetation in meters and is derived from Hagemann (2002). The value of K_{cfull} is limited to 1.2 in case of h >2m. If the climatic and wind speed conditions mentioned for 4.5 are not met, the value of K_{cfull} is determined by using equation 4.6

$$K_{\text{cfull}} = K_{\text{cfull}} + (0.04(u_2 - 2) - 0.004(RH_{\min} - 45)) * (h/3)^{0.3}) \tag{4.6}$$

where u_2 is wind speed ($m.s^{-1}$) at 2m elevation and RH_{min} is the minimum daily relative humidity (%).

Similarly, the values for vegetation ground cover (G_c) (m^2/m^2) and Interception storage (I_s) (m) are calculated based on LAI using the equations 4.7 and 4.8 respectively.

$$G_c = 1 - exp(-\alpha * LAI) \tag{4.7}$$

where the α is the extinction factor assumed to be 0.4.

$$I_s = \gamma * LAI \tag{4.8}$$

where γ is unit interception depth assumed to be 2 X 10^{-4}m.

The bare soil potential evaporation (ES_o, $m.day^{-1}$) and the potential transpiration (T_c, $m.day^{-1}$) are calculated by using the relationship 4.9 and 4.10 respectively.

$$ES_o = K_{c,\min} * ET_o \tag{4.9}$$

$$T_c = ET_c - ES_o = (K_c * ET_o) - (K_{c,\min} * ET_o) = ET_o * (K_c - K_{c,\min}) \tag{4.10}$$

where T_c is the crop specific monthly potential transpiration in $m.day^{-1}$ and $K_{c,min}$, K_c are the minimum crop factor and monthly crop factor for bare soil

evaporation respectively. The reductions in the ET_c and T_c are based on the soil moisture availability (see 4.11). The ET_c is drawn from the top soil layer and for the saturated fraction (x), no reduction is applicable. Only condition is that the rate of potential evaporation cannot exceed the saturated hydraulic conductivity of the top soil layer. In case of unsaturated fraction (1-x), the rate is based on the unsaturated hydraulic conductivity of the top soil layer:

$$ET_{\mathrm{a}} = x * min(K_{\mathrm{s}}, ET_{\mathrm{c}} + (1 - x) * min(K_{\mathrm{s1}}, ET_{\mathrm{c}})) \tag{4.11}$$

where s1 is the effective degree of saturation. Transpiration takes place only from the unsaturated fraction since in the saturated fraction the uptake of water by the plants is restricted owing to lack of aeration. Over the unsaturated fraction, the actual transpiration is a function of total available soil moisture in the soil layer. The reduction of potential transpiration to actual transpiration is done as

$$T_{\mathrm{a}} = (1 - x) * f_{\mathrm{t}} * T_{\mathrm{c}} \tag{4.12}$$

where f_t is the ratio of actual transpiration to potential transpiration and is given by 4.13

$$f_{\mathrm{t}} = 1/1 + (S_{\mathrm{E}}/S_{\mathrm{E50}})^{-3\beta} \tag{4.13}$$

where S_{E50} is the average degree of saturation at which potential transpiration is halved. Its value is usually taken to be equivalent to the degree of saturation in reference to a matric potential of 33.3 KPa. β is the coefficient of the soil water retention curve. The average degree of saturation is calculated based on the properties of two soil layers weighted by the capacity of soil to store moisture and root fractions. Based on the improved Arno scheme, the average degree of saturation over the unsaturated fraction of the cell is calculate as (van Beek and Bierkens, 2009)

$$S_E = \frac{W_{max} + b(W_{max} - W_{min}) * \left[1 - \frac{b+1}{b} * \left(\frac{W_{max} - W}{W_{max} - W_{min}}\right)^{\frac{1}{b+1}}\right]}{W_{max} + b(W_{max} - W_{min}) * \left[1 - \left(\frac{W_{max} - W}{W_{max} - W_{min}}\right)^{\frac{1}{b+1}}\right]} \tag{4.14}$$

where W_{max}, W_{min} and W is the minimum moisture storage capacity, maximum moisture storage capacity and total soil moisture averaged over the cell layer respectively and b is the shape factor that describes the distribution of local soil moisture storage capacity.

4.2.2 Computation of Quick and Slow Runoff

Quick Runoff

The water can reach the first soil store from non intercepted liquid precipitation and as a result of snow melt. The melt water, upto the maximum storage capacity, can be stored into snow pack where it can either refreeze or is subjected to evaporation. The melt water exceeding the maximum storage capacity adds up to the non intercepted liquid precipitation. Conversion of this net amount (P_n) into surface runoff depends upon the fraction of saturated soil and is given by equation 4.15

$$x = \left[1 - \left(\frac{W_{max} - W}{W_{max} - W_{min}}\right)^{\frac{b}{b+1}}\right] \tag{4.15}$$

Where, W, W_{max} and W_{min} are the cell average, maximum cell average and minimum cell average water storage in the top soil store respectively. The distribution of the soil water storage is defined by a dimensionless shape factor,b, which is calculated based on the rooting depths obtained from GLCC Data Base Version 2.0. Based on this parameterization following relationships hold. Quick runoff (Q_s) can occur only when sum of cell averaged moisture storage and the the net amount (P_n exceeds the minimum cell average water storage (W_{min}) in the top soil store (see equation 4.16).

If,

$$P_n < W - W_{min}; \tag{4.16}$$

$$Q_s = 0 \tag{4.17}$$

Equation 4.19 calculates the fast runoff when $W_{min} < P_n + W < W_{max}$. Expressed in terms of cell average water storage capacity this relates to the following.

If,

$$W - W_{min} \leq P_n < (b+1)(W_{max} - Wmin)\left(\frac{W_{max} - W}{W_{max} - W_{min}}\right)^{\frac{1}{b+1}} : \tag{4.18}$$

$$Q_s = P_n - (W_{max} - W) + (W_{max} - W_{min})\left[\left(\frac{W_{max} - W}{W_{max} - W_{min}}\right)^{\frac{1}{b+1}} - \frac{P_n}{(W_{max} - W_{min})(b+1)}\right]^{b+1} \tag{4.19}$$

Equation 4.21 calculates quick runoff when $P_n + W \geq W_{max}$.

If,

$$P_n \geq (b+1)(W_{max} - W_{min})(W_{max} - Wmin)\left(\frac{W_{max} - W}{W_{max} - W_{min}}\right)^{\frac{1}{b+1}} : \tag{4.20}$$

$$Q_s = P_n - (W_{max} - W_{min}) \tag{4.21}$$

In this case, the infiltration (P_{0i} is the difference between the net liquid rainfall (P_{ni}) and the quick runoff (Q_{si}). The infiltration excess adds up to the quick runoff when the infiltration rate exceeds the saturated hydraulic conductivity. In the case when total infiltration exceeds the storage capacity of the top soil layer, the infiltration excess passed on to the second soil layer.

Slow Runoff

Interflow

The computation of lateral flow in the model is based on the simplified approach (see equation 4.22) suggested by (Sloan and Moore, 1984) which

assumes soil as a uniform, sloping slab having an average inclination and depth. Interflow is computed when the soil water content of the second soil store exceeds its field capacity.

$$Q_i(t) = \left[1 - \frac{\Delta T}{TCL}\right] Q_i(t - \Delta T) + \frac{\Delta T}{TCL} L\,(q_{12}(t) - q_{23}(t)) \tag{4.22}$$

Where, Q_i is interflow per m slope width, $[L^2T^{-1}]$, L is the average slope length or drainage distance [L], q_{12} & q_{23} are fluxes from/to first soil store and groundwater store and ΔT is the time step. The parameter TCL represents the response time and is given by

$$TCL = \frac{L(\theta_s - \theta_{fc})}{2k_{s,2} tan\beta} \tag{4.23}$$

where, θ_s and θ_{fc} represent soil moisture content at saturation and field capacity respectively, $k_{s,2}$ is the saturated hydraulic conduictivity of second soil store and β is the average slope of the soil profile.

BaseFlow

The recharge of the third store (groundwater reservoir) consists of the difference between the amount of water percolating from the second store to the third store and the capillary rise from the third store to the second store. Discharge from this groundwater reservoir adds up to the total discharge as base flow. In the model this discharge is modeled by a linear reservoir approach (see equation 4.24).

$$Q_3 = \alpha S_3 \Delta t \tag{4.24}$$

Where, α is the recession coefficient in day^{-1} and S_3 is the storage in the third layer in m.

4.2.3 Computation of irrigation water demand

For estimating the net and gross irrigation water demand, PCR-GLOBWB uses the MIRCA data set that provides monthly growing area data on 26 irrigated crops representing the cropping situation in the year 2000(Portmann et al., 2008). This includes the global crop calenders and cropping pattern at the spatial resolution of 0.0833333°. The net crop water demand ($D_{c,net}$) in m.day^{-1}, which is the amount of water needed by the crops for ensuring full growth, is calculated using the equation 4.25

$$D_{c,net} = ET_c = k_c ET_o = T_c - ES_o \tag{4.25}$$

The net irrigation water demand ($D_{irri,net}$) is the amount of water that needs to be additionally supplied to the crops by irrigation for ensuring maximum evapotranspiration. This is because if the precipitation does not satisfy the crop water demand the evapotranspiration can no longer take place at the potential rate. $D_{irri,net}$ does not account for the losses such as evaporation and percolation that may occur during transport and application. Estimation of the net irrigation water demand is done using equation 4.26

$$D_{irri,net} = (T_c - T_a) + (ES_o - ES_a) \tag{4.26}$$

where, ES_a is the actual bare soil evaporation (m.day$_{-1}$).

Gross irrigation water demand ($D_{irri,gross}$) which also accounts for the aforementioned losses is calculates using equation 4.27.

$$D_{irri,gross} = e_{irri} * D_{irri,net} \tag{4.27}$$

where, e_{irri} is a dimensionless country specific irrigation efficiency factor which are taken from Rohwer et al. (2007).

4.3 Experimental Setup

To answer the research questions mentioned in the section 3.1.2 the research was divided into six experiment. Table 4.2 gives the overview of each experiment and the changes made in the each experiment. Experiment 1, hereafter referred

Exp.No.	Name	Data Used
1	P-Def	CRU TS 3.21 meteorological forcing and default vegetation parameterization
2	P-RSLAI	CRU TS 3.21 meteorological forcing and vegetation parameterization based on remote sensing LAI
3	P-RSLAI-APHRO	Same as P-RSLAI, except for the precipitation forcing using APHRODITE data
4	P-RSLAI-Cor-APHRO	Same as P-RSLAI, except for the precipitation forcing using corrected APHRODITE data
5	P-RSLAI-CHIRPS	Same as P-RSLAI, except for the precipitation forcing using CHIRPS data
6	P-RSLAI-ET	Vegetation parameterization based on remote sensing LAI, Potential Evapotranspiration based on the ETensemble product and precipitation forcing based on the best performing precipitaion product from previous five experimetns

Table 4.2: Overview of the experimental setup and data used in each experiment

to as P-Def, consists of the PCR-GLOBWB simulation with the default vegetation parametrization and the meteorological forcing using CRU 3.21 time series. The detailed formulation of the default vegetation parametrization is as discussed in section 4.2.1. In the experiment 2, hereafter referred to as P-RSLAI, the default vegetation parametrization are replaced and are derived from remote sensing based on the MOD15A2 LAI data. The details of the changes in the parametrization are discussed in section 4.3.1. The experiment number 3,4 and 5 are similar to that of P-RSLAI except for the different precipitation data

as mentioned in 4.2 are used for evaluation of their performance in model simulations. In the Experiment 6, hereafter referred to as P-RSLAI-ET, the vegetation parameterization is again based on the MOD15A2 LAI product. The precipitation product that performed relatively better in previous experiments was chosen as a forcing in this experiment. The major change in this experiment compared to the precious ones is that the ETensemble data was directly introduced into the model as an estimate of potential ET. The details are further discussed in the section 4.3.2.

4.3.1 P-RSLAI

The crop factors calculated in P-Def model using the climatology serve as the vegetation response for the average year and the monthly values of these crop factors are repeated in multi-year model simulations. In this experiment, instead of using the LAI values generated based on the temperature driven growth function, the LAI values derived from remote sensing data set were used for calculating the crop factors, interception storage and ground cover. This is because it is anticipated that the LAI values derived from remote sensing can provide more accurate representation of the spatial as well as temporal response of the vegetated land surfaces. For this purpose the MOD15A2 LAI dataset which is available every 8 days was was downloaded for the study years (2001-2007) and processed so as to use it as an input for calculation of the vegetation parameters. Prior to the processing, the downloaded tiles were checked if the imagery was affected by cloud cover using the quality assurance metadata and omitted from the further processing if it resulted in unreliable estimates. These LAI values were plugged directly into the equations 4.4, 4.7 and 4.8 to calculate the vegetation parameters at the frequency of eight days. These remote sensing derived crop factors can provide better represent inter-annual variability and therefore take into account the factors like temporary crop stress and variations in the timing of the seasons.

4.3.2 P-RSLAI-ET

For this experiment, the ET from remote sensing (ETensemble product) was directly used to force the model by inputting it as a potential ET ($ET_{c,ensemble}$). As briefly mentioned in 4.1, the ETensemble product was available at monthly time steps and at the spatial resolution of 0.0025°. Since the model runs on a daily temporal resolution, primary step was to disaggregate the ETensemble monthly data into daily ETensemble values. This disaggregation was done by calculating the daily weights using the CRU reference ET data. These weights were generated as the factor of amount of total evapotranspiration in a day of the month to the total evapotranspiration in that month. The weights so generated were then used to disaggregate the ETensemble values to a daily temporal resolution by simple multiplicative relationship. This disaggregated daily evapotranspiration is then incorporated into the model as potential ET and is subjected to reduction based on 4.11. The partitioning of the bare soil potential evaporation ($ES_{o,new}$) and monthly potential transpiration ($T_{c,new}$) is revised as shown in equations 4.28 and 4.29

$$ES_{o,new} = min(ET_{c,ensemble}, ES_o) \tag{4.28}$$

$$T_{c,new} = ET_{c,ensemble} - ES_{o,new} \tag{4.29}$$

It must be note here that since the ensemble ET is directly used as potential ET, underestimations in the model simulated ET are implicit when enough water is unavailable to meet the ET requirements. However, as briefly mentioned in the section 3.1.1, the information on water withdrawals can be obtained indirectly from soil moisture and evapotranspiration measurements. The soil moisture data sets have a very coarse spatial resolution (approximately 12.5 Km) as against the 250m ETensemble data. Also, such remote sensing based evapotranspiration data set reflect upon the climate, land use, irrigation, and myriad anthropogenic influences in a spatially distributed manner. Provided that enough water is available to meet the ET requirements, significant enrichment can be achieved in the estimation of water withdrawals in a spatially distributed way by using 250 m ETensemble data.

4.4 Model Validation

To assess the model performance and to reduce the errors, it is imperative to evaluate the input data and validate the model outputs against the in-situ observations. In this study, the simulated evapotranspiration was compared against the ETensemble product. Further the simulated river discharge was validated at 16 high quality discharge gauging locations (see table 4.3 & figure 3.1) located across the entire study area. All the stations, except Bahadurabad, Hardinge Bridge, Konta and Amababal, are located in the upstream areas of the river basin and the flows at these locations are least affected by anthropogenic activities. Thus evaluation of the model simulations against the values from these gauging locations ensures verification of catchment scale hydrological processes. These observed data set were obtained from the Water and Power Development Authority (WAPDA) of Pakistan, International Water Management Institute (IWMI), and Bhakra Beas Management Board (BBMB) and were either daily or monthly observations. The fit between the simulated and observed discharge was assessed using the Nash-Sutcliffe efficiency (NSE) method (Nash and Sutcliffe, 1970), Pearsons coefficient of determination (R^2), and the Bias. The NSE, R^2,and Bias were calculated using equations 4.30, 4.31, and 4.32 respectively.

Sr.No.	Station/Place Name	River Basin	LAT (dd)	LON (dd)	Observation Interval	Source
1	**Tarbela Reservoir**	Indus	34.3286	72.8560	Daily	WAPDA
2	**Mangla Reservoir**	Indus	33.2000	73.6500	Daily	WAPDA
3	**Bahadurabad**	Brahmaputra	25.2000	89.7000	Daily	Walter
4	**Hardinge_Bridge**	Ganges	24.0698	89.0295	Daily	IWMI
5	**Asaraghat**	Ganges	28.9530	81.4447	Monthly	IWMI
6	**Benighat**	Ganges	28.9611	81.1194	Monthly	IWMI
7	**Humla**	Ganges	29.1589	81.5911	Monthly	IWMI
8	**Turkeghat**	Ganges	27.3320	87.1882	Monthly	IWMI
9	**Angsing**	Ganges	27.8834	83.7939	Monthly	IWMI
10	**Bhimgoda**	Ganges	29.9574	78.1809	Monthly	IWMI
11	**Ambabal**	Godavari	19.2900	81.7900	Daily	IWMI
12	**Konta**	Godavari	17.8200	81.3900	Daily	IWMI
13	**Mandi**	Indus	31.7131	76.9333	Daily	BBMB
14	**Nadaun**	Indus	31.7892	76.3472	Daily	BBMB
15	**Pando**	Indus	31.6869	77.0456	Daily	BBMB
16	**Sujanpur**	Indus	31.8383	76.5111	Daily	BBMB

Table 4.3: River discharge gauge locations at which the model performance was evaluated

$$NSE = 1 - \left[\frac{\sum_{i=1}^{n} (Q_i^{obs} - Q_i^{sim})^2}{\sum_{i=1}^{n} (Q_i^{obs} - \overline{Q_i^{obs}})^2} \right] \tag{4.30}$$

where, Q^{obs}, Q^{sim} and $\overline{Q^{sim}}$ represent the observed, simulated and mean simulated discharge respectively and n is the total number of observations. The NSE range lies between ∞ to 1 and the NSE value of 0 suggests that the accuracy of the simulated discharge is as close as the observed discharge. In essence, the close the NSE value the better the model performance. The negative values of NSE on the other hand indicates that the observed discharge is the better predictor than the simulated outcomes.

$$R^2 = \left[\frac{\sum_{i=1}^{n} (Q_i^{obs} - \overline{Q_i^{obs}})(Q_i^{sim} - \overline{Q_i^{sim}})}{\sqrt{\sum_{i=1}^{n} (Q_i^{obs} - \overline{Q_i^{obs}})^2} \sqrt{\sum_{i=1}^{n} (Q_i^{sim} - \overline{Q_i^{sim}})^2}} \right]^2 \tag{4.31}$$

The value of R^2, indicator of how closely the simulated discharge fits against the observed discharge, ranges between 0 and 1. Closer the value of R^2 to 1, the better the fit between the simulated and observed data.

$$Bias = \frac{\sum_{i=1}^{n} (Q_i^{obs} - Q_i^{sim})}{\sum_{i=1}^{n} (Q_i^{obs})} \tag{4.32}$$

Bias which indicates the mean deviation of the simulated discharge compared to the observed discharge. The positive values of Bias indicate that the model simulations are underestimated compared to the observed values whereas the negative value of Bias indicate otherwise.

CHAPTER 5

RESULTS

5.1 Model Performance

Owing to the data availability, the primary method for evaluating the improvements in the model simulations was by comparing the various simulated discharges with the in-situ observation data set. The river discharge was simulated using the default model (P-Def) as well as different data - enhanced versions (P-RSLAI, P-RSLAI-APHRO, P-RSLAI-cor-APHRO P-RSLAI-CHIRPS and P-RSLAI-ET-cor-APHRO). Due to the nature of model forcing changes made in the aforesaid model versions, the impact on the model performance is expected to manifest at different temporal scales. Incorporation of MODIS LAI into the model was specifically done so as to incorporate the site specific spatio-temporal vegetation dynamics into the model. The analyses was therefore conducted at two temporal scales, daily and monthly.

5.1.1 Incorporation of RS LAI

Compared to the P-Def simulations, the daily and monthly cycle of discharge showed a significant improvement at most discharge stations. Although the underestimation of the peak flows persisted, the daily and monthly NSE values at these gauging stations showed improvements along with a significant reduction in the model bias (see Appendix F, E). Also the daily and monthly low flows in the P-RSLAI run are comparatively better simulated at most gauging stations. Figure 5.1 and Figure 5.2 depict the observed vs. simulated daily and monthly discharge at the river discharge gauging stations respectively. It clearly displays that the dominant improvements occur in both daily and monthly discharge simulations especially in the drier seasons. This is because the greatest changes in the simulate ET between the P-Def and P-RSLAI model occurs during these months (see figure 5.3). Figure 5.3 displays the seasonal mean ET simulated by the P-DEF and P-RSLAI models, the ETensemble and the difference between the ETensemble and the simulated ET. From the difference maps it is clear that during the Winter (DJF) and Summer(MAM) months the P-RSLAI ET is

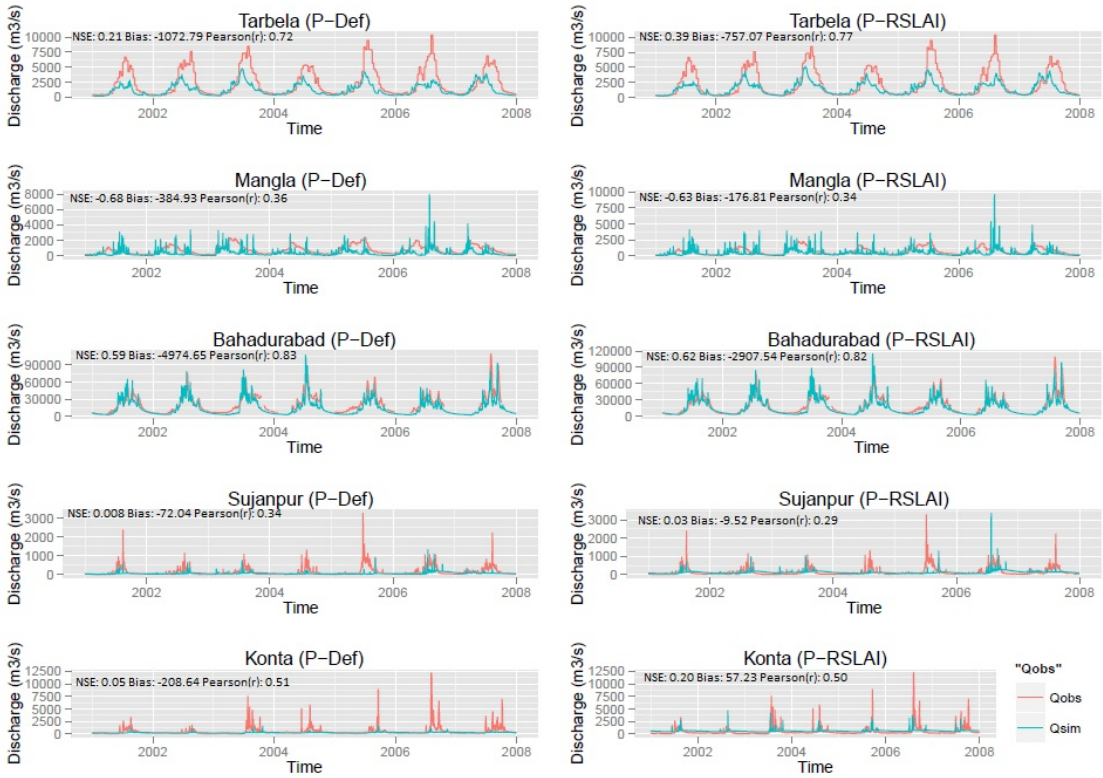

Figure 5.1: Daily observed and simulated discharge (m^3/s) at Tarbela, Mangla, Bahadurabad, Sujanpur & Konta gauging stations (Exp. 1 & 2)

in better agreement with the ETensemble values especially in some parts of Indo-Gangetic plains and parts of Godavari basin. Figure 5.4, that displays the spatial correlation between the simulated ET and the ETensemble over the entire simulation period, shows improved correlation in the aforesaid regions of the basin further strengthening the argument. It can be seen that the ET simulated by the P-RSLAI experiment has a strong linear relationship with the ETensemble values in most parts of the Indo-Gangetic plains as well as the Narmada, Mahi, Tapi, and Godavari basins.

To assess the simulated ET more closely the monthly basin average values were compared to the ETensemble values. In order to avoid the effect of extreme conditions, such as the dry Indus basin or the wet Brahmaputra basin, on the entire IGBMNTG basin averages and its further translation into the analyses, the comparison was split into three basins (Indus (I), Ganges-Brahmaputra (GB),

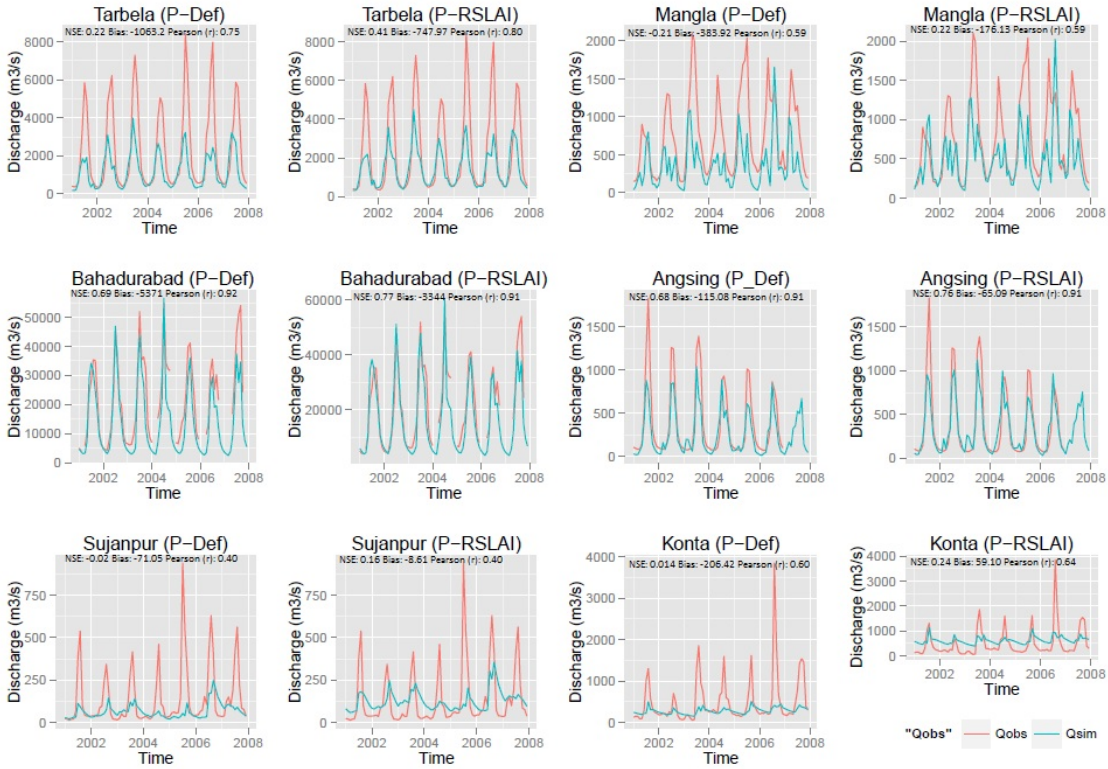

Figure 5.2: Monthly observed and simulated discharge (m^3/s) at Tarbela, Mangla, Bahadurabad, Sujanpur & Konta gauging stations (Exp. 1 & 2)

Mahi-Narmada-Tapi-Godavari(MNTG). The regression analysis (see figure 5.5) between the simulated ET and the ETensemble for both the experiments showed relatively high values, indicating that the seasonal timing of the simulations are fairly well represented in both the experiments. The slope of the regression line, however, was smaller in the P-RSLAI experiment compared to the P-Def. This, as can be seen from the figure 5.5, could be because there is a better association between lower values of ET simulated by P-RSLAI run and the ETensemble product but the higher values seem to be underestimated. The correlation and RMSE-observed standard deviation ratio (RSR) for the weighted monthly average ET for each basin can be found in table 5.1. Although the correlation values have not changed much the RSR values have almost doubled. This could be explained by the underestimations of the higher ET values.

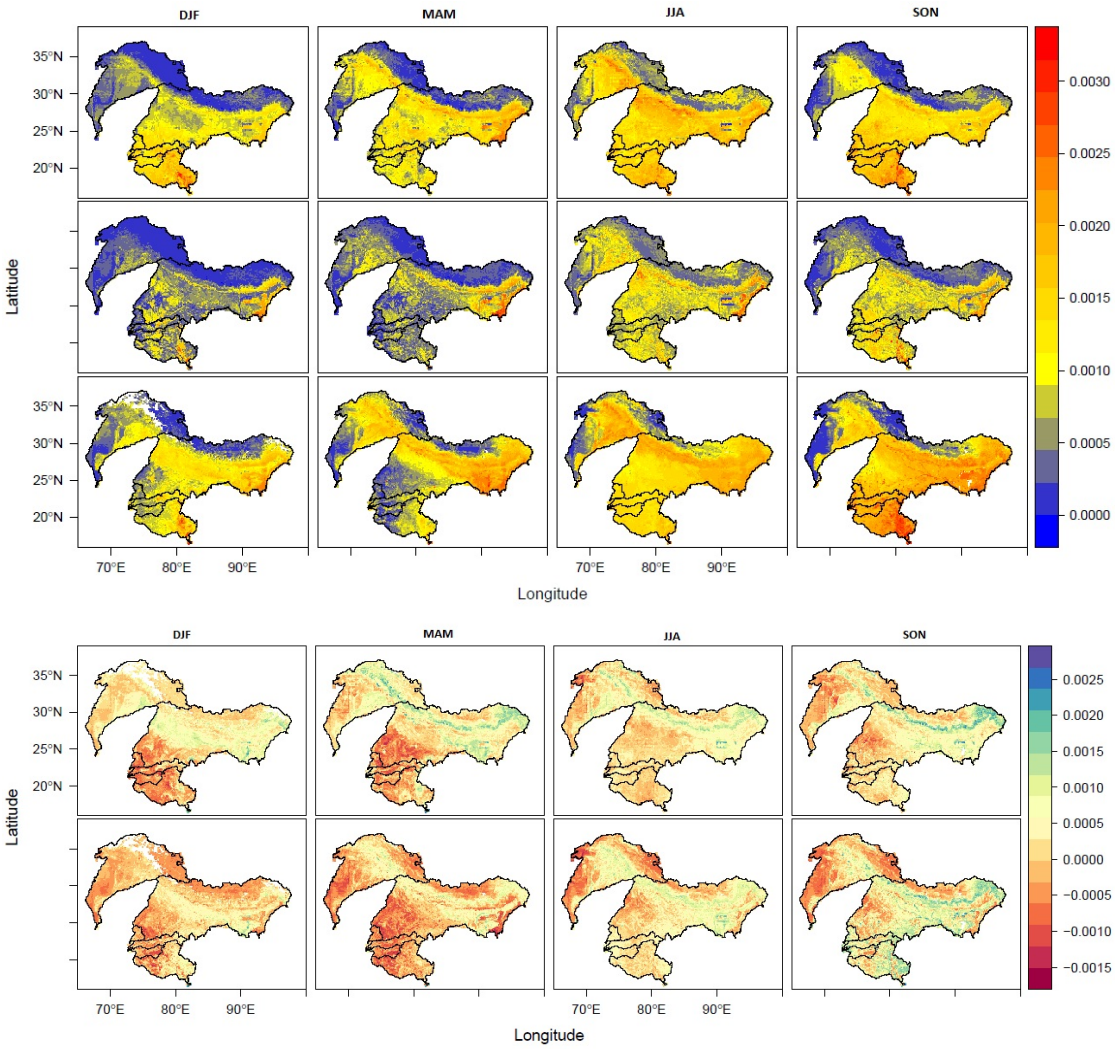

Figure 5.3: Seasonal mean ET (m.day^{-1}): P-Def (1st row), P-RSLAI (2nd row), ETensemble (3rd row), ETensemble-P-Def (4th row) and ETensemble-P-RSLAI (5th row)

.

Exp.No.	Correlation			RSR		
	I	GB	MNTG	I	GB	MNTG
1	0.96	0.91	0.84	0.44	0.63	0.60
2	0.94	0.88	0.86	0.93	1.27	1.11

Table 5.1: Comparison of weighted monthly average (m.day^{-1}) simulated ET and ETensemble for each basin in terms of the correlation and RSR (Exp 1 & 2)

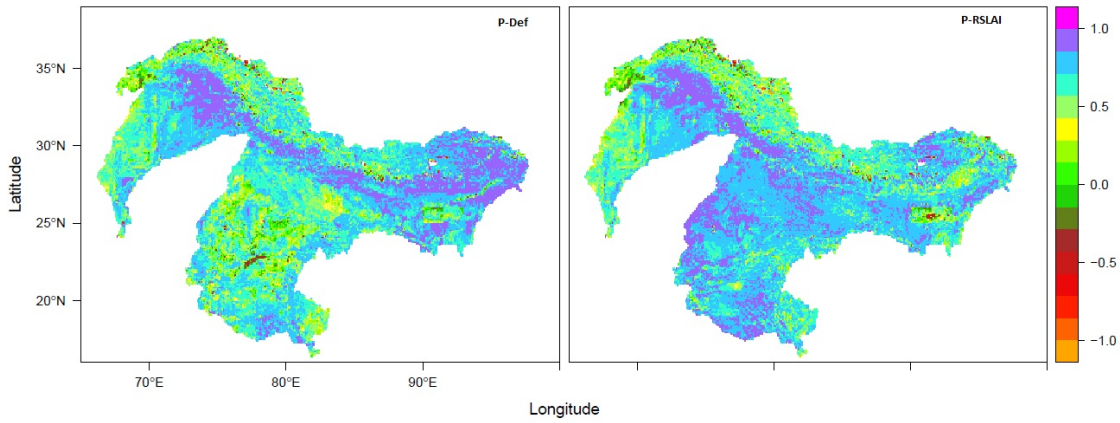

Figure 5.4: Spatial correlation between the monthly average ETensemble and simulated ET for 2003-2007.

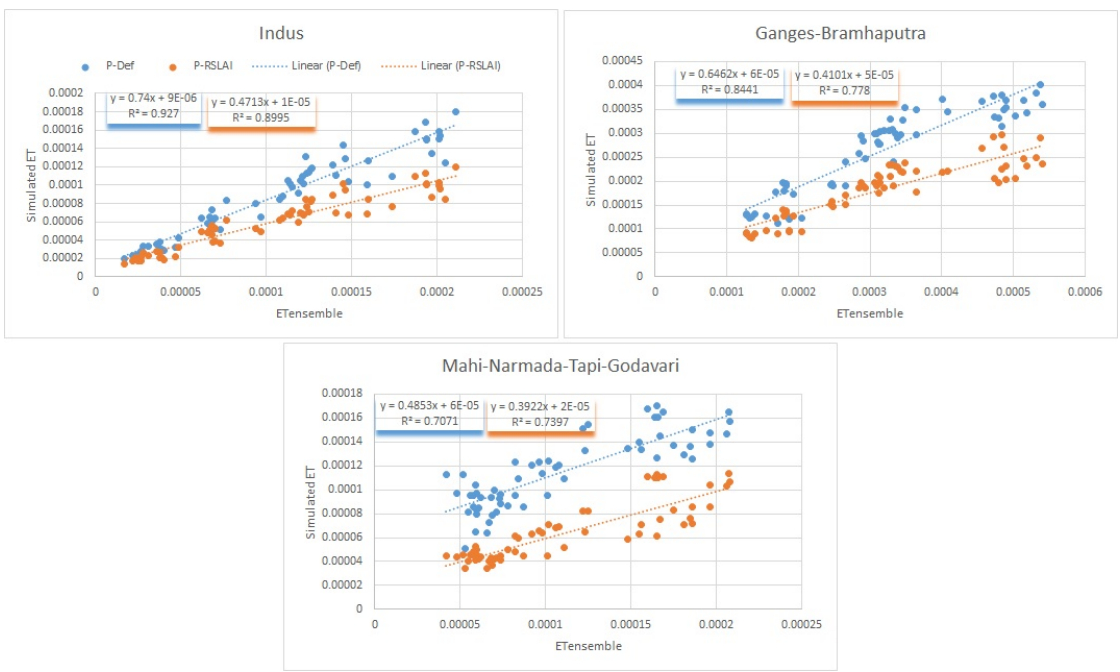

Figure 5.5: Regression analysis between basin weighted monthly average (m.day^{-1}) ETensemble and simulated ET for Exp. 1 & 2

5.1.2 Different Precipitation Products

Once it was established that, compared to P-Def, the incorporation of LAI resulted in marked model improvements in terms of better simulating the river discharge, the effectiveness of different precipitation data products in simulating the river discharge was assessed using P-RSLAI model. For this, the P-RSLAI simulation was re-run by changing the precipitation forcings. Similar to the assessment in the 5.1.1 section, the simulated ET was compared with the ETensemble. Figure 5.6 shows the regression analysis between the differnt simulated ET and ETensemble, while the table 5.2 shows the correlation and RSR values for these runs. From these it can be seen that, compared to the P-RSLAI run, the model runs with different precipitation products showed increase in the R^2 and correlation values across the entire IGBMNTG basin. However, the RSR values were also on the higher side compared to the P-Def and P-RSLAI experiments. This can be partly explained by the fact that although the spatial variability is well represented the absolute values of CHIRPS and APHRODITE precipitation products are lower compared to the CRU data.

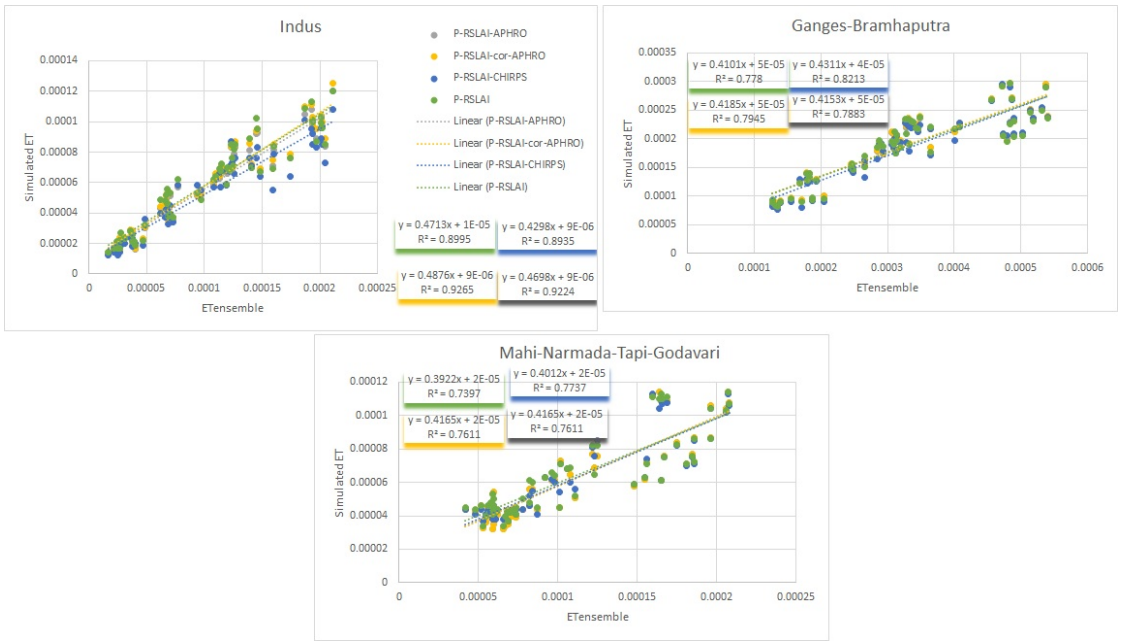

Figure 5.6: Regression analysis between basin weighted monthly average ($m.day^{-1}$) ETensemble and simulated ET for Exp. 2 to 5

Exp.No.	Correlation			RSR		
	I	GB	MNTG	I	GB	MNTG
3	0.96	0.89	0.87	0.95	1.26	1.12
4	0.96	0.88	0.87	0.92	1.25	1.12
5	0.94	0.90	0.87	1.03	1.28	1.12

Table 5.2: Comparison of weighted monthly average (m.day^{-1}) simulated ET and ETensemble for each basin in terms of the correlation and RSR (Exp 3 to 5)

Figure 5.7 and figure 5.8 depict the observed vs. simulated daily and monthly discharge for experiments 3,4 and 5 at several river discharge gauging stations respectively. The NSE values for the discharge simulated by P-RSLAI-APHRO

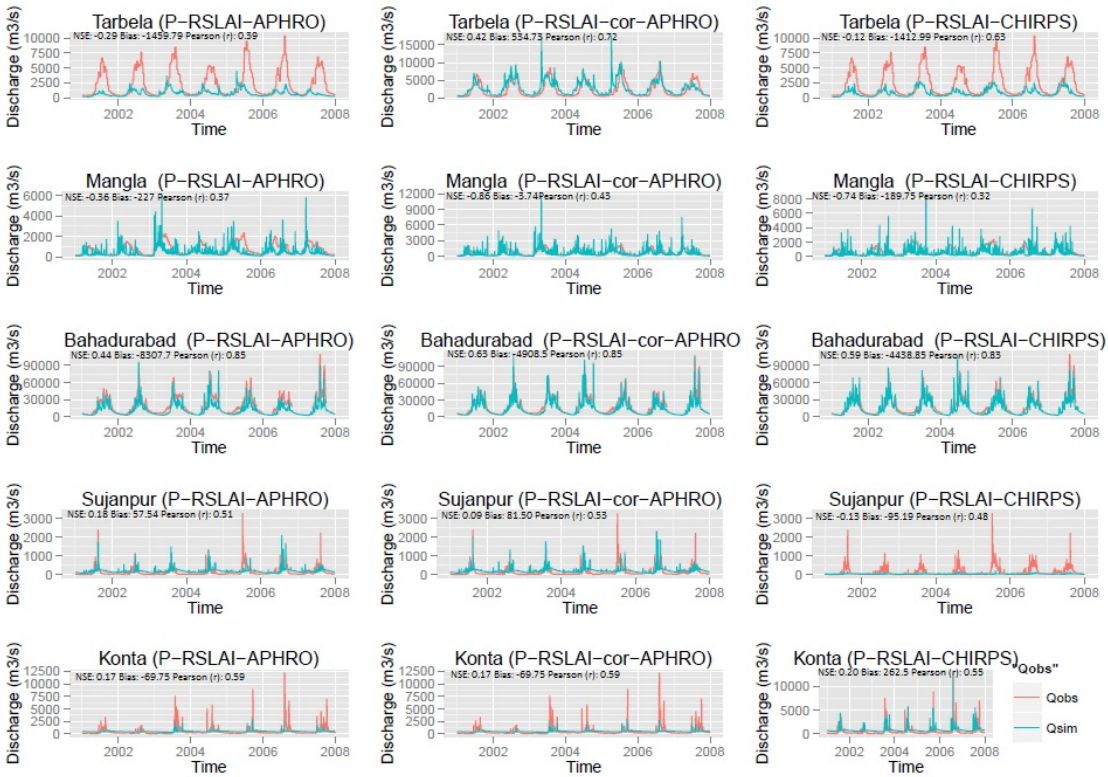

Figure 5.7: Daily observed and simulated discharge (m^3/s) at Tarbela, Mangla, Bahadurabad, Sujanpur & Konta gauging stations (Exp. 3 to 5)

and P-RSLAI-cor-APHRO runs were comparatively better than those simulated

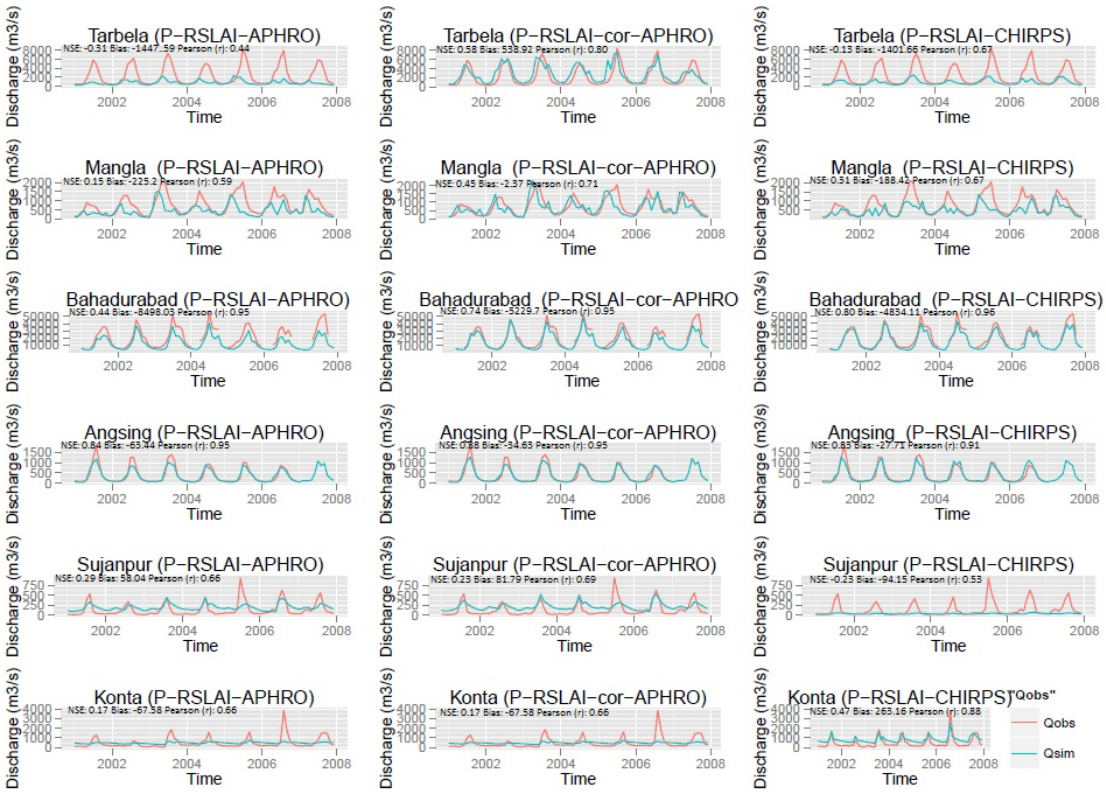

Figure 5.8: Daily observed and simulated discharge (m^3/s) at Tarbela, Mangla, Bahadurabad, Sujanpur & Konta gauging stations (Exp. 3 to 5)

by the P-RSLAI run, while those for the P-RSLAI-CHIRPS did not show much improvement(see Appendix F, E). However, similar to experiments 1 and 2, the monthly and daily simulated flows, particularly peak flows, in experiments 3 and 5 tend to be underestimated at most locations, especially in the upstream parts of the Indus, Ganges and Brahmaputra Basins. The P-RSLAI-cor-APHRO run, among all the five runs, proved to be the best model run providing the more accurate estimate of the observed discharge including the upstream IGB locations where the other model runs underestimated the discharge.

5.1.3 Incorporation of the ETensemble as a Potential ET

The best performing model run in terms of best simulation of the discharge estimates, P-RSLAI-cor-APHRO, was used in the experiment and the ETensemble was incorporated into the model run as the potential ET. This was done so as to correct for the bias in the simulated ET. Table 5.3 shows the correlation and RSR values for the weighted basin average simulated ET and ETensemble product.

Exp.No.	Correlation			RSR		
	I	GB	MNTG	I	GB	MNTG
6	0.97	0.98	0.98	0.63	0.65	0.68

Table 5.3: Comparison of weighted monthly average (m.day^{-1}) simulated ET and ETensemble for each basin in terms of the correlation and RSR (Exp 6)

Figure 5.9 and figure 5.10 depict the observed vs. simulated daily and monthly discharge for experiments 6 at several river discharge gauging stations respectively. Compared to the P-RSLAI-cor-APHRO run, the daily and monthly discharge simulations showed a reasonable performance. The NSE values for the gauge stations located in the upstreams of Indus basin as well as those located in the Godavari basin dipped slightly. For instance the daily NSE value at Tarbela reservoir decreased from 0.41 to -0.40 while the monthly value showed a slight decrease from 0.57 to 0.39. This decrease in NSE value can be associated with the reduction of the simulated ET especially in the drier months causing the overestimation of river discharge. Similarly, the daily NSE value at Konta station located in Godavari basin decreased from, while the monthly value decreased from 0.16 to -0.09. Apart from these few stations, the daily and monthly discharge at most gauging stations was fairly well simulated both in terms of timing and magnitude, which is reflected in the slight increase of the NSE value compared to the P-RSLAI-cor-APHRO run.

Figure 5.9: Daily observed and simulated discharge (m^3/s) at several gauging stations (Exp. No. 6)

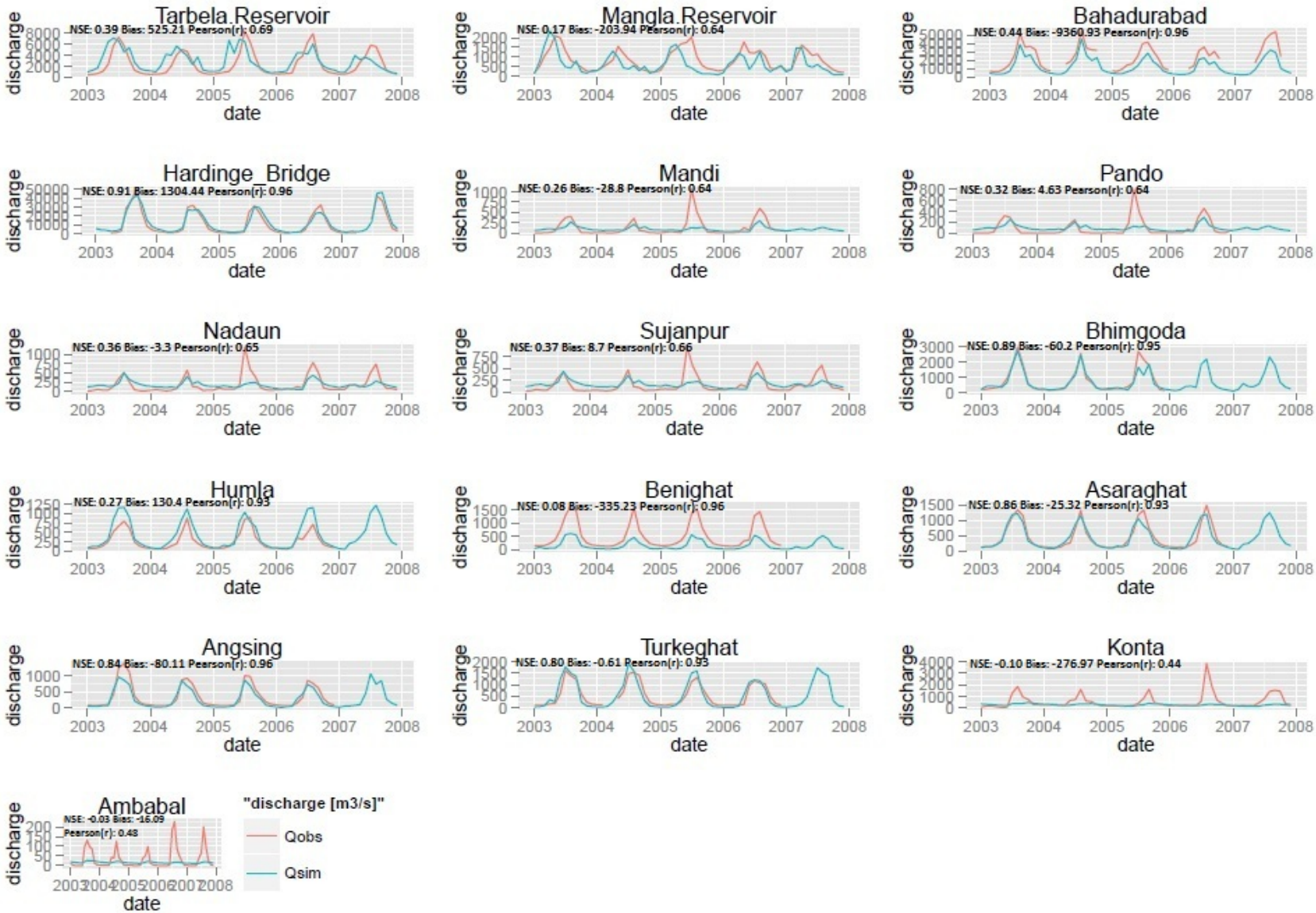

Figure 5.10: Monthly observed and simulated discharge (m^3/s) at several gauging stations (Exp. No. 6)

5.1.4 Water Budget Components, Water Demand and Use

After establishing that the hydrological model PCR-GLOBWB after incorporating the remote sensing information is capable of more accurately reproducing the historical variability and magnitude of the river discharge, it was also important to examine water budged components, water demands and use simulated by the model. Figure 5.11 displays the basin-wise annual average values of of the precipitation, evapotranspiation and runoff for the P-RSLAI-ET experiment.

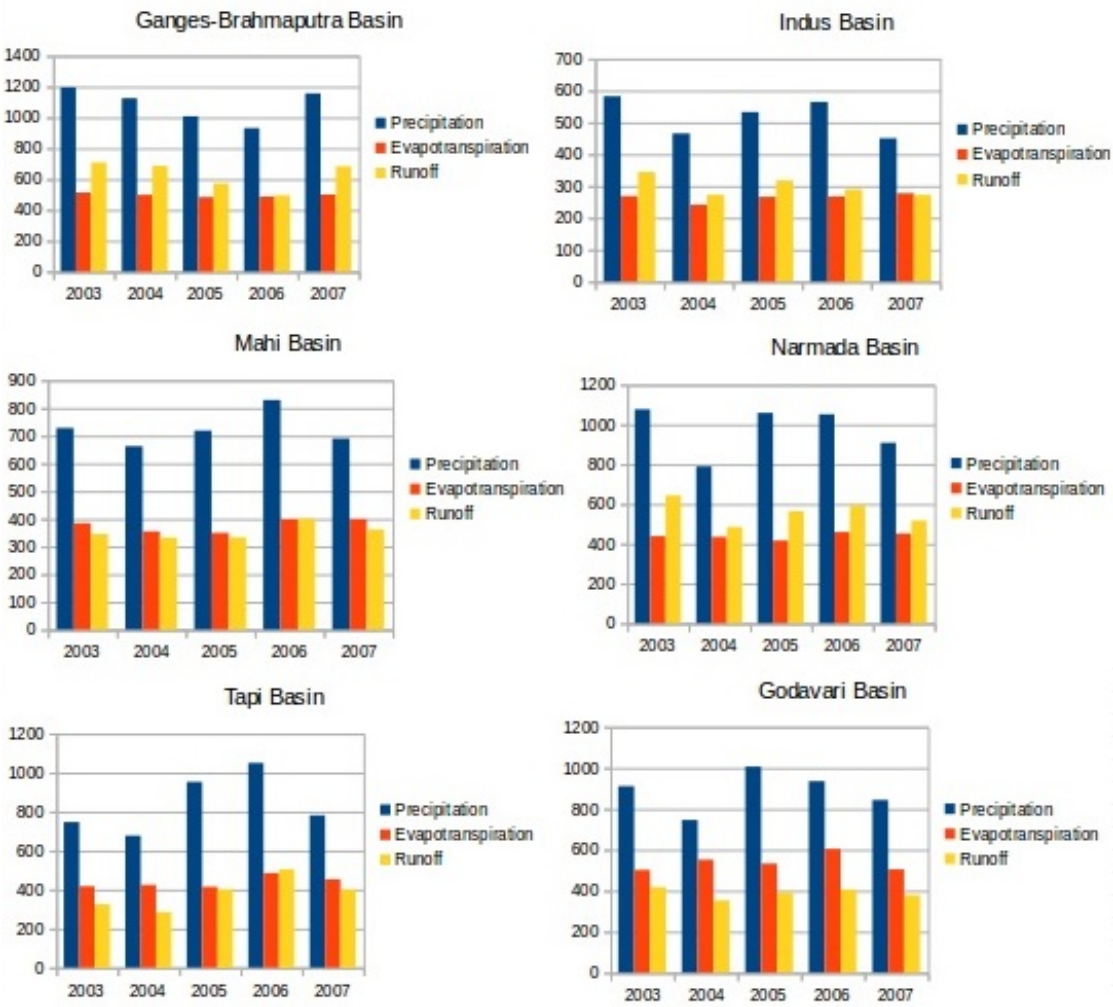

Figure 5.11: Main water budget components (mm.year^{-1}) for different river basins as assessed using P-RSLAI-ET run

The average precipitation, evapotranspiration and runoff between 2003 and

	Ganges-Brahmaputra	Indus	Mahi	Narmada	Tapi	Godavari
Precipitation(mm)	1082	518	724	976	840	887
Evapotranspiration(mm)	495	264	376	439	438	538
Runoff(mm)	628	298	354	560	382	388

Table 5.4: Multi-year average (2003-2007) water budget components for different river basins

2007 for different river basins are summarized in table 5.4. Evapotranspration was observed to be the dominant flux in the Mahi, Tapi and Godavari basin compared to the discharge.

Figures 5.12 and figure 5.13 provide the water demand and water use dynamics in all the basins between the years 2003 and 2007 as simulated by the P-RSLAI-ET-cor-APHRODITE run.

The average potential gross demand in Ganges-Brahmaputra basin between 2003 and 2007 accounted to about 74.88 $Km^3.year^{-1}$ of which approximately 86% was for irrigation and 14% was for non irrigation purpose. This gross irrigation demand was further divided into approximately 70% and 30% for paddy and non paddy irrigation. On an average, the irrigation evaporation water use and non irrigation water use were approximately 25.67 $Km^3.year^{-1}$ and 10.81 $Km^3.year^{-1}$ respectively. In the Indus basin, the average potential gross demand was accounted to about 42.52 $Km^3.year^{-1}$ (irrigation: 39.71 and non irrigation 2.80). The gross demand for paddy irrigation in this basin increased from about 16.47 $Km^3.year^{-1}$ in 2001 to 22.34 $Km^3.year^{-1}$ in 2007. The average gross demand in Godavari basin was about 10 $Km^3.year^{-1}$ of which 70% was consumed by irrigation. The average irrigation evaporation water use in this basin accounted to about $3.40^3.year^{-1}$. In the Mahi, Narmada and Tapi basins the average gross water demand was approximately 0.76, 1.80 and 1.06 $Km^3.year^{-1}$ respectively. Approximately 50% of these demands were for non paddy irrigation while the remaining fraction was for non irrigation demand. Overall it can be seen that between 2003 and 2007 the gross irrigation water demand has significantly increased in the IGBMNTG basin especially in the heavily irrigated IGB basin.

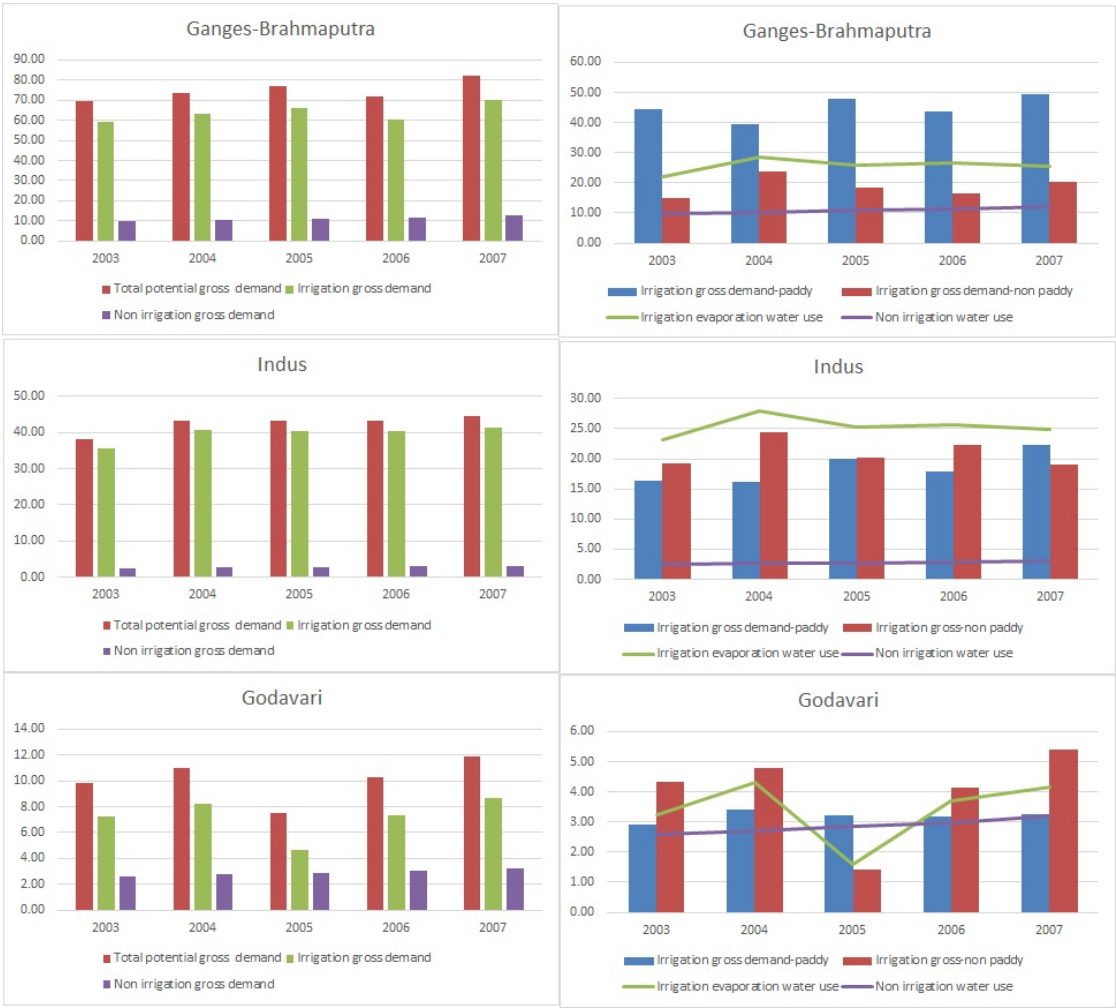

Figure 5.12: Water demand and use dynamics (all in $Km^3.year^{-1}$ for irrigated and non irrigated areas in Indus, Ganges-Brahmaputra and Godavari basin.

Figure 5.13: Water demand and use dynamics (all in $Km^3.year^{-1}$ for irrigated and non irrigated areas in Mahi, Narmada and Tapi basin.

CHAPTER 6
DISCUSSION

From the section 5 it is evident that incorporating remote sensing hydrological information into the PCR-GLOBWB displayed a significant improvement in terms of reproducing the historic river discharge observations in the IGBMNTG basin. These improvements indicate that the incorporation of remote sensing hydrological information into the hydrological models not only provides greater model accuracy and better understanding of the historic hydrology but can also, to an extent, help in characterizing the model related uncertainties in the simulations. Uncertainties in the hydrological model may arise in four different ways namely(Sood and Smakhtin, 2014): uncertainty in input data owing to the measurement errors, output uncertainty that can be attributed to errors in analysis, model uncertainties which is attributed to the representation of hydrological processes in the model and finally the uncertainty arising from the model parameters. In this study, an attempt was made to reduce the input uncertainty by incorporating the remote sensing LAI and accurate precipitation and evapotranspiration data.

The lower simulated value of P-RSLAI ET when compared to the P-Def ET during the drier period (see Figure 5.3) can be attributed to LAI values incorporated from the remote sensing being lower than those used in the P-Def. It is because of this reason that the simulated river discharge are slightly higher and correspond better with the in-situ observations in the P-RSLAI run compared to the P-Def run. Although the reconstruction of the magnitude of the simulated discharge,especially peak flows, continues to be an issue, the incorporation of LAI results into better capture of the low flows and the timing. The model performance statistics for both the model experiments are enlisted in the Appendix E andF. It can be seen that the with the discharge simulated by the P-RSLAI experiment shows a better correlation with the observed data with a significant reduction in the bias. The P-RSLAI showed a better capability of improving the accuracy of river discharge simulation on the monthly and annual scale because of the incorporation of remote sensing LAI.

In the experiments with different precipitation forcings, the best estimates of river discharge were obtained by P-RSLAI-cor-APHRO run. The NSE

values and the correlation with the in-situ discharge at most gauging stations were comparatively better for this experiment compared to all other experiments (P-RSLAI, P-RSLAI-APHRO and P-RSLAI-CHIRPS) and the RMSE was significantly lower. The poor performance in the other runs can be associated with the biases in the precipitation products in terms of how well the precipitation product captured the spatial and temporal distribution as well as the magnitude of the extreme wet and dry events. Figure 6.1 shows the seasonal spatial variation and magnitude as captured by the different precipitation products. It is stressed

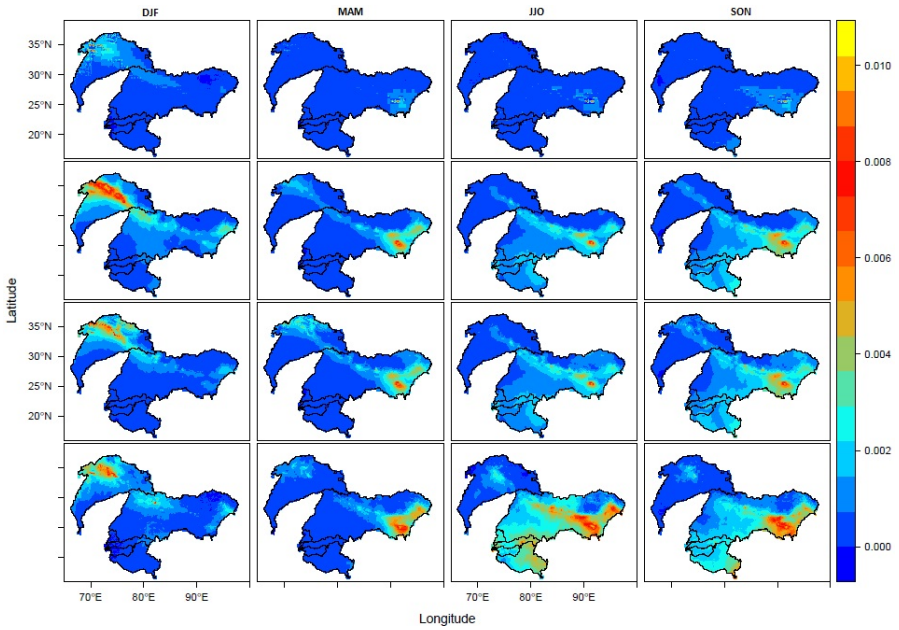

Figure 6.1: Seasonal mean precipitation (2001 to 2007) ordered rowwise as: CRU, APHRODITE, UIGB-Corrected-APHRODITE and CHIRPS

that, in this study, the accuracy of different precipitation products against the in situ rain gauge stations was not evaluated. However, the propagation of bias in the precipitation product into the simulated discharge can be clearly seen and is in agreement with the studies that evaluated the precipitation product against the rain gauge data. Duncan and Biggs (2012) assessed the TRMM and APHRODITE precipitation over the Nepal and concluded that the satellite based precipitation overestimated the precipitation in all seasons and the larges error was found during the monsoon season. Another study by Khandu et al. (2016) which compared the APHRODITE, TRMM, CMORPH, and CHIRPS against the rain gauge observations over Bhutan concluded that APHRODITE was in better

agreement with the gauge data, while the CMORPH, and CHIRP products did not show much correlation over the mountains, during the pre and post monsoon seasons. It therefore is fair to consider the UIGB-corrected-APHRODITE performed better in comparison with other precipitation forcings in terms of simulating the river discharge. Also, the validation of P-RSLAI-cor-APHRO simulated discharge at location other than those used by (Immerzeel et al., 2015) displayed a good agreement with the observed data.

For the P-RSLAI-ET-cor-APHRO run, the choice of ETensemble product was driven by several facts. First, it is difficult to find a single best ET product as every individual energy balance model has its uncertainties. The ETensemble product addresses these uncertainties by combining the predictions from individual energy balance models. These uncertainties in the different individual ET products were minimized by removing the outlier values during the preparation of ensemble. Also, the product is available at 250m resolution and better reflects on the local conditions such as natural vegetation and anthropogenic withdrawals. The ETensemble product, although has not been extensively validated yet, the ET back calculated from the precipitation and discharge over Thailand was compared with the ETensemble by the Water Accounting group at UNESCO-IHE and it presented an overall good agreement with small bias (overestimations) in the ETensemble. The ET simulation using P-RSLAI-ET-cor-APHRO showed a good agreement with the ETensemble, especially in wet period. However, the ET was underestimated in the drier months which can be attributed to the irrigation water scheduling in the model. The lack of moisture in the root zone to meet the potential ET in the drier months resulted in the reduced actual ET. Owing to this reduction in ET, the simulated discharge at some stations was overestimated. However, at most gauging stations the discharge simulated by P-RSLAI-ET-cor-APHRO run was more satisfactory compared to the P-RSLAI-cor-APHRO run. This reduction in ET is anticipated if sufficient water is not available to meet the requirements. One way to address this issue is by improving the timing of the irrigation that is scheduled in the model. Alternatively, the soil moisture function that is responsible for reduction of ET_c can be set to unity such that the ETensemble values incorporated as potential ET can be conserved.

CHAPTER 7
CONCLUSIONS AND RECOMMENDATIONS

The main objective of this study was to assess whether the incorporation of remote sensing hydrological information into the distributed global hydrological model PCR-GLOBWB can provide improved quantification of the hydrological fluxes. The study specifically analysed the influence of uncertaininty in input data on the model simulation uncertainty. First the hydrological changes as a result of vegetation parametrization using RS LAI were investigated. Further the capability of newly emerged precipitation data sets in reproducing the river discharge was studied. Finally, the ETensemble product was directly incorporated into the model to account for the bias in the simulated evapotranspiration and to evaluate the resulting model performance.

From the present study it can be concluded that the incorporation of remote sensing LAI, specifically to represent site specific inter annual variation in vegetation response, led to better evapotranspiration and discharge estimates and exhibited an overall better model performance. The model simulations with CRU, APHRODITE and CHIRPS precipitation products tend to underestimate the discharge, especially in the upstream of Indus, Ganges and Brahmaputra basins, owing to the uncertainty (under catch of high altitude precipitation) in the data sets. Among the model simulations with different precipitation forcings, the UIGB corrected APHRODITE performed relatively better in reproducing the historical river discharge observations. More notable is the model performance by P-RSLAI-cor-APHRO which displayed significant improvements in the simulations of river discharge at both monthly and daily scales.

It must be noted here that the need for accurate precipitation product remains persistent owing to the limited availability of APHRODITE data (not updated since 2007) and under-catch of high altitude precipitation in remote sensing precipitation products as highlighted by Khandu et al. (2016). In this study the different precipitation products were not individually evaluated against the rain gauge staions. In the future studies it is recommended to carry out evaluation of precipitation products against the station data to ensure clear conclusions on the model performance when incorporated with different precipitation products.

The P-RSLAI-ET-cor-APHRO run improved the ET simulations across the

basin and therefore the discharge estimates at most gauging stations. However, some underestimations of ET in the drier periods persisted. This issue can be possibly addressed by improving the irrigation scheduling in the model or by adjusting the soil moisture reduction function. In the future studies it is also recommended to evaluate the ETensemble against the data from flux towers and correct the data for the bias. Also, the ETensemble data currently incorporated into the model lacked values for water. This needs to be taken into account in the future study and evaporation values for water must be computed.

Although the study focuses on IGBMNTG basin, the method developed for incorporating the remote sensing ET data into the model is applicable globally. In fact, the availability of ETensemble data at 250m spatial resolution and covers most parts of the globe (+45°to -45°), makes it particularly useful in the global irrigated areas and areas that are data scarce. Using this data with the PCR-GLOBWB at the spatial resolution of approximately 0.008°could be interesting especially when it comes to water accounting.

The IGB plains experience highly intensive groundwater abstractions. In the future studies these abstractions could be verified against the piezometric measurements and the anomaly of total water storage simulated by the model can be compared with the anomalies estimated by GRACE satellite.

APPENDIX A

MEAN ANNUAL ET (2003-2007) (M/DAY) FOR VARIOUS EXPERIMENTS

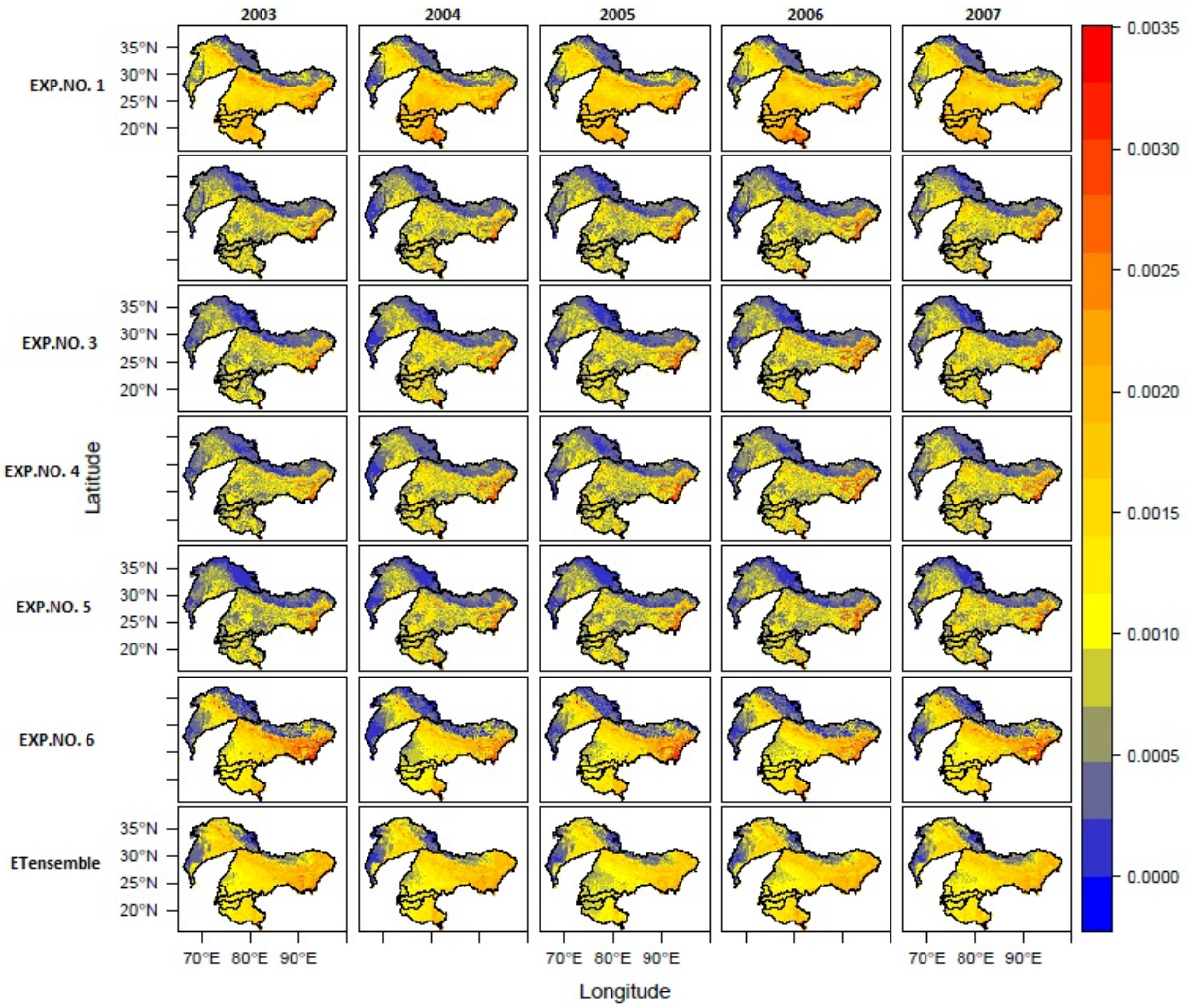

Figure A.1: Ordered rowwise as: P-Def, P-RSLAI, P-RSLAI-APHRO, P-RSLAI-cor-APHRO,P-RSLAI-CHIRPS, P-RSLAI-ET-cor-APHRO, ETensemble

APPENDIX B

DIFFERENCE MAP BETWEEN MEAN ANNUAL PRECIPITAITON AND ET

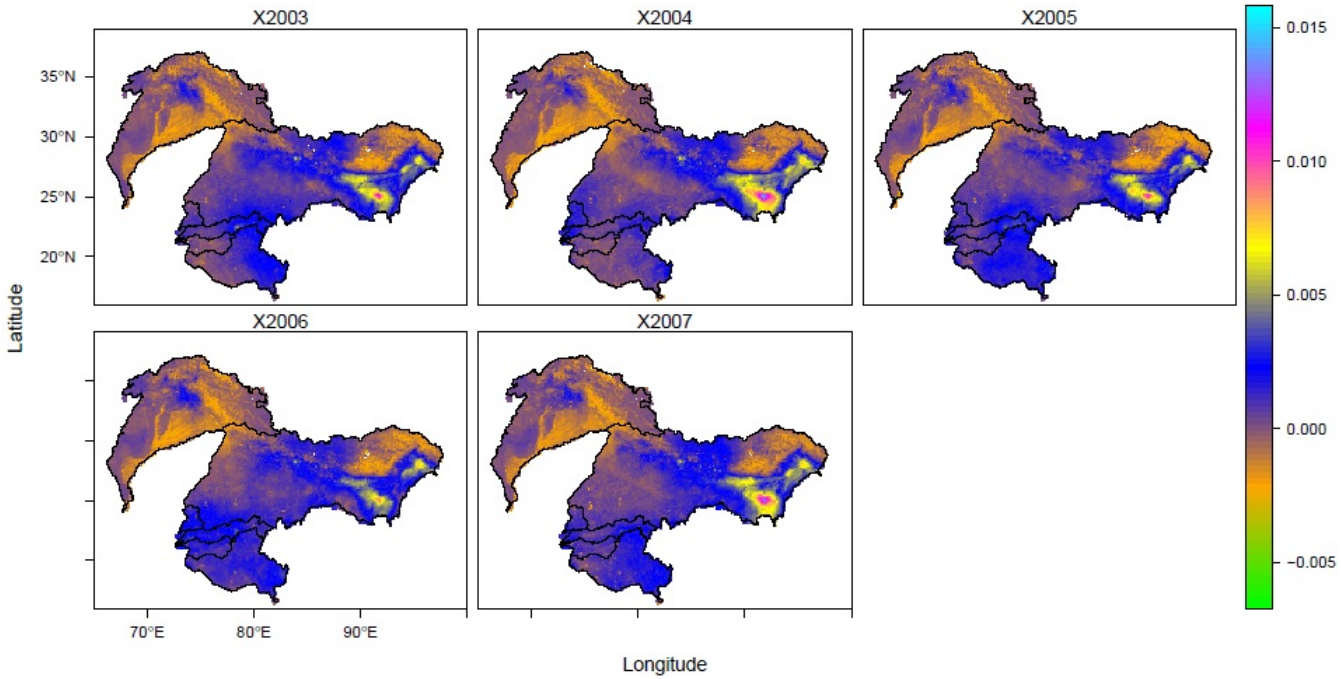

Figure B.1: Difference map between mean annual CHIRPS precipitation and ETensemble (2003-2007) (m.day^{-1})

APPENDIX C

PLOTS SHOWING MONTHLY OBSERVED VS. SIMULATED RIVER DISCHARGE (M^3/S) AT SEVERAL GAUGE STATIONS FOR VARIOUS EXPERIMENTS

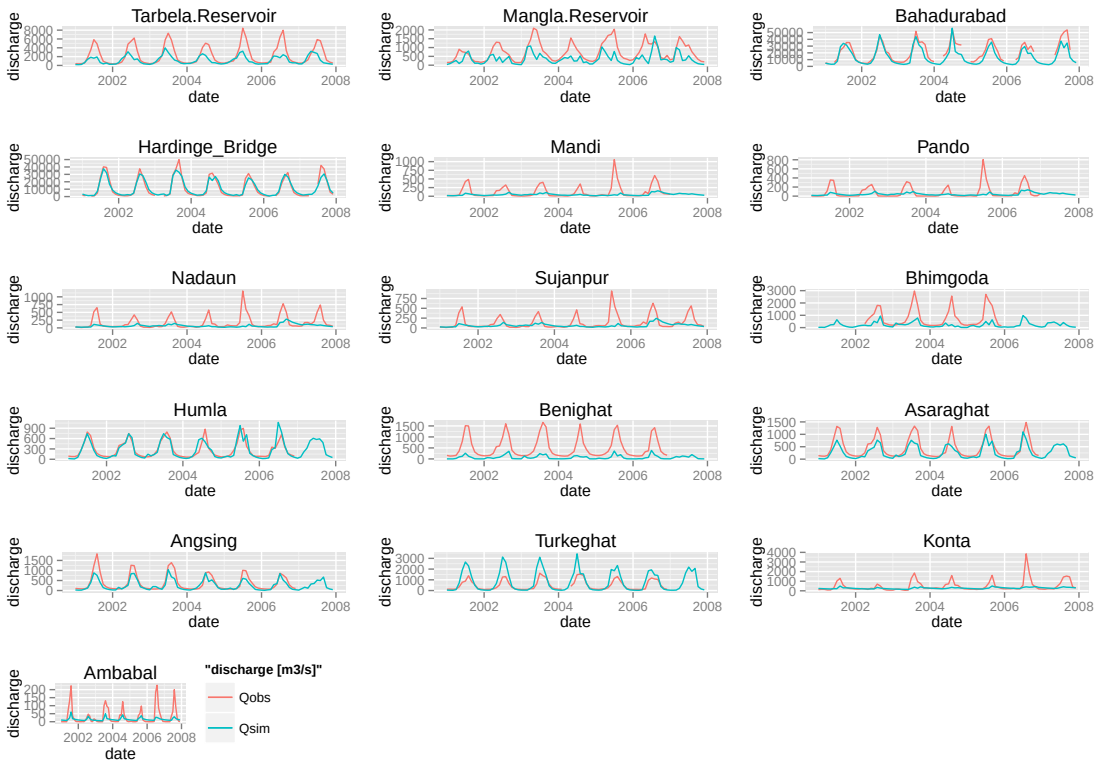

Figure C.1: P-Def

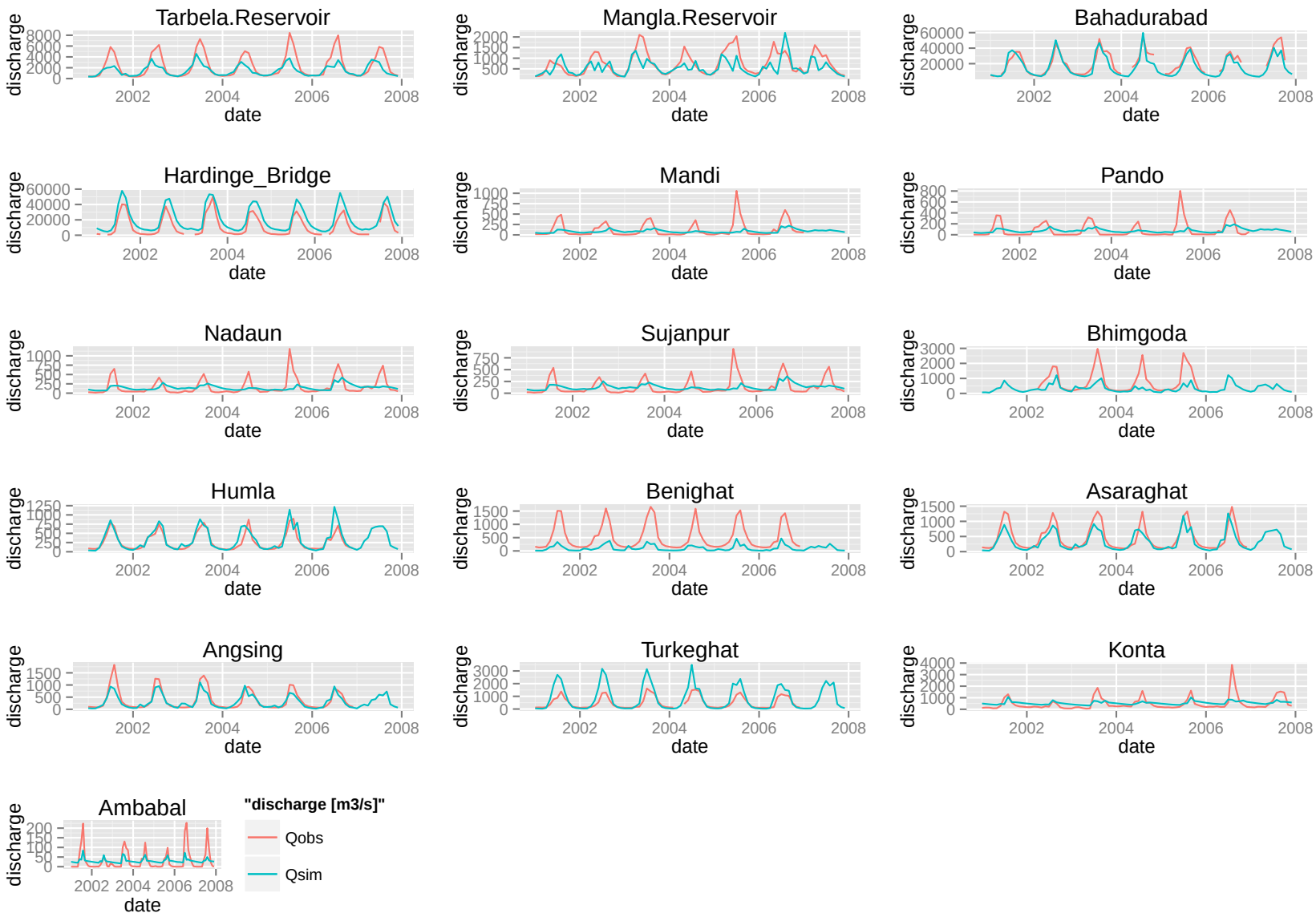

Figure C.2: P-RSLAI

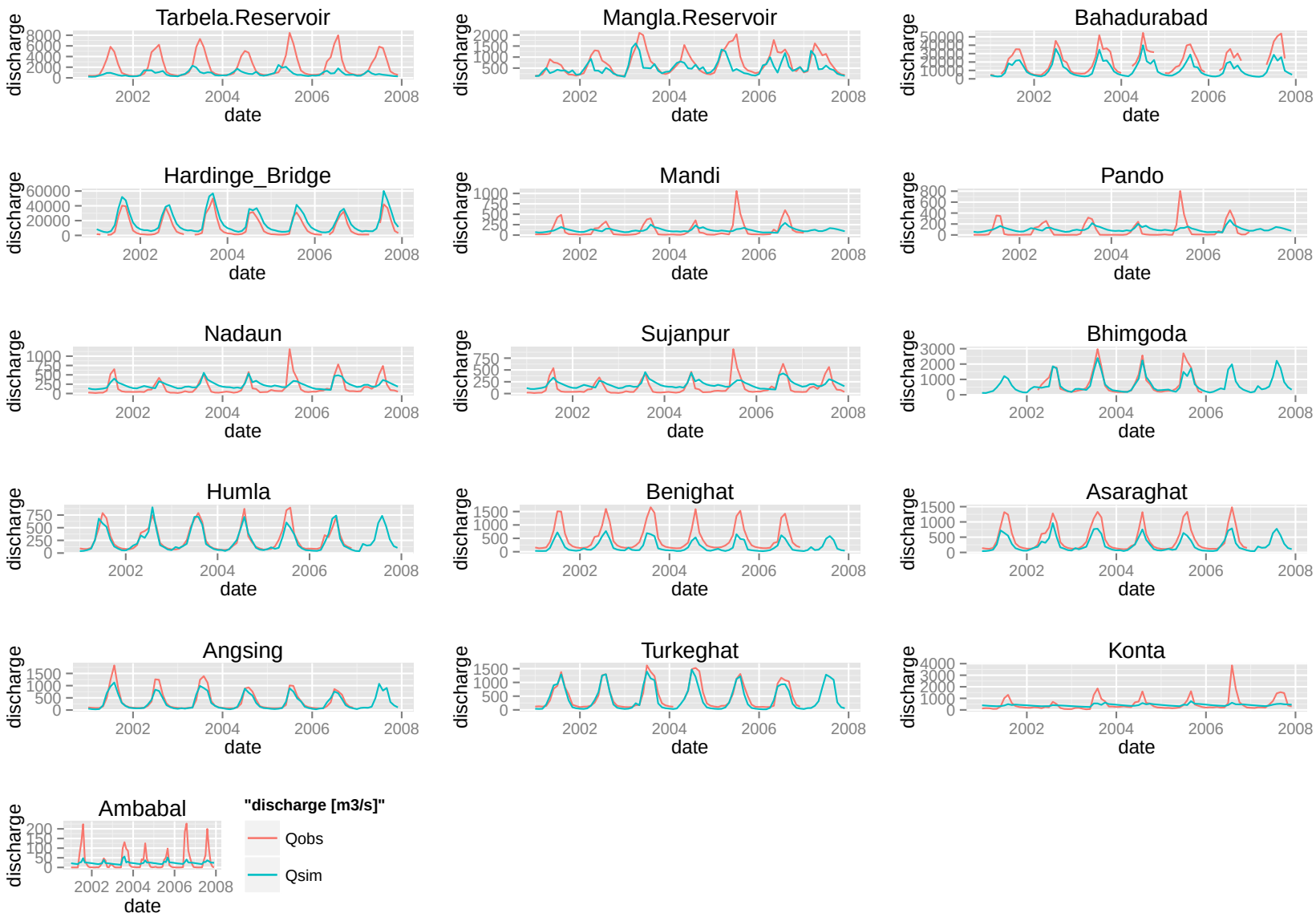

Figure C.3: P-RSLAI-APHRO

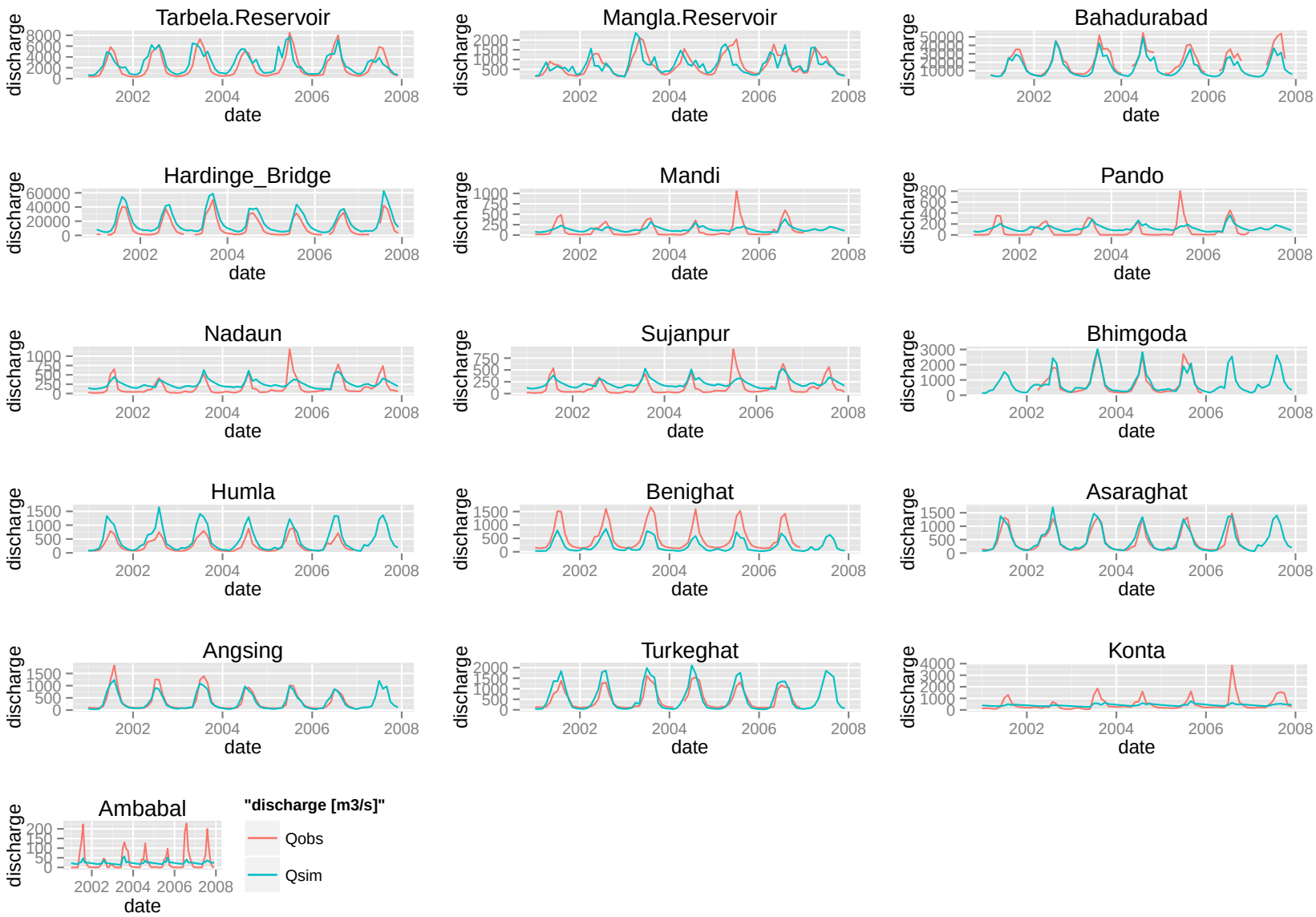

Figure C.4: P-RSLAI-cor-APHRO

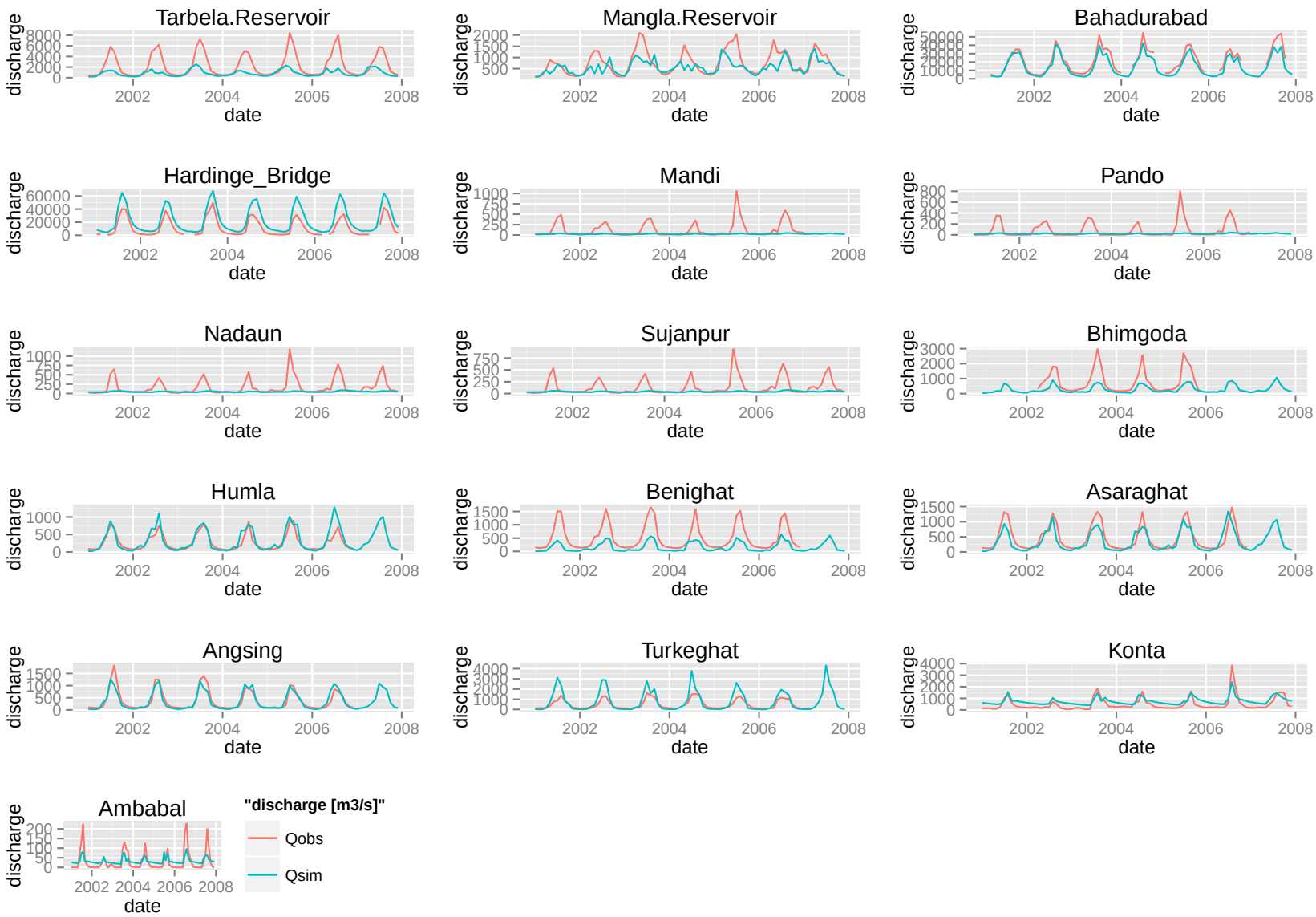

Figure C.5: P-RSLAI-CHIRPS

APPENDIX D

PLOTS SHOWING MONTHLY OBSERVED VS. SIMULATED RIVER DISCHARGE (M^3/S) AT SEVERAL GAUGE STATIONS FOR VARIOUS EXPERIMENTS

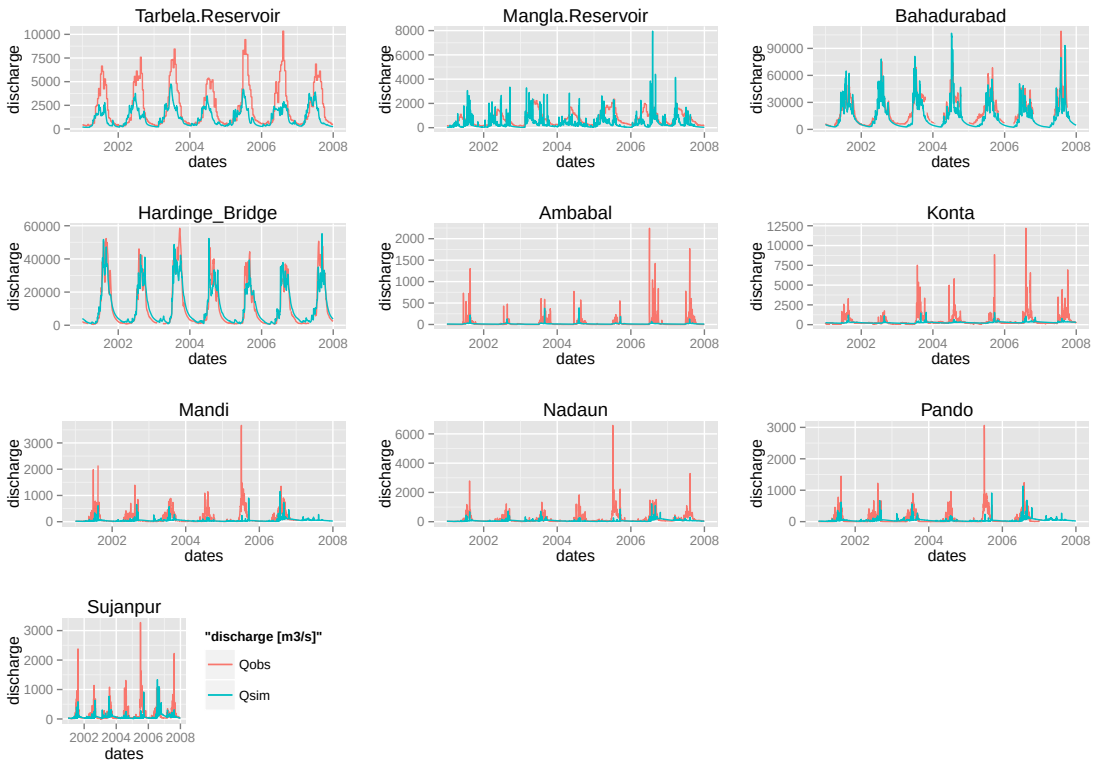

Figure D.1: P-Def

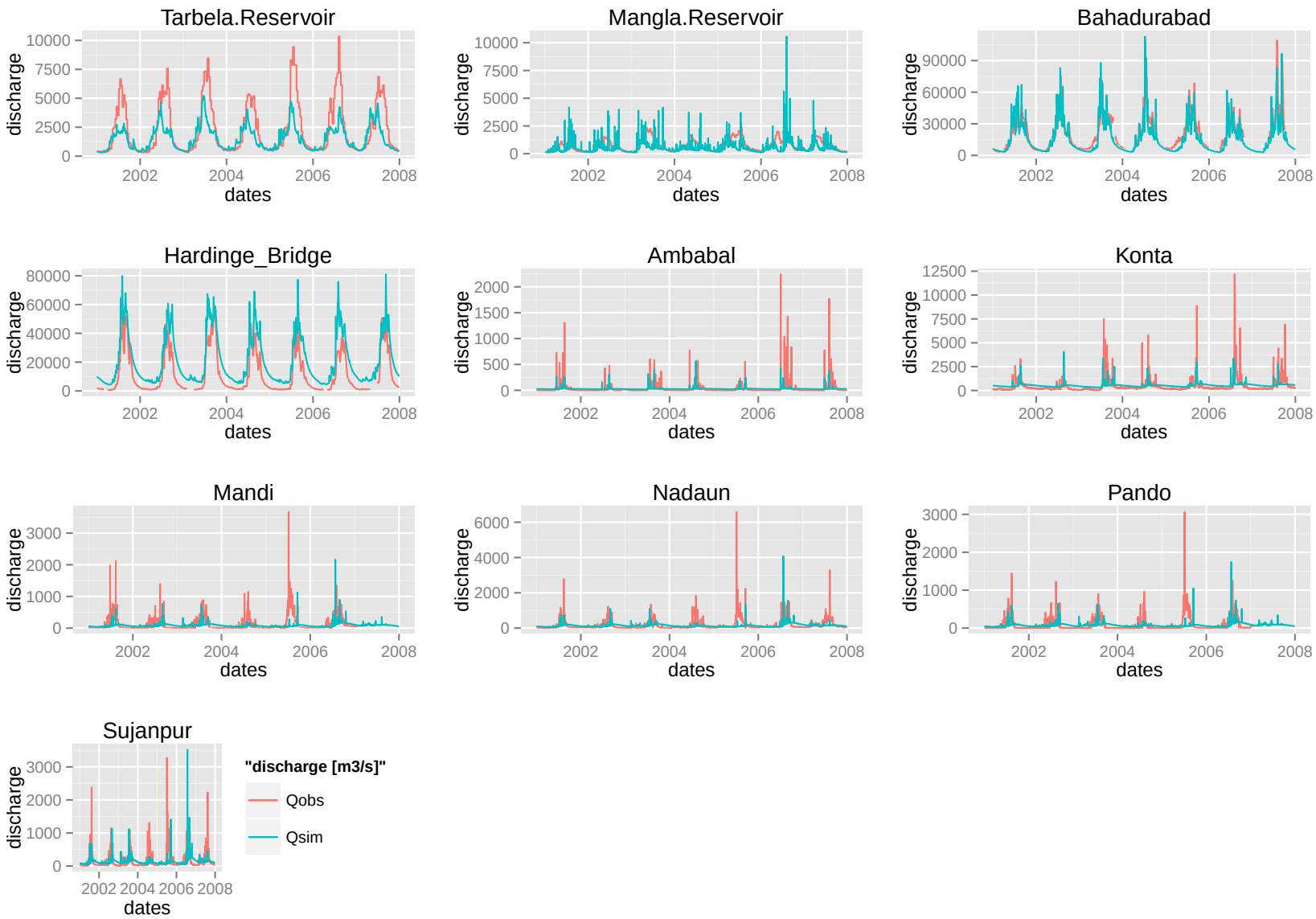

Figure D.2: P-RSLAI

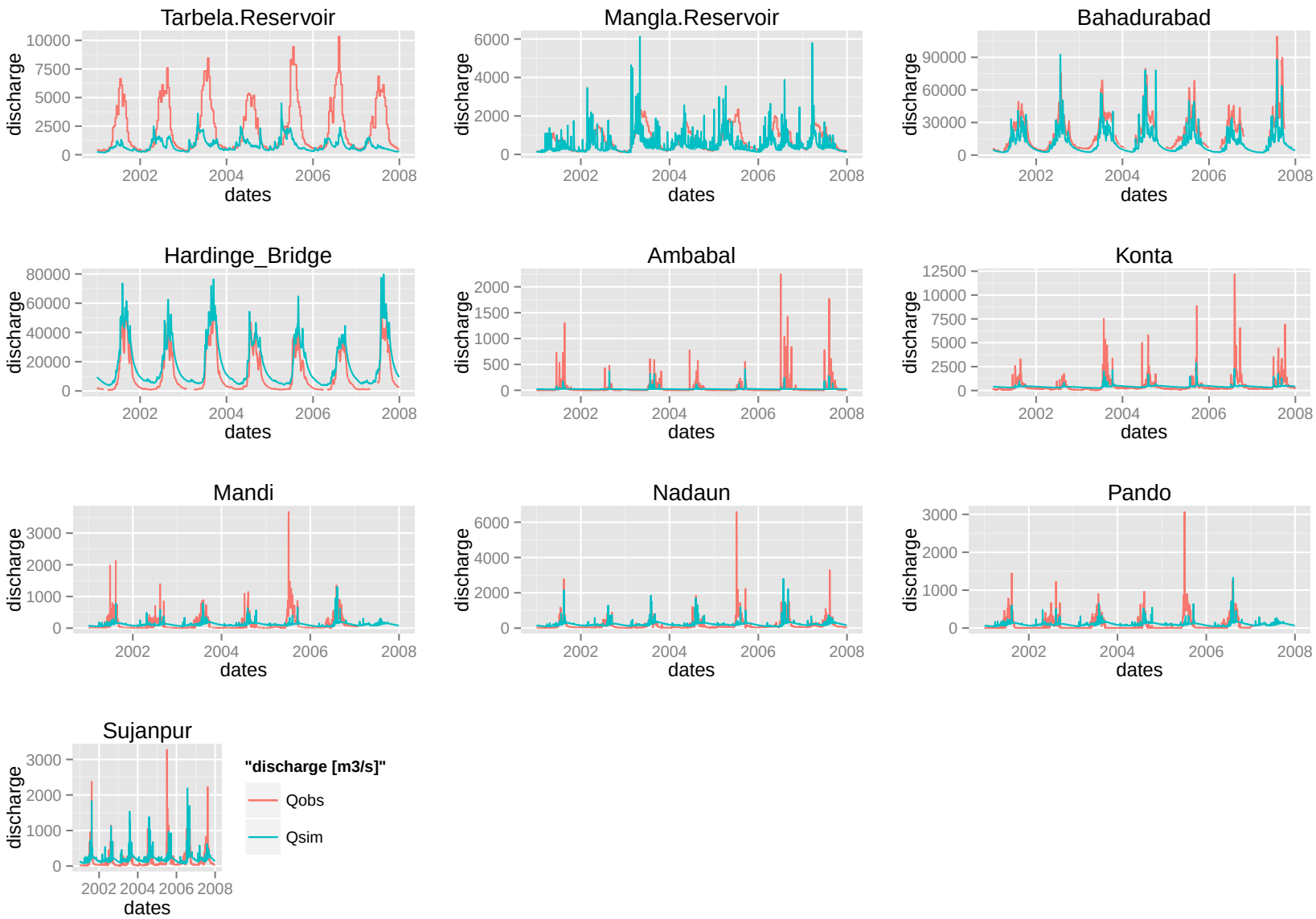

Figure D.3: P-RSLAI-APHRO

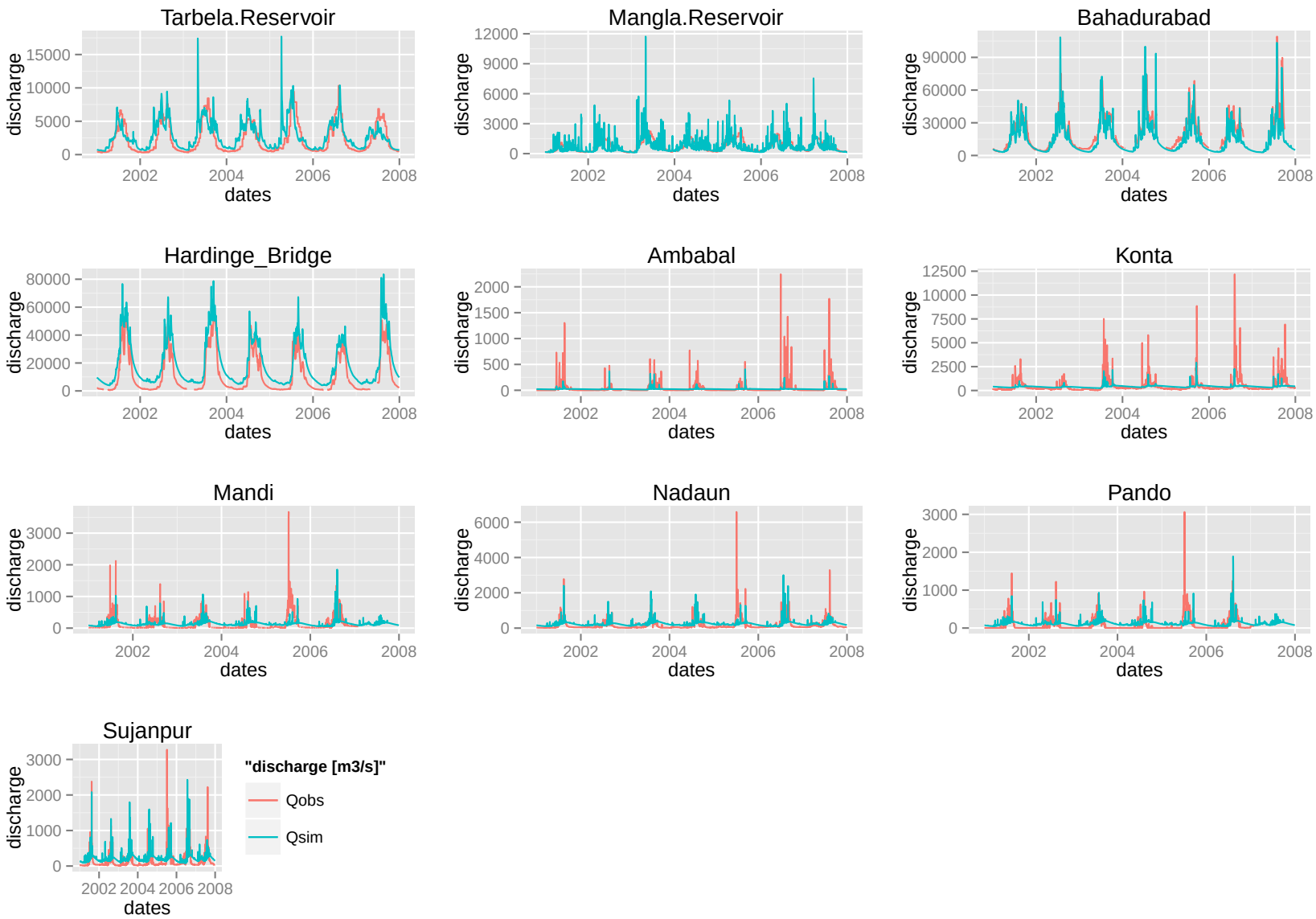

Figure D.4: P-RSLAI-cor-APHRO

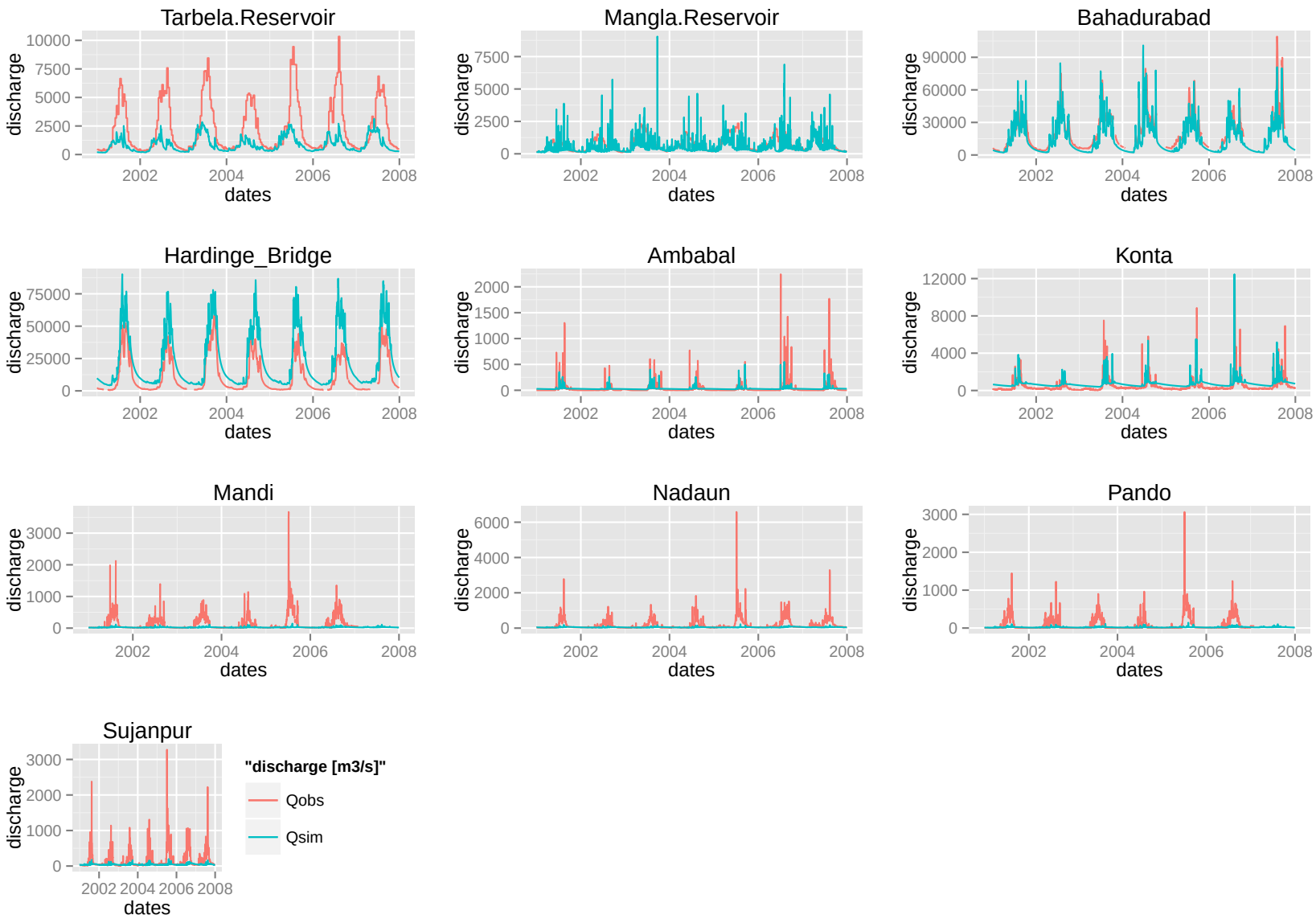

Figure D.5: P-RSLAI-CHIRPS

APPENDIX E

TABLES SHOWING MONTHLY MODEL PERFORMANCE FOR VARIOUS EXPERIMENTS

	P-Def															
	Tarbela	**Mangla**	**Sujanpur**	**Nadaun**	**Mandi**	**Pando**	**Bhimgoda**	**Humla**	**Benighat**	**Asaraghat**	**Angsing**	**Turkeghat**	**Bahadurabad**	**Hardinge_Bridge**	**Ambabal**	**Konta**
avg_obs	2257.71	741.12	135.65	165.89	122.61	82.94	785.10	273.85	506.35	446.61	371.38	500.71	21631.67	11578.57	30.48	484.32
avg_sim	1194.47	357.20	64.59	69.80	46.99	42.99	223.85	260.47	72.45	266.30	256.30	823.83	16260.38	11638.37	15.34	277.90
NSE	0.22	-0.21	-0.03	-0.08	-0.04	0.07	-0.23	0.73	-0.58	0.54	0.68	-0.92	0.70	0.91	0.18	0.01
LNSE	0.45	-0.93	0.15	0.07	0.28	0.06	-1.66	0.44	-9.53	-0.17	0.47	0.28	0.57	0.87	0.18	0.32
rmse	1894.47	563.75	175.71	223.22	187.03	137.45	849.07	124.78	588.53	276.14	232.30	647.41	7670.72	4087.18	47.46	568.35
mae	1181.37	396.48	94.92	119.14	94.66	75.73	567.42	76.06	433.90	197.47	144.00	393.48	6053.13	2765.90	26.16	275.40
bias	-1063.24	-383.92	-71.05	-96.10	-75.63	-39.95	-561.25	-13.38	-433.90	-180.31	-115.09	323.12	-5371.29	59.80	-15.15	-206.42
R2	0.58	0.35	0.16	0.15	0.21	0.21	0.49	0.78	0.67	0.78	0.83	0.81	0.85	0.93	0.66	0.37
R2ad	0.57	0.34	0.15	0.14	0.20	0.20	0.48	0.78	0.67	0.78	0.83	0.81	0.84	0.93	0.66	0.36
correlation	0.76	0.59	0.40	0.38	0.46	0.46	0.70	0.88	0.82	0.89	0.91	0.90	0.92	0.96	0.81	0.61

	P-RSLAI															
	Tarbela	**Mangla**	**Sujanpur**	**Nadaun**	**Mandi**	**Pando**	**Bhimgoda**	**Humla**	**Benighat**	**Asaraghat**	**Angsing**	**Turkeghat**	**Bahadurabad**	**Hardinge_Bridge**	**Ambabal**	**Konta**
avg_obs	2257.71	741.12	135.65	165.89	122.61	82.94	785.10	273.85	506.35	446.61	371.38	500.71	21631.67	11578.57	30.48	484.32
avg_sim	1509.73	564.99	127.03	146.38	85.43	74.49	344.37	317.14	105.28	328.32	306.29	845.04	18286.86	21046.65	30.30	543.43
NSE	0.41	0.22	0.16	0.14	0.10	0.15	0.05	0.62	-0.39	0.67	0.76	-1.05	0.78	0.36	0.32	0.25
LNSE	0.72	0.49	0.03	0.06	0.08	-0.40	0.13	0.75	-3.80	0.55	0.74	0.39	0.77	0.11	-0.43	-0.02
rmse	1648.07	451.57	158.81	199.91	173.82	131.25	744.78	147.07	553.25	233.92	200.79	668.86	6566.97	10679.16	43.15	497.17
mae	992.70	285.41	101.44	122.02	103.33	87.57	456.58	84.78	402.26	158.34	121.50	405.26	4839.28	9468.08	30.00	341.10
bias	-747.98	-176.13	-8.61	-19.52	-37.19	-8.45	-440.74	43.29	-401.07	-118.29	-65.09	344.34	-3344.81	9468.08	-0.19	59.11
R2	0.65	0.35	0.17	0.15	0.19	0.18	0.55	0.78	0.70	0.77	0.84	0.82	0.84	0.92	0.64	0.41
R2ad	0.65	0.34	0.16	0.14	0.17	0.17	0.54	0.77	0.69	0.77	0.84	0.81	0.84	0.92	0.63	0.40
correlation	0.81	0.59	0.41	0.39	0.43	0.43	0.74	0.88	0.84	0.88	0.92	0.90	0.92	0.96	0.80	0.64

P-RSLAI-APHRO																
	Tarbela	**Mangla**	**Sujanpur**	**Nadaun**	**Mandi**	**Pando**	**Bhimgoda**	**Humla**	**Benighat**	**Asaraghat**	**Angsing**	**Turkeghat**	**Bahadurabad**	**Hardinge_Bridge**	**Ambabal**	**Konta**
avg_obs	2257.71	741.12	135.65	165.89	122.61	82.94	785.10	273.85	506.35	446.61	371.38	500.71	21631.67	11578.57	30.48	484.32
avg_sim	810.12	515.91	193.69	227.09	119.28	103.18	699.14	242.70	195.34	257.94	307.94	415.75	13133.64	18894.12	24.21	416.74
NSE	-0.31	0.15	0.29	0.32	0.24	0.23	0.84	0.86	0.21	0.55	0.84	0.87	0.44	0.62	0.19	0.17
LNSE	-0.15	0.38	-0.37	-0.29	-0.14	-0.70	0.84	0.84	-1.08	0.45	0.85	0.41	0.44	0.27	-0.31	0.20
rmse	2456.47	472.20	146.20	177.72	159.85	124.76	303.70	89.82	415.43	274.78	162.93	166.27	10461.72	8201.13	47.13	523.10
mae	1528.36	301.87	116.99	136.74	109.24	93.25	194.22	59.63	311.03	192.60	98.60	120.99	8498.03	7399.73	30.28	310.23
bias	-1447.59	-225.21	58.04	61.19	-3.33	20.24	-85.97	-31.15	-311.00	-188.67	-63.44	-84.95	-8498.03	7315.55	-6.27	-67.58
R2	0.19	0.34	0.44	0.44	0.35	0.32	0.89	0.88	0.90	0.89	0.91	0.91	0.90	0.95	0.58	0.44
R2ad	0.18	0.34	0.43	0.44	0.34	0.31	0.88	0.87	0.90	0.89	0.91	0.91	0.90	0.94	0.58	0.43
correlation	0.44	0.59	0.66	0.67	0.59	0.57	0.94	0.94	0.95	0.94	0.95	0.95	0.95	0.97	0.76	0.66

P-RSLAI-cor-APHRO																
	Tarbela	**Mangla**	**Sujanpur**	**Nadaun**	**Mandi**	**Pando**	**Bhimgoda**	**Humla**	**Benighat**	**Asaraghat**	**Angsing**	**Turkeghat**	**Bahadurabad**	**Hardinge_Bridge**	**Ambabal**	**Konta**
avg_obs	2257.71	741.12	135.65	165.89	122.61	82.94	785.10	273.85	506.35	446.61	371.38	500.71	21631.67	11578.57	30.48	484.32
avg_sim	2796.63	738.75	217.62	251.01	140.77	124.61	859.45	476.26	215.41	491.99	336.75	602.05	16401.92	19836.97	24.21	416.74
NSE	0.58	0.45	0.23	0.29	0.31	0.25	0.88	-0.56	0.31	0.84	0.88	0.66	0.74	0.53	0.19	0.17
LNSE	0.55	0.64	-0.53	-0.41	-0.25	-0.84	0.83	0.54	-0.82	0.87	0.87	0.52	0.75	0.21	-0.31	0.20
rmse	1399.00	380.41	151.69	181.03	152.77	123.38	261.00	299.42	388.35	162.52	142.10	270.61	7083.25	9118.65	47.13	523.10
mae	1070.30	276.73	126.70	145.55	108.76	95.50	193.38	204.51	291.09	101.01	86.77	203.38	5277.53	8266.02	30.28	310.23
bias	538.92	-2.37	81.97	85.12	18.16	41.67	74.34	202.41	-290.93	45.38	-34.63	101.35	-5229.75	8258.40	-6.27	-67.58
R2	0.64	0.50	0.48	0.48	0.40	0.38	0.89	0.88	0.90	0.88	0.90	0.89	0.90	0.95	0.58	0.44
R2ad	0.64	0.49	0.47	0.47	0.40	0.37	0.89	0.87	0.90	0.87	0.90	0.89	0.90	0.95	0.58	0.43
correlation	0.80	0.71	0.69	0.69	0.64	0.62	0.95	0.94	0.95	0.94	0.95	0.94	0.95	0.98	0.76	0.66

P-RSLAI-CHIRPS																
	Tarbela	**Mangla**	**Sujanpur**	**Nadaun**	**Mandi**	**Pando**	**Bhimgoda**	**Humla**	**Benighat**	**Asaraghat**	**Angsing**	**Turkeghat**	**Bahadurabad**	**Hardinge_Bridge**	**Ambabal**	**Konta**
avg_obs	2257.71	741.12	135.65	165.89	122.61	82.94	785.10	273.85	506.35	446.61	371.38	500.71	21631.67	11578.57	30.48	484.32
avg_sim	856.05	552.70	41.50	48.33	24.81	20.98	291.11	321.06	157.55	340.34	343.67	758.00	16797.56	23024.11	33.57	747.48
NSE	-0.13	0.31	-0.23	-0.25	-0.24	-0.13	0.05	0.53	-0.02	0.69	0.83	-0.78	0.80	-0.04	0.45	0.47
LNSE	0.06	0.56	-0.11	-0.20	0.01	0.17	-0.15	0.65	-2.65	0.37	0.74	-0.02	0.69	0.14	-0.43	-0.30
rmse	2287.22	425.65	192.32	240.64	204.12	151.50	743.93	164.06	474.39	226.97	168.66	622.98	6282.02	13547.07	38.91	415.64
mae	1456.68	265.13	101.58	125.32	103.66	78.22	494.00	96.58	350.00	165.80	102.00	367.00	5056.40	11445.54	28.68	379.34
bias	-1401.66	-188.42	-94.15	-117.56	-97.80	-61.96	-494.00	47.20	-348.80	-106.27	-27.71	257.30	-4834.11	11445.54	3.09	263.16
R2	0.45	0.45	0.28	0.18	0.37	0.39	0.83	0.78	0.81	0.76	0.84	0.83	0.93	0.94	0.73	0.78
R2ad	0.44	0.44	0.27	0.17	0.36	0.38	0.82	0.77	0.80	0.76	0.83	0.82	0.93	0.94	0.73	0.78
correlation	0.67	0.67	0.53	0.43	0.61	0.62	0.91	0.88	0.90	0.87	0.91	0.91	0.96	0.97	0.85	0.88

P-RSLAI-ET-cor-APHRODITE																
	Tarbela	**Mangla**	**Sujanpur**	**Nadaun**	**Mandi**	**Pando**	**Bhimgoda**	**Humla**	**Benighat**	**Asaraghat**	**Angsing**	**Turkeghat**	**Bahadurabad**	**Hardinge_Bridge**	**Ambabal**	**Konta**
avg_obs	2356.60	830.31	148.45	181.73	130.78	87.90	773.21	270.94	499.60	435.94	346.75	529.66	24130.52	11613.13	32.21	552.47
avg_sim	2881.81	626.37	157.15	178.42	101.97	92.53	713.01	401.34	164.38	410.62	266.63	529.05	14769.62	12917.57	16.12	275.50
NSE	0.39	0.17	0.37	0.36	0.26	0.32	0.89	0.27	0.08	0.86	0.84	0.80	0.44	0.91	-0.03	-0.10
LNSE	0.44	-0.04	0.05	0.14	0.10	-0.44	0.90	0.73	-1.58	0.84	0.62	0.17	0.22	0.84	-0.09	0.12
rmse	1719.76	487.62	146.57	183.95	173.39	127.37	270.59	209.60	448.83	155.45	147.91	220.17	10629.53	4006.90	53.59	669.02
mae	1271.45	353.45	100.21	116.22	99.49	82.16	145.52	140.05	335.23	103.35	107.51	172.71	9360.90	3175.07	32.26	337.19
bias	525.21	-203.94	8.70	-3.31	-28.81	4.63	-60.20	130.40	-335.23	-25.32	-80.11	-0.61	-9360.90	1304.44	-16.09	-276.97
R2	0.48	0.41	0.43	0.43	0.41	0.41	0.91	0.87	0.93	0.86	0.91	0.87	0.93	0.92	0.23	0.19
R2ad	0.47	0.40	0.42	0.42	0.40	0.40	0.90	0.86	0.93	0.86	0.91	0.87	0.93	0.92	0.22	0.18
correlation	0.69	0.64	0.66	0.65	0.64	0.64	0.95	0.93	0.96	0.93	0.96	0.93	0.96	0.96	0.48	0.44

APPENDIX F

TABLES SHOWING DAILY MODEL PERFORMANCE FOR VARIOUS EXPERIMENTS

P-Def										
	Tarbela	**Mangla**	**Sujanpur**	**Nadaun**	**Mandi**	**Pando**	**Bahadurabad**	**Hardinge_Bridge**	**Ambabal**	**Konta**
avg_obs	2271.08	742.66	136.75	167.23	125.80	83.78	21810.71	11640.25	30.77	486.84
avg_sim	1198.29	357.72	64.70	69.91	47.30	43.09	16836.06	11697.04	15.39	278.20
NSE	0.21	-0.68	0.01	-0.01	-0.01	0.05	0.60	0.85	0.09	0.05
LNSE	0.42	-1.67	0.05	-0.02	0.19	-0.12	0.54	0.85	0.02	0.33
rmse	2003.10	697.14	214.38	290.55	235.00	174.76	10182.18	5475.86	103.29	821.01
mae	1236.43	492.35	101.41	124.79	102.77	82.94	7127.92	3539.82	28.76	289.72
bias	-1072.79	-384.94	-72.04	-97.32	-78.50	-40.69	-4974.65	56.79	-15.38	-208.64
R2	0.53	0.13	0.12	0.11	0.11	0.10	0.71	0.87	0.18	0.27
R2ad	0.53	0.13	0.12	0.11	0.11	0.10	0.70	0.87	0.18	0.27
correlation	0.73	0.37	0.35	0.33	0.33	0.32	0.84	0.93	0.42	0.52

P-RSLAI										
	Tarbela	**Mangla**	**Sujanpur**	**Nadaun**	**Mandi**	**Pando**	**Bahadurabad**	**Hardinge_Bridge**	**Ambabal**	**Konta**
avg_obs	2271.08	742.66	136.75	167.23	125.80	83.78	21810.71	11640.25	30.77	486.84
avg_sim	1514.01	565.84	127.23	146.59	85.71	74.63	18903.17	21132.96	30.37	544.07
NSE	0.39	-0.64	0.04	0.05	0.05	0.08	0.63	0.34	0.19	0.20
LNSE	0.69	0.13	-0.05	-0.02	0.00	-0.61	0.73	0.09	-0.76	-0.12
rmse	1761.53	687.86	211.20	282.32	227.65	172.04	9808.66	11566.44	97.23	754.03
mae	1052.49	408.80	115.96	139.89	115.63	97.29	6336.39	9811.54	36.60	382.39
bias	-757.07	-176.82	-9.52	-20.64	-40.08	-9.14	-2907.54	9492.71	-0.41	57.23
R2	0.60	0.12	0.09	0.08	0.08	0.09	0.69	0.86	0.25	0.25
R2ad	0.60	0.12	0.09	0.08	0.08	0.09	0.69	0.86	0.25	0.25
correlation	0.78	0.34	0.29	0.28	0.29	0.30	0.83	0.92	0.50	0.50

P-RSLAI-APHRO										
	Tarbela	**Mangla**	**Sujanpur**	**Nadaun**	**Mandi**	**Pando**	**Bahadurabad**	**Hardinge_Bridge**	**Ambabal**	**Konta**
avg_obs	2271.08	742.66	136.75	167.23	125.80	83.78	21810.71	11640.25	30.77	486.84
avg_sim	811.29	515.65	194.21	227.71	119.57	103.46	13502.93	18970.71	24.25	417.09
NSE	-0.29	-0.36	0.18	0.17	0.18	0.16	0.44	0.61	0.14	0.17
LNSE	-0.16	0.07	-0.45	-0.39	-0.23	-0.93	0.41	0.25	-0.58	0.14
rmse	2560.85	627.43	195.17	264.35	211.01	164.41	12048.92	8874.79	100.28	770.06
mae	1587.24	399.25	136.28	160.75	123.36	107.24	8956.88	7728.59	33.45	332.58
bias	-1459.79	-227.01	57.46	60.48	-6.22	19.68	-8307.78	7330.46	-6.52	-69.75
R2	0.15	0.14	0.26	0.22	0.20	0.17	0.72	0.90	0.24	0.35
R2ad	0.15	0.14	0.26	0.22	0.20	0.17	0.72	0.90	0.24	0.35
correlation	0.39	0.37	0.51	0.47	0.44	0.42	0.85	0.95	0.49	0.59

P-RSLAI-cor-APHRO										
	Tarbela	**Mangla**	**Sujanpur**	**Nadaun**	**Mandi**	**Pando**	**Bahadurabad**	**Hardinge_Bridge**	**Ambabal**	**Konta**
avg_obs	2271.08	742.66	136.75	167.23	125.80	83.78	21810.71	11640.25	30.77	486.84
avg_sim	2805.81	738.88	218.24	251.74	141.27	124.98	16902.19	19920.98	24.25	417.09
NSE	0.42	-0.86	0.09	0.12	0.21	0.12	0.63	0.53	0.14	0.17
LNSE	0.52	0.31	-0.61	-0.51	-0.35	-1.09	0.71	0.19	-0.58	0.14
rmse	1723.56	732.77	205.59	271.66	208.30	167.93	9797.29	9769.91	100.28	770.06
mae	1169.73	413.68	148.35	172.21	127.39	114.66	6608.72	8524.03	33.45	332.58
bias	534.73	-3.78	81.50	84.52	15.47	41.21	-4908.52	8280.74	-6.52	-69.75
R2	0.52	0.18	0.28	0.23	0.21	0.19	0.72	0.91	0.24	0.35
R2ad	0.52	0.18	0.28	0.23	0.21	0.19	0.72	0.91	0.24	0.35
correlation	0.72	0.43	0.53	0.48	0.46	0.43	0.85	0.95	0.49	0.59

P-RSLAI-CHIRSP										
	Tarbela	**Mangla**	**Sujanpur**	**Nadaun**	**Mandi**	**Pando**	**Bahadurabad**	**Hardinge_Bridge**	**Ambabal**	**Konta**
avg_obs	2271.08	742.66	136.75	167.23	125.80	83.78	21810.71	11640.25	30.77	486.84
avg_sim	858.09	552.92	41.56	48.39	24.90	21.02	17375.86	23131.98	33.68	749.34
NSE	-0.12	-0.74	-0.13	-0.13	-0.15	-0.08	0.59	-0.04	0.15	0.20
LNSE	0.03	-0.08	-0.05	-0.11	0.06	0.09	0.56	0.12	-0.78	-0.46
rmse	2386.55	708.21	229.25	307.07	250.48	186.21	10234.91	14492.23	99.96	757.10
mae	1492.95	428.39	103.90	128.48	108.52	82.43	7067.35	11582.95	37.35	459.63
bias	-1412.99	-189.75	-95.19	-118.83	-100.90	-62.75	-4434.85	11491.74	2.91	262.50
R2	0.40	0.10	0.23	0.16	0.18	0.18	0.68	0.88	0.15	0.31
R2ad	0.40	0.10	0.23	0.16	0.18	0.18	0.68	0.88	0.15	0.31
correlation	0.63	0.32	0.48	0.40	0.42	0.43	0.83	0.94	0.39	0.55

P-RSLAI-ET-cor-APHRO										
	Tarbela	**Mangla**	**Sujanpur**	**Nadaun**	**Mandi**	**Pando**	**Bahadurabad**	**Hardinge_Bridge**	**Ambabal**	**Konta**
avg_obs	2370.26	831.83	149.59	183.10	134.32	88.74	24626.01	11662.00	32.50	555.33
avg_sim	2888.90	626.03	157.60	178.94	102.39	92.87	15396.61	12973.43	16.13	275.68
NSE	-0.41	-0.85	0.13	0.15	0.12	0.08	0.49	0.85	0.01	-0.01
LNSE	0.41	-1.02	-0.08	-0.01	-0.01	-0.64	0.23	0.81	-0.24	0.19
rmse	2749.27	769.55	212.31	287.96	235.14	185.17	12025.60	5545.77	112.47	969.02
mae	1417.31	512.38	122.86	140.97	117.62	102.32	9368.95	3894.05	34.08	347.12
bias	518.64	-205.80	8.01	-4.16	-31.92	4.13	-9229.40	1311.43	-16.37	-279.65
R2	0.22	0.18	0.18	0.17	0.14	0.13	0.83	0.86	0.14	0.20
R2ad	0.22	0.18	0.18	0.16	0.14	0.13	0.83	0.86	0.14	0.20
correlation	0.47	0.43	0.43	0.41	0.37	0.36	0.91	0.93	0.37	0.45

BIBLIOGRAPHY

Alcamo, J., Döll, P., Kaspar, F., and Siebert, S. (1997). Global change and global scenarios of water use and availability: an application of WaterGAP 1.0. *Center for Environmental* . . . .

Allen, R. G. (1998). FAO Irrigation and Drainage Paper Crop by. *Irrigation and Drainage*, 300(56):300.

Andermann, C., Bonnet, S., and Gloaguen, R. (2011). Evaluation of precipitation data sets along the Himalayan front. *Geochemistry, Geophysics, Geosystems*, 12(7):n/a–n/a.

Andersen, J., Dybkjaer, G., Jensen, K., Refsgaard, J., and Rasmussen, K. (2002). Use of remotely sensed precipitation and leaf area index in a distributed hydrological model. *Journal of Hydrology*, 264(1-4):34–50.

Anderson, M. C., Norman, J. M., Mecikalski, J. R., Otkin, J. A., and Kustas, W. P. (2007). A climatological study of evapotranspiration and moisture stress across the continental United States based on thermal remote sensing: 2. Surface moisture climatology. *Journal of Geophysical Research Atmospheres*, 112(11):1–13.

Arnell, N. (1999a). A simple water balance model for the simulation of streamflow over a large geographic domain. *Journal of Hydrology*, 217(3-4):314–335.

Arnell, N. (1999b). Climate change and global water resources. *Global Environmental Change*, 9:S31–S49.

Ashouri, H., Hsu, K.-L., Sorooshian, S., Braithwaite, D. K., Knapp, K. R., Cecil, L. D., Nelson, B. R., and Prat, O. P. (2015). PERSIANN-CDR: Daily Precipitation Climate Data Record from Multisatellite Observations for Hydrological and Climate Studies. *Bulletin of the American Meteorological Society*, 96(1):69–83.

Bárdossy, A. and Singh, S. K. (2008). Robust estimation of hydrological model parameters. *Hydrology and Earth System Sciences*, 12(6):1273–1283.

Bastiaanssen, W. G. M., Cheema, M. J. M., Immerzeel, W. W., Miltenburg, I. J., and Pelgrum, H. (2012). Surface energy balance and actual evapotranspiration of the transboundary Indus Basin estimated from satellite measurements and the ETLook model. *Water Resources Research*, 48(11):n/a–n/a.

Bastiaanssen W.G.M., M. Meneti, R.A. Feddes, and Holtslag, a. a. M. (1998). A remote sensing surface energy balance algorithm for land (SEBAL)\n1.Formulation. *Journal of Hydrology*, 212-213(JANUARY):198–212.

Bayabil, H. K., Tebebu, T. Y., Stoof, C. R., and Steenhuis, T. S. (2016). Effects of a deep-rooted crop and soil amended with charcoal on spatial and temporal runoff patterns in a degrading tropical highland watershed. *Hydrology and Earth System Sciences*, 20(2):875–885.

Beven, K. (1989). Changing ideas in hydrology - The case of physically-based models. *Journal of Hydrology*, 105:157–172.

Beven, K. (2006). A manifesto for the equifinality thesis. In *Journal of Hydrology*, volume 320, pages 18–36.

Beven, K. and Freer, J. (2001). Hydrology Equifinality, data assimilation, and uncertainty estimation in mechanistic modelling of complex environmental systems using the GLUE methodology. *lournal of Hydrology*, 249:11–29.

Biemans, H., Hutjes, R. W. a., Kabat, P., Strengers, B. J., Gerten, D., and Rost, S. (2009). Effects of Precipitation Uncertainty on Discharge Calculations for Main River Basins. *Journal of Hydrometeorology*, 10(4):1011–1025.

Biemans, H., Speelman, L. H., Ludwig, F., Moors, E. J., Wiltshire, A. J., Kumar, P., Gerten, D., and Kabat, P. (2013). Future water resources for food production in five South Asian river basins and potential for adaptation–a modeling study. *The Science of the total environment*, 468-469 Su:S117–31.

Bierkens, M. F. P. (2015). Global hydrology 2015: State, trends, and directions. *Water Resources Research*, 51(7):4923–4947.

Bounoua, L., Collatz, G. J., Los, S. O., Sellers, P. J., Dazlich, D. A., Tucker, C. J., and Randall, D. A. (2000). Sensitivity of Climate to Changes in NDVI. *Journal of Climate*, 13(13):2277–2292.

Bronstert, A., Carrera, J., Kabat, P., and Lütkemeier, S. (2005). *Coupled Models for the Hydrological Cycle*.

Cheema, M. J. M. and Bastiaanssen, W. G. M. (2012). Local calibration of remotely sensed rainfall from the TRMM satellite for different periods and spatial scales in the Indus Basin. *International Journal of Remote Sensing*, 33(8):2603–2627.

Cheema, M. J. M., Immerzeel, W. W., and Bastiaanssen, W. G. M. (2014). Spatial quantification of groundwater abstraction in the irrigated indus basin. *Groundwater*, 52(1):25–36.

Chen, F., Mitchell, K., Schaake, J., Xue, Y., Pan, H.-L., Koren, V., Duan, Q. Y., Ek, M., and Betts, A. (1996). Modeling of land surface evaporation by four schemes and comparison with FIFE observations. *Journal of Geophysical Research*, 101(D3):7251.

Clark, M. P. and Vrugt, J. a. (2006). Unraveling uncertainties in hydrologic model calibration: Addressing the problem of compensatory parameters. *Geophysical Research Letters*, 33(6):1–5.

Crow, W. T. and Ryu, D. (2008). A new data assimilation approach for improving hydrologic prediction using remotely-sensed soil moisture retrievals. *Hydrology and Earth System Sciences Discussions*, 5(4):2005–2044.

De Lannoy, G. J. M., Reichle, R. H., Houser, P. R., Arsenault, K. R., Verhoest, N. E. C., and Pauwels, V. R. N. (2010). Satellite-Scale Snow Water Equivalent Assimilation into a High-Resolution Land Surface Model. *Journal of Hydrometeorology*, 11(2):352–369.

Dickinson, E., Henderson-Sellers, A., and Kennedy, J. (1993). Biosphere-atmosphere Transfer Scheme (BATS) Version 1e as Coupled to the NCAR Community Climate Model. *NCAR Tech. Rep. NCAR/TN-3871STR, 72*, (August):77.

Dingman, S. L. (2015). *Physical Hydrology: Third Edition*. Waveland Press.

Duncan, J. M. A. and Biggs, E. M. (2012). Assessing the accuracy and applied use of satellite-derived precipitation estimates over Nepal. *Applied Geography*, 34:626–638.

Eagleson, P. S. (1986). The emergence of global scale hydrology. *Water Resources Research*, 22(9):6s–14s.

Eckhardt, K., Breuer, L., and Frede, H.-G. (2003). Parameter uncertainty and the significance of simulated land use change effects. *Journal of Hydrology*, 273(1-4):164–176.

Fauchereau, N., Trzaska, S., Rouault, M., and Richard, Y. (2003). Rainfall variability and changes in southern Africa during the 20th century in the global warming context. *Natural Hazards*.

Fekete, B. M., Vörösmarty, C. J., Roads, J. O., and Willmott, C. J. (2004). Uncertainties in precipitation and their impacts on runoff estimates. *Journal of Climate*, 17(2):294–304.

Fisher, J. B., Tu, K. P., and Baldocchi, D. D. (2008). Global estimates of the land-atmosphere water flux based on monthly AVHRR and ISLSCP-II data, validated at 16 FLUXNET sites. *Remote Sensing of Environment*, 112(3):901–919.

Fraedrich, K., Kleidon, A., and Lunkeit, F. (1999). A Green Planet versus a Desert World: Estimating the Effect of Vegetation Extremes on the Atmosphere. *Journal of Climate*, 12(10):3156–3163.

Funk, C. C., Peterson, P. J., Landsfeld, M. F., Pedreros, D. H., Verdin, J. P., Rowland, J. D., Romero, B. E., Husak, G. J., Michaelsen, J. C., and Verdin, a. P. (2014). A Quasi-Global Precipitation Time Series for Drought Monitoring. *U.S. Geological Survey Data Series*, 832:4.

Gain, A. K. and Wada, Y. (2014). Assessment of Future Water Scarcity at Different Spatial and Temporal Scales of the Brahmaputra River Basin. *Water Resources Management*, 28(4):999–1012.

Garratt, J. R. (1993). Sensitivity of Climate Simulations to Land-Surface and Atmospheric Boundary-Layer Treatments-A Review. *Journal of Climate*, 6(3):419–448.

Gholz, H. L., Fitz, F. K., and Waring, R. H. (1976). Leaf area differences associated with old-growth forest communities in the western Oregon Cascades. *Canadian Journal of Forest Research*, 6(1):49–57.

Gigante, V., Iacobellis, V., Manfreda, S., Milella, P., and Portoghese, I. (2009). Influences of Leaf Area Index estimations on water balance modeling in a Mediterranean semi-arid basin. *Natural Hazards and Earth System Science*, 9(3):979–991.

Gleick, P. H. (2000). The Changing Water Paradigm - A Look at Twenty-first Century Water Resources Development. *Water International*, 25(1):127–138.

Gleick, P. H. (2003). Water Use. *Annual Review of Environment and Resources*, 28(1):275–314.

Guerschman, J. P., Van Dijk, A. I. J. M., Mattersdorf, G., Beringer, J., Hutley, L. B., Leuning, R., Pipunic, R. C., and Sherman, B. S. (2009). Scaling of potential evapotranspiration with MODIS data reproduces flux observations and catchment water balance observations across Australia. *Journal of Hydrology*, 369(1-2):107–119.

Gumma, M. K. (2011). Mapping rice areas of South Asia using MODIS multitemporal data. *Journal of Applied Remote Sensing*, 5(1):053547.

Hagemann, S. (2002). An Improved Land Surface Parameter Dataset for Global and Regional Climate Models. Technical report, Max Planck Institute for Meteorology, Hamburg, Germany.

Hanasaki, N., Kanae, S., Oki, T., Masuda, K., Motoya, K., Shirakawa, N., Shen, Y., and Tanaka, K. (2008). An integrated model for the assessment of global water resources Part 1: Model description and input meteorological forcing. *Hydrology and Earth System Sciences*, 12(4):1007–1025.

Hoerling, M. and Kumar, A. (2003). The perfect ocean for drought. *Science (New York, N.Y.)*, 299(5607):691–4.

Hu, G. and Jia, L. (2015). *Monitoring of evapotranspiration in a semi-arid inland river basin by combining microwave and optical remote sensing observations*, volume 7.

Immerzeel, W. (2008). Spatial modelling of mountainous basins. pages 1–146.

Immerzeel, W., Wanders, N., a.F. Lutz, Shea, J., and Bierkens, M. (2015). Reconciling high altitude precipitation with glacier mass balances and runoff. *Hydrology and Earth System Sciences Discussions*, 12:4755–4784.

Jhorar, R. K., Van Dam, J. C., Bastiaanssen, W. G. M., and Feddes, R. a. (2004). Calibration of effective soil hydraulic parameters of heterogeneous soil profiles. *Journal of Hydrology*, 285(1-4):233–247.

Joyce, R. J., Janowiak, J. E., Arkin, P. a., and Xie, P. (2004). CMORPH: A Method that Produces Global Precipitation Estimates from Passive Microwave and Infrared Data at High Spatial and Temporal Resolution. *Journal of Hydrometeorology*, 5(3):487–503.

Khandu, J. L., Awange, J. L., and Forootan, E. (2016). An evaluation of high-resolution gridded precipitation products over Bhutan (1998-2012). *International Journal of Climatology*, 36(3):1067–1087.

Kite, G. and Droogers, P. (2000). Comparing evapotranspiration estimates from satellites, hydrological models and field data. *Journal of Hydrology*, 229(1-2):3–18.

Koren, V., Schaake, J., Mitchell, K., Duan, Q.-Y., Chen, F., and Baker, J. M. (1999). A parameterization of snowpack and frozen ground intended for NCEP weather and climate models. *Journal of Geophysical Research*, 104(D16):19569.

Koster, R. D. and Suarez, M. J. (1992). Modeling the land surface boundary in climate models as a composite of independent vegetation stands. *Journal of Geophysical Research*, 97(D3):2697.

Krakauer, N., Pradhanang, S., Lakhankar, T., and Jha, A. (2013). Evaluating Satellite Products for Precipitation Estimation in Mountain Regions: A Case Study for Nepal. *Remote Sensing*, 5(8):4107–4123.

Kunnath-Poovakka, A., Ryu, D., Renzullo, L. J., and George, B. (2016). The efficacy of calibrating hydrologic model using remotely sensed evapotranspiration and soil moisture for streamflow prediction. *Journal of Hydrology*, 535:509–524.

Kustas, W. P. and Norman, J. M. (1997). A two-source approach for estimating turbulent fluxes using multiple angle thermal infrared observations. *Water Resources Research*, 33(6):1495–1508.

Laghari, A. N., Vanham, D., and Rauch, W. (2012). The Indus basin in the framework of current and future water resources management. *Hydrology and Earth System Sciences*, 16(4):1063–1083.

Lark, M. A. P. C., Slater, A. G., and Clark, M. P. (2006). Snow Data Assimilation via an Ensemble Kalman Filter. *Journal of Hydrometeorology*, 7(3):478–493.

Lei, H., Huang, M., Leung, L. R., Yang, D., Shi, X., Mao, J., Hayes, D. J., Schwalm, C. R., Wei, Y., and Liu, S. (2014). Sensitivity of global terrestrial gross primary production to hydrologic states simulated by the Community Land Model

using two runoff parameterizations. *Journal of Advances in Modeling Earth Systems*, 6(3):658–679.

Liang, X., Lettenmaier, D. P., and Wood, E. F. (1996). One-dimensional statistical dynamic representation of subgrid spatial variability of precipitation in the two-layer variable infiltration capacity model. *Journal of Geophysical Research*, 101(D16):21403.

Liang, X., Lettenmaier, D. P., Wood, E. F., and Burges, S. J. (1994). A simple hydrologically based model of land surface water and energy fluxes for general circulation models. *Journal of Geophysical Research*, 99(D7):14415.

Lopez Lopez, P., Wanders, N., Schellekens, J., Renzullo, L. J., Sutanudjaja, E. H., and Bierkens, M. F. P. (2015). Improved large-scale hydrological modelling through the assimilation of streamflow and downscaled satellite soil moisture observations. *Hydrology and Earth System Sciences Discussions*, 12(10):10559–10601.

Los, S. O., Pollack, N. H., Parris, M. T., Collatz, G. J., Tucker, C. J., Sellers, P. J., Malmström, C. M., DeFries, R. S., Bounoua, L., and Dazlich, D. A. (2000). A Global 9-yr Biophysical Land Surface Dataset from NOAA AVHRR Data. *Journal of Hydrometeorology*, 1(2):183–199.

Maltese, A., Cannarozzo, M., Capodici, F., La Loggia, G., and Santangelo, T. (2008). <title>A sensitivity analysis of a surface energy balance model to LAI (Leaf Area Index)</title>. In Neale, C. M. U., Owe, M., and D'Urso, G., editors, *Remote Sensing for Agriculture*, volume 7104, pages 71040K–71040K–10.

Manabe, S. (1969). Climate and the Ocean Circulation 1. *Monthly Weather Review*, 97(11):739–774.

McMichael, C. E., Hope, A. S., and Loaiciga, H. A. (2006). Distributed hydrological modelling in California semi-arid shrublands: MIKE SHE model calibration and uncertainty estimation. *Journal of Hydrology*, 317(3-4):307–324.

Mekonnen, M. M. and Hoekstra, A. Y. (2016). Four billion people facing severe water scarcity. *Science Advances*, 2(2):e1500323–e1500323.

Ménégoz, M., Gallée, H., and Jacobi, H. W. (2013). Precipitation and snow cover in the Himalaya: From reanalysis to regional climate simulations. *Hydrology and Earth System Sciences*, 17(10):3921–3936.

Miralles, D. G., Holmes, T. R. H., De Jeu, R. A. M., Gash, J. H., Meesters, A. G. C. A., and Dolman, A. J. (2011). Global land-surface evaporation estimated from satellite-based observations. *Hydrology and Earth System Sciences*, 15(2):453–469.

Mo, K. C. and Schemm, J. E. (2008). Relationships between ENSO and drought over the southeastern United States. *Geophysical Research Letters*, 35(15):L15701.

Mu, Q., Cleugh, H. a., Leuning, R., and Running, S. W. (2007). Regional evaporation estimates from flux tower and MODIS satellite data. *Remote Sensing of Environment*, 106(3):285–304.

Mu, Q., Jones, L. A., Kimball, J. S., McDonald, K. C., and Running, S. W. (2009). Satellite assessment of land surface evapotranspiration for the pan-Arctic domain. *Water Resources Research*, 45(9):1–20.

Mu, Q., Zhao, M., and Running, S. W. (2011). Improvements to a MODIS global terrestrial evapotranspiration algorithm. *Remote Sensing of Environment*, 115(8):1781–1800.

Nash, J. and Sutcliffe, J. (1970). River flow forecasting through conceptual models part I A discussion of principles. *Journal of Hydrology*, 10(3):282–290.

Olson, J. (1994a). Global Ecosystem Framework- Definitions: Internal Report. Technical report, USGS EROS Data Centre, Sioux Falls, South Dakota.

Olson, J. (1994b). Global Ecosystem Framework- Translation Strategy. Technical report, USGS EROS Data Center, Sioux Falls, South Dakota.

Olson, J., Watts, J., and & Allison, L. (1983). Carbon in live vegetation of major world ecosystems. *Oak Ridge National Laboratory*, pages ORNL–5862.

Parr, D., Wang, G., and Bjerklie, D. (2015). Integrating Remote Sensing Data on Evapotranspiration and Leaf Area Index with Hydrological Modeling: Impacts on Model Performance and Future Predictions. *Journal of Hydrometeorology*, 16(5):2086–2100.

Portmann, F., Siebert, S., Bauer, C., and Döll, P. (2008). Global dataset of monthly growing areas of 26 irrigated crops. *Frankfurt Hydrology Paper*, (06):400.

Postel, S. (1999). *Pillar of Sand: Can the Irrigation Miracle Last?* W.W. Norton.

Prigent, C., Papa, F., Aires, F., Jimenez, C., Rossow, W. B., and Matthews, E. (2012). Changes in land surface water dynamics since the 1990s and relation to population pressure. *Geophysical Research Letters*, 39(8):n/a–n/a.

Pulliainen, J. (2006). Mapping of snow water equivalent and snow depth in boreal and sub-arctic zones by assimilating space-borne microwave radiometer data and ground-based observations. *Remote Sensing of Environment*, 101(2):257–269.

Reddy, S. T. S. (2007). Declining groundwater levels in India. *International Journal of Water Resources Development*.

Refsgaard, J. C. and Henriksen, H. J. (2004). Modelling guidelinesterminology and guiding principles. *Advances in Water Resources*, 27(1):71–82.

Richard, Y., Trzaska, S., Roucou, P., and Rouault, M. (2000). Modification of the southern African rainfall variability/ENSO relationship since the late 1960s. *Climate Dynamics*, 16(12):883–895.

Rohwer, J., Gerten, D., and Lucht, W. (2007). Development of functional types of irrigation for improved global crop modelling. Technical report.

Running, S., Peterson, D., Spanner, M., and Teuber, K. (1986). Remote sensing of coniferous leaf area. *Ecology*, 67(1):273–276.

Schuurmans, J., Troch, P., Veldhuizen, A., Bastiaanssen, W., and Bierkens, M. (2003). Assimilation of remotely sensed latent heat flux in a distributed hydrological model. *Advances in Water Resources*, 26(2):151–159.

Sellers, P. J., Tucker, C. J., Collatz, G. J., Los, S. O., Justice, C. O., Dazlich, D. A., and Randall, D. A. (1996). A Revised Land Surface Parameterization (SiB2) for Atmospheric GCMS. Part II: The Generation of Global Fields of Terrestrial Biophysical Parameters from Satellite Data. *Journal of Climate*, 9(4):706–737.

Senay, G. B., Bohms, S., Singh, R. K., Gowda, P. H., Velpuri, N. M., Alemu, H., and Verdin, J. P. (2013). Operational Evapotranspiration Mapping Using

Remote Sensing and Weather Datasets: A New Parameterization for the SSEB Approach. *Journal of the American Water Resources Association*, 49(3):577–591.

Sharma, B., Amarasinghe, U., and Sikka, A. (2008). Indo-Gangetic River Basins: Summary situation analysis.

Sharma, B., Amarasinghe, U., Xueliang, C., de Condappa, D., Shah, T., Mukherji, A., Bharati, L., Ambili, G., Qureshi, A., Pant, D., Xenarios, S., Singh, R., and Smakhtin, V. (2010). The Indus and the Ganges: river basins under extreme pressure. *Water International*, 35(5):493–521.

Shiklomanov, I. a. (2000). Appraisal and Assessment of World Water Resources. *Water International*, 25(1):11–32.

Shrestha, M., Artan, G., Bajracharya, S., and Sharma, R. (2008). Using satellite-based rainfall estimates for streamflow modelling: Bagmati Basin. *Journal of Flood Risk Management*, 1(2):89–99.

Silvestro, F., Gabellani, S., Rudari, R., Delogu, F., Laiolo, P., and Boni, G. (2015). Uncertainty reduction and parameter estimation of a distributed hydrological model with ground and remote-sensing data. *Hydrology and Earth System Sciences*, 19(4):1727–1751.

Sloan, P. G. and Moore, I. D. (1984). Modeling subsurface stormflow on steeply sloping forested watersheds. *Water Resources Research*, 20(12):1815–1822.

Smith, P. J., Thornhill, G. D., Dance, S. L., Lawless, a. S., Mason, D. C., and Nichols, N. K. (2013). Data assimilation for state and parameter estimation: Application to morphodynamic modelling. *Quarterly Journal of the Royal Meteorological Society*, 139(671):314–327.

Sood, A. and Smakhtin, V. (2014). Global hydrological models: a review. *Hydrological Sciences Journal*, 6667(April):18.

Sutanudjaja, E. H., Van Beek, L. P. H., De Jong, S. M., Van Geer, F. C., and Bierkens, M. F. P. (2014). Calibrating a large-extent high-resolution coupled groundwater-land surface model using soil moisture and discharge data. *Water Resources Research*, 50(1):687–705.

Takata, K., Emori, S., and Watanabe, T. (2003). Development of the minimal advanced treatments of surface interaction and runoff. *Global and Planetary Change*, 38(1-2):209–222.

Tesemma, Z., Wei, Y., Peel, M., and Western, A. (2015). The effect of year-to-year variability of leaf area index on Variable Infiltration Capacity model performance and simulation of runoff. *Advances in Water Resources*, 83:310–322.

Thirel, G., Salamon, P., Burek, P., and Kalas, M. (2013). Assimilation of MODIS Snow Cover Area Data in a Distributed Hydrological Model Using the Particle Filter. *Remote Sensing*, 5(11):5825–5850.

van Beek, L. and Bierkens, M. (2009). The Global Hydrological Model PCR-GLOBWB: Conceptualization, Parameterization and Verification, Report Department of Physical Geography, Utrecht. *vanbeek. geo. uu. nl/suppinfo/vanbeekbierkens2009. . . . .*

van Beek, L. P. H., Wada, Y., and Bierkens, M. F. P. (2011). Global monthly water stress: 1. Water balance and water availability. *Water Resources Research*, 47(7):n/a–n/a.

Vorosmarty, C. J. (2000). Global Water Resources: Vulnerability from Climate Change and Population Growth. *Science*, 289(5477):284–288.

Vörösmarty, C. J., Federer, C. A., and Schloss, A. L. (1998). Potential evaporation functions compared on US watersheds: Possible implications for global-scale water balance and terrestrial ecosystem modeling. *Journal of Hydrology*, 207(3-4):147–169.

Wada, Y., van Beek, L. P. H., van Kempen, C. M., Reckman, J. W. T. M., Vasak, S., and Bierkens, M. F. P. (2010). Global depletion of groundwater resources. *Geophysical Research Letters*, 37(20):n/a–n/a.

Wada, Y., van Beek, L. P. H., Wanders, N., and Bierkens, M. F. P. (2013). Human water consumption intensifies hydrological drought worldwide. *Environmental Research Letters*, 8(3):034036.

Wada, Y., Wisser, D., and Bierkens, M. F. P. (2014). Global modeling of withdrawal, allocation and consumptive use of surface water and groundwater resources. *Earth System Dynamics*, 5(1):15–40.

Wanders, N., Bierkens, M., Sutanudjaja, E., and van Beek, R. (2014a). The PCR-GLOBWB global hydrological reanalysis product. *EGU General Assembly 2014*, 16:5369.

Wanders, N., Bierkens, M. F. P., de Jong, S. M., de Roo, A., and Karssenberg, D. (2014b). The benefits of using remotely sensed soil moisture in parameter identification of large-scale hydrological models. *Water Resources Research*, 50(8):6874–6891.

Weiß, M. and Menzel, L. (2008). A global comparison of four potential evapotranspiration equations and their relevance to stream flow modelling in semi-arid environments. *Advances in Geosciences*, 18:15–23.

Widén-Nilsson, E., Halldin, S., and Xu, C.-y. (2007). Global water-balance modelling with WASMOD-M: Parameter estimation and regionalisation. *Journal of Hydrology*, 340(1-2):105–118.

Wilson, M. F. and Henderson-Sellers, A. (1985). A global archive of land cover and soils data for use in general circulation climate models. *Journal of Climatology*, 5(2):119–143.

Winsemius, H. C., Savenije, H. H. G., and Bastiaanssen, W. G. M. (2008). Constraining model parameters on remotely sensed evaporation: justification for distribution in ungauged basins? *Hydrology and Earth System Sciences*, 12(4):1403–1413.

Wipfler, E. L., Metselaar, K., Van Dam, J. C., Feddes, R. A., Van Meijgaard, E., Van Ulft, L. H., Van Den Hurk, B., Zwart, S. J., and Bastiaanssen, W. G. M. (2011). Seasonal evaluation of the land surface scheme HTESSEL against remote sensing derived energy fluxes of the Transdanubian region in Hungary. *Hydrology and Earth System Sciences*, 15(4):1257–1271.

Wisser, D., Fekete, B. M., Vörösmarty, C. J., and Schumann, a. H. (2009). Reconstructing 20th century global hydrography: a contribution to the Global Terrestrial Network- Hydrology (GTN-H). *Hydrology and Earth System Sciences Discussions*, 6(2):2679–2732.

World Economic Forum (2016). The Global Risks Report 2016 11th Edition. Technical report.

Yong, B., Liu, D., Gourley, J. J., Tian, Y., Huffman, G. J., Ren, L., and Hong, Y. (2015). Global View Of Real-Time Trmm Multisatellite Precipitation Analysis: Implications For Its Successor Global Precipitation Measurement Mission. *Bulletin of the American Meteorological Society*, 96(2):283–296.

Zhang, Y. and Wegehenkel, M. (2006). Integration of MODIS data into a simple model for the spatial distributed simulation of soil water content and evapotranspiration. *Remote Sensing of Environment*, 104(4):393–408.